03424-17-T

THE UNIVERSITY OF MICHIGAN

COLLEGE OF ENGINEERING

DEPARTMENT OF NUCLEAR ENGINEERING
LABORATORY FOR FLUID FLOW AND HEAT TRANSPORT PHENOMENA

Technical Report No. 17

Cavitation Damage Characteristics in Water and Mercury from Studies in a Cavitating Venturi

M. J. ROBINSON

F. G. HAMMITT

Under grant from:

National Aeronautics and Space Administration

Grant NsG-39-60

Administered through:

April 1966

OFFICE OF RESEARCH ADMINISTRATION · ANN ARBOR

03424-17-T

Laboratory for Fluid Flow and Heat Transport Phenomena
Department of Nuclear Engineering
The University of Michigan

CAVITATION DAMAGE CHARACTERISTICS IN WATER AND MERCURY FROM STUDIES IN A CAVITATING VENTURI

Technical Report Number 17

M. J. Robinson
F. G. Hammitt

April, 1966

Under grant from:

National Aeronautics and Space Administration
(Grant No. NsG-39-60)

ABSTRACT

29748

This report summarizes data gathered to date from a continuing cavitation research investigation concerned with basic cavitation flow regime studies, individual cavitation bubble collapse studies, and damage to materials associated with both. The studies have been conducted using water at 64.7, 97.2 and 200 ft./sec., and mercury at 24, 34 and 65 ft./sec. The bulk of the data was taken at 200 ft./sec. for water and 34 ft./sec. for mercury due to ease of facility operation under these conditions.

Among the topics considered are:

a) Correlations of damage data with specimen material mechanical properties;

b) microexamination of individual pits including (1) sensitive surface traces of individual pits, and (2) metallographic sections of materials through damage areas;

c) microhardness versus specimen exposure time;

d) damage as a function of material grain size for comparable strength ranges of materials;

e) correlation of pitting rate, pit size, spatial distribution of pits, bubble distribution, and pressure above vapor pressure on the specimen surface, all as a function of axial position on the test specimen polished surface;

f) photographic studies of single bubble collapses in a venturi both away from and near a solid boundary.

Conclusions resulting from interpretation of the data are drawn throughout the report.

ACKNOWLEDGMENTS

The authors would like to acknowledge the assistance of Messrs. Ericson, Olson, Garcia and Mitchell, whose unpublished data has been generously referred to in this report, and also numerous other research assistants who worked on this grant.

TABLE OF CONTENTS

	Page
ABSTRACT	ii
ACKNOWLEDGMENTS	iv
NOMENCLATURE	vii
LIST OF TABLES	ix
LIST OF FIGURES	x
Chapter	
I. INTRODUCTION	1
II. EQUIPMENT AND EXPERIMENTAL PROCEDURES	3
A. Mercury System	
B. Water System	
C. Experimental Procedures	
III. MERCURY SYSTEM RESULTS	36
A. Water Content	
B. Damage Tabulations	
C. Damage Correlations	
D. Microexaminations	
E. Pit Correlations	
IV. WATER SYSTEM RESULTS	62
A. Damage Tabulations	
B. Damage Correlations	
C. Microexaminations	
V. CONCLUSIONS	88
A. Damage Correlations	
B. Microexaminations	
C. Pit Correlations	

Page

APPENDICES 92

A. MDP Computational Program
B. Damage Correlation Program
C. Definition of Cavitation Conditions

BIBLIOGRAPHY 102

NOMENCLATURE

Symbol	Description
AcI	Acoustic Impedance Ratio of Material and Fluid = $\frac{(\rho\,(E/\rho)^{1/2})_{\text{fluid}}}{(\rho\,(E/\rho)^{1/2})_{\text{material}}}$
As Rec'd	As Received Material Condition = 60% Cold-Worked
BHN	Brinell Hardness Number, 500 Kg Load
CS	Carbon Steel
Cb-1Zr	Columbium-1% Zirconium Alloy
DPH	Diamond Pyramid Hardness
ESE	Engineering Strain Energy
E	Elastic Modulus
H.H.Trt.	High Heat Treat, Highest Temperature Anneal for Copper, Zinc, Nickel Alloys
L.H.Trt.	Low Heat Treat, Lowest Temperature Anneal for Copper, Zinc, Nickel Alloys
MDP	Mean Depth of Penetration, Total Weight Loss Divided by Material Density per Unit Area
p	Pressure, $lbf/inch^2$
p_v	Vapor Pressure
ppm	Parts per Million
%El	Percent Elongation
%RA	Percent Reduction of Area
SS	Stainless Steel

Symbol	Description
TBS	True Breaking Stress
TSE	True Strain Energy
TS	Tensile Strength
YS	Yield Strength

LIST OF TABLES

Table		Page
1.	"Wet" Mercury Damage Tabulations	39
2.	"Dry" Mercury Damage Tabulations	40
3.	Mechanical Property versus Damage Correlations for Mercury Data at 50 Hours Duration	43
4.	Water Damage Tabulations	64
5.	Mechanical Properties of Test Specimen Materials	68
6.	Mechanical Property versus Damage Correlations for Water Data at 50 Hours Duration	71
7.	Mechanical Property versus Damage Correlations for Water Data at 100 Hours Duration	74

LIST OF FIGURES

Figure		Page
1.	Mercury Loop Schematic	4
2.	Mercury Loop Photograph	5
3.	Photograph of Water Content Measurement Apparatus	8
4.	Schematic of Gas Content Apparatus, Δ H Rig.	9
5.	Photograph of Stainless Steel Sample Capsule	10
6.	Modified Van Slyke Schematic	11
7.	Basic Venturi Dimensions	13
8.	1/2" Plexiglas Venturi, Pressure Tapped, in Mercury Loop	14
9.	1/8" Stainless Steel Venturi and Plexiglas, Pressure Tapped, in Mercury Loop	15
10.	1/2" Stainless Steel Venturi, Pressure Tapped, in Mercury Loop	16
11.	1/2" Plexiglas Damage Venturi, 120° 2-Specimen Orientation	17
12.	1/2" Stainless Steel Damage Venturi, 180° 2-Specimen Orientation	18
13.	1/2" Plexiglas Damage Venturi, 180° 2-Specimen Orientation	20
14.	Schematic of Pressure Tapped Specimen-Holder Combination	21
15.	Schematic of Electrode Specimen-Holder Combination	22
16.	Schematic of Transparent Photographic Specimen-Holder Combination	23

Figure		Page
17.	Schematic of Sonic Probe Apparatus	24
18.	Schematic of Water Loop	25
19.	Photograph of Water Loop	26
20.	Schematic of Regular Van Slyke Apparatus	28
21.	3/4" Plexiglas Venturi, Pressure Tapped, in Water Loop	29
22.	1/2" Plexiglas Venturi, Pressure Tapped, in Water Loop	30
23.	1/4" Plexiglas Venturi, Pressure Tapped, in Water Loop	31
24.	1/8" Plexiglas Venturi, Pressure Tapped, in Water Loop	32
25.	1/2" Plexiglas Damage Venturi, 120° 3-Specimen Orientation	33
26.	Schematic of Two-Dimensional Venturi	34
27.	Schematic of Test Specimen Geometry	35
28.	Cavitation Damage on 302 SS versus H_2O Content in Mercury	37
29.	Typical Proficorder Trace of Cavitation Damage on 304 SS in Mercury Facility	46
30.	Comparison of Jet Impact Craters to Cavitation Craters	48
31.	Comparison of Number of Bubbles, Number of Pits, and $p-p_v$ per unit Time versus Axial Distance Along Test Specimen Polished Surface in Mercury	50
32.	Pit Size Spectrum for Downstream Position on Specimen Surface for SS in H_2O and SS, CS, Cb-1Zr in Hg	53
33.	Pit Size Spectrum versus Distance Along Test Specimen Surface for Cb-1Zr in Mercury	55
34.	Ratio of Number of Bubbles Per Second to Number of Pits Per Second on SS and Cb-1Zr in Mercury	56
35.	Sequence of Bubble Collapse in Water from Two-Dimensional Venturi Tests	58

Figure Page

36. Sequence of Bubble Collapse in Water Near a Wedge From Two-Dimensional Venturi Tests 59

37. Directional Variation of Cavitation Damage Pits versus Venturi Test Velocity in Water 61

38. Typical Photomicrograph and Corresponding Proficorder Traces of Cavitation Damage Pits on SS in Water 76

39. Typical Photomicrograph and Corresponding Proficorder Traces of Cavitation Damage Pits on Copper-Nickel Alloy in Water 77

40. Typical Photomicrograph and Corresponding Proficorder Traces of Cavitation Damage Pits on Copper-Nickel Alloy in Water 78

41. Microhardness versus Axial Distance on Cavitated Copper at Several Durations of Test 81

42. Microhardness versus Axial Distance on Cavitated Brass at Several Durations of Test 82

43. Microhardness versus Axial Distance on Cavitated Copper-Nickel Alloy at Several Durations of Test 83

44. Microphotograph of Full Surface of Microhardness Test Specimen Showing Damage Distribution and Location of DPH Marks 84

45. Cavitation Damage on Copper-Zinc-Nickel Alloys versus Grain Size for Selected Ranges of Mechanical Properties 86

CHAPTER I

INTRODUCTION

For the past several years a continuing investigation of the causes and effects of cavitating flow regimes has been conducted in the authors' laboratories. During this investigation many concepts and observations have been made which shed considerable light on the damaging nature of cavitation. It is the primary purpose of this report to gather some of these and consolidate the results and conclusions thereof into a more comprehensible form. The areas considered in this report include: (i) the effects of material properties on cavitation damage resistance, (ii) the detailed pitting characteristics of cavitation flow regimes in both mercury and water on a variety of materials, (iii) comparison of pitting with that incurred with jet and droplet impact devices, (iv) comparison of bubble and pressure distribution with the pitting distribution, (v) a preliminary attempt to correlate the above with possible mechanisms of damage from bubble collapse, (vi) the effects of specimen grain size on damage resistance, and (vii) the effect of cavitation on the specimen surface hardness.

A previous report[2] gave the initial results of the damage versus mechanical properties correlations from the venturi tests to that time.

However, additional data at longer duration of exposure has been since obtained and is presented in this report.

CHAPTER II

EQUIPMENT AND EXPERIMENTAL PROCEDURES

The major portion of the equipment used during the course of the investigation has been described in many past reports.[1,2,etc.] However, a brief summary of the major components will be presented here for convenience. In addition to the equipment described herein, much supporting equipment has been supplied from other sources to complement the general overall capability of the laboratory. These include: the Department of Nuclear Engineering for such items as oscilloscopes, scope cameras, barometers, scintillation detection equipment, etc.; the National Science Foundation under Grant No. G22529, which supplied the equipment for the parallel investigation of cavitation damage in an ultrasonic facility; the Michigan Memorial-Phoenix Project for use of the Ford Nuclear Reactor for sample irradiations and examination facilities. The description of the major components utilized follows.

A. Mercury System

The mercury loop is shown schematically in Figure 1, and Figure 2 is a photograph of the facility with the top half of the heater section removed for clearer visualization. The facility is capable of operating over a temperature range from about 50 to 500°F and with sump

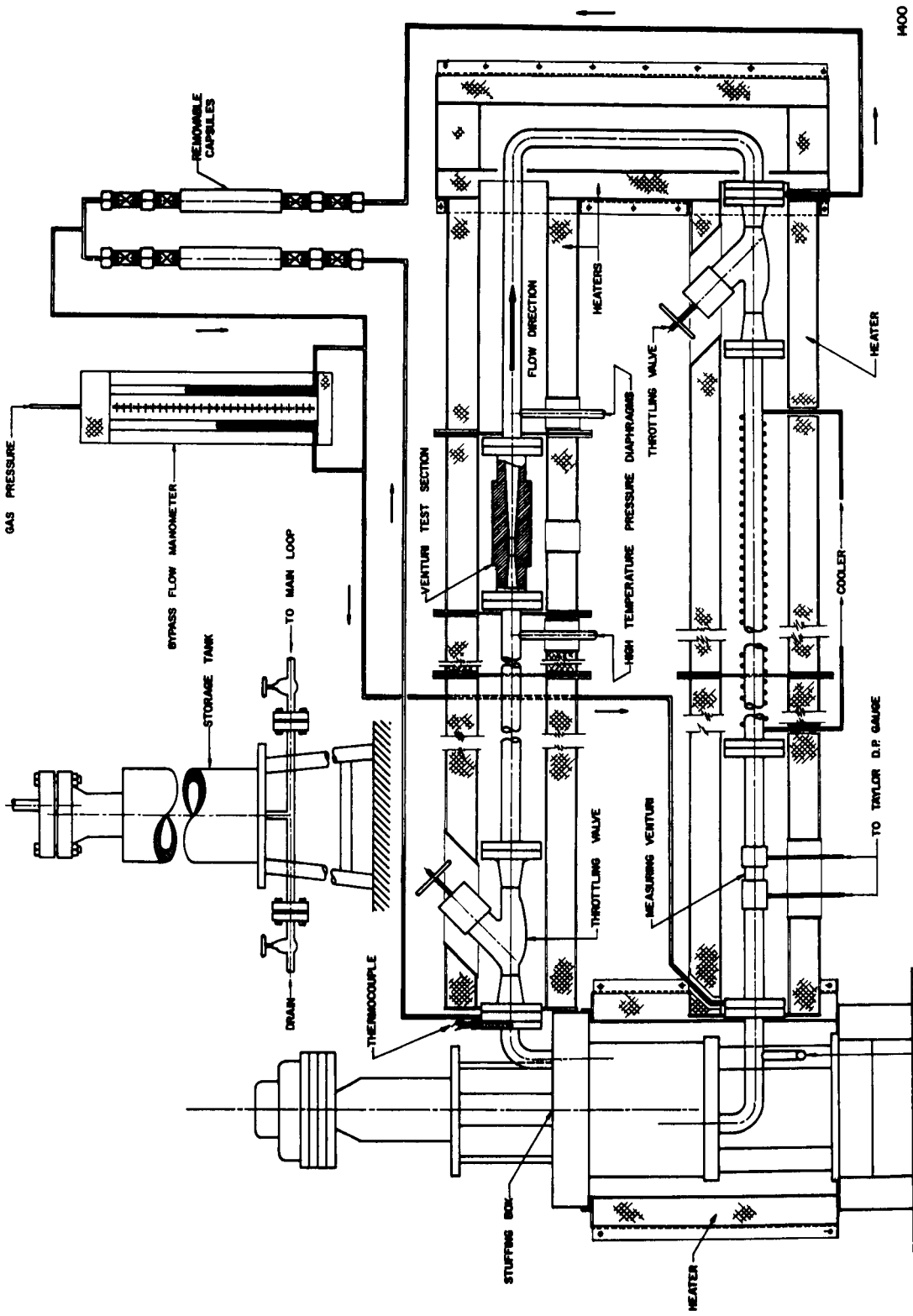

Fig. 1.--Schematic of mercury loop and sample bypass lines.

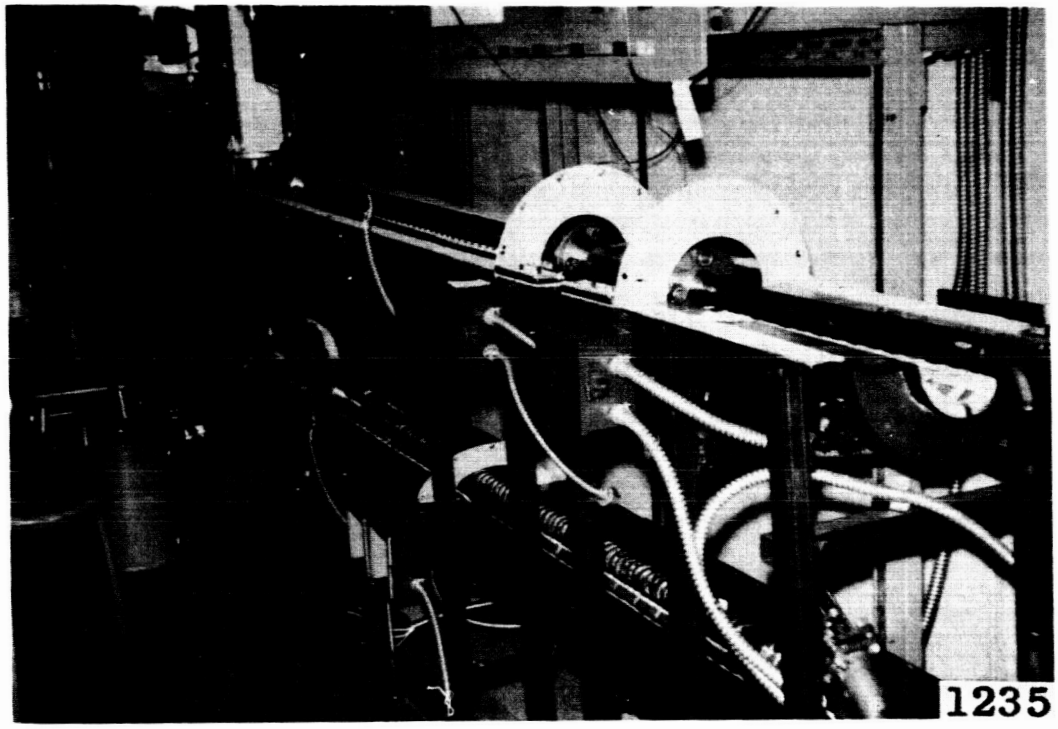

Fig. 2.--Photograph of mercury facility with top half of heater sections removed.

pressurization from about atmospheric to 100 psig. With a one-half inch throat diameter venturi installed, this provides a throat velocity range, with cavitation occurring in the venturi, from about 20 to 50 feet per second. Plexiglas venturis have been used for most of the low temperatures and stainless steel venturis for the high temperature as well as some of the low temperature tests. Relatively few tests have been conducted in the high temperature range in the venturi facilities.

Supporting equipment that has been utilized in conjunction with this facility and that has been developed expressly for this purpose consists of: water in mercury content measurement apparatus, gas in mercury content measurement apparatus, special venturis for pressure profile and test specimen pressure measurements, sonic probe apparatus for cavitation detection in opaque systems, electrode probe apparatus for cavitation extent measurements in opaque systems, and gamma-ray densitometry equipment.

In the early series of tests in this system, water was used as a pressurizing fluid in the sump region of the pump, floating on the mercury, in order to obtain higher flow rates by virtue of the additional sump pressure. This eliminated cavitation in the pump impeller and increased pump discharge pressure, thus obtaining higher velocities in the venturi test section. A liquid rather than gas was required for this purpose, since the sump region is sealed by a stuffing box which would not operate satisfactorily in a dry condition which exists when gas is the sealing fluid. The mercury-water interface was maintained at a level of 5 inches above the impeller inlet, which was thought

sufficient to prevent water entrainment. However, it was later discovered that somehow traces of water were being carried over into the flowing mercury system from this region. When this was discovered, an apparatus was developed to measure the quantity of water in the mercury in order to evaluate its effect on the damage capabilities. Figure 3 is a photograph of the apparatus that was developed for this determination. This is capable of measuring the content between about 15 ppm and 3000 ppm, with an accuracy of about $\pm$ 10 ppm, by weight of a relatively volatile component such as water in a fluid of relatively low volatility such as mercury.

Another variable affecting the amount of damage inflicted in a given cavitation flow regime is the entrained gas content of the fluid.[3] Also, the amount of gas in a fluid affects the flow performance of the cavitating venturi itself.[4] Hence, an apparatus for determining the amount of gas existing in the mercury was developed, partially for a parallel investigation for Atomics International.[5] This is shown schematically in Figure 4. It measures the amount of mercury displaced into a calibrated capillary tube for the sample capsule filled from the loop, when the capsule is vented through a U-tube from the sampling pressure of about 100 psi to atmospheric pressure. It is capable of measuring gas contents from about 0.0 to 4.0 per cent by volume with an accuracy of about $\pm$ 0.1 per cent. Figure 5 is a photograph of the stainless steel sample capsules which were used, and Figure 6 is a schematic of a modified Van Slyke apparatus used to obtain a measurement of the total mass of gas in the sample (as opposed to the volume measurement obtained

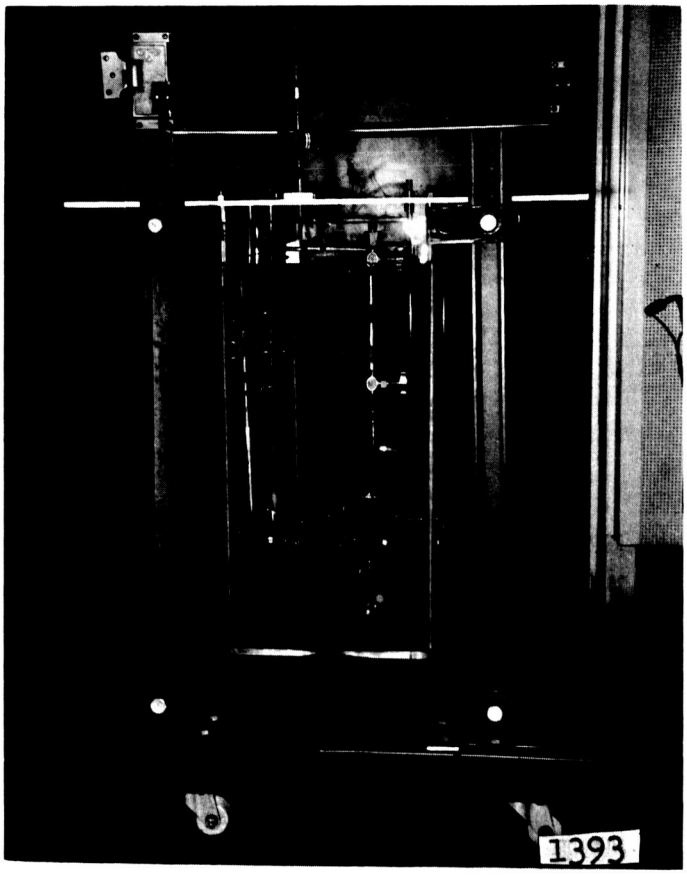

Fig. 3.--Photograph of water content measurement apparatus.

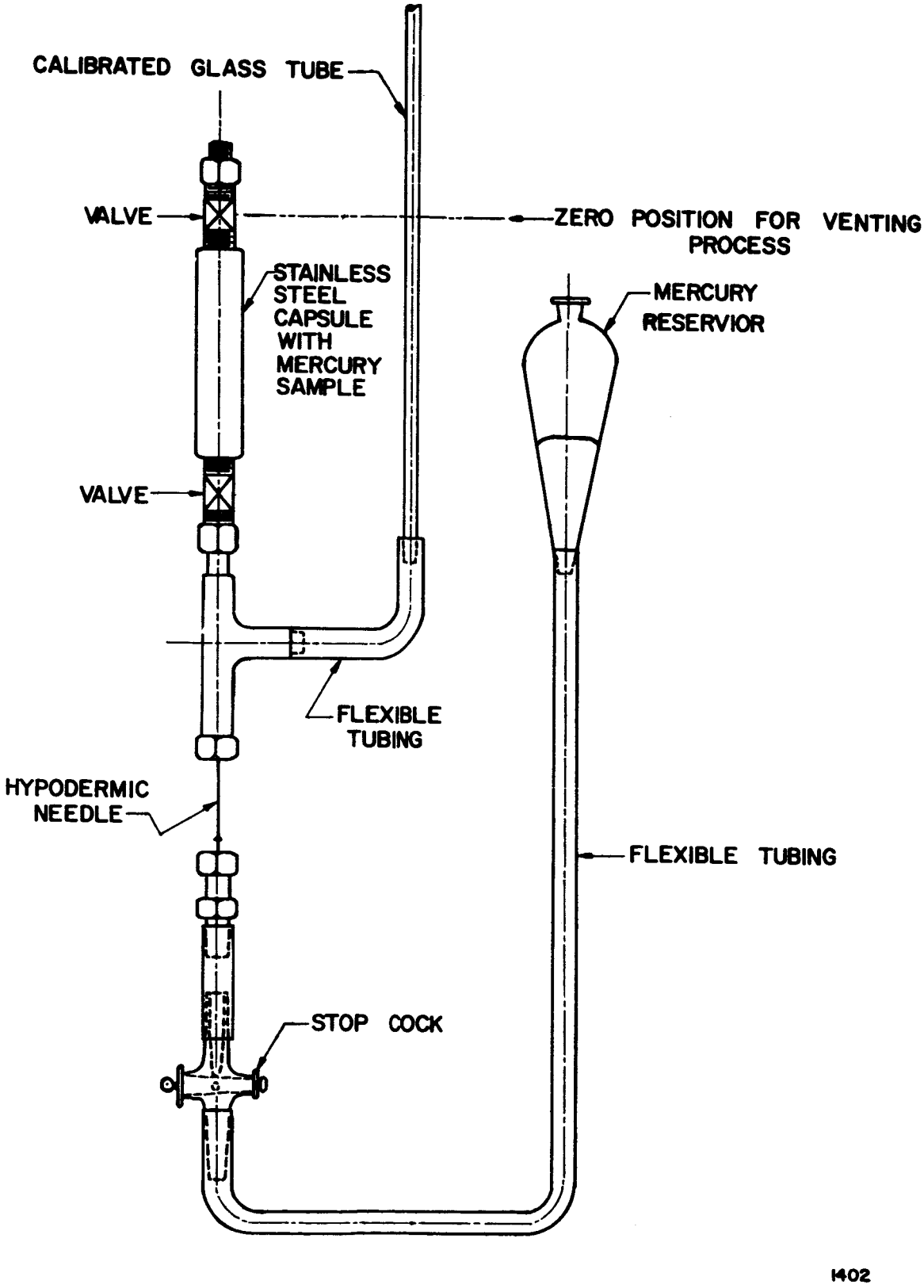

Fig. 4.--Capsule venting and Δ H apparatus.

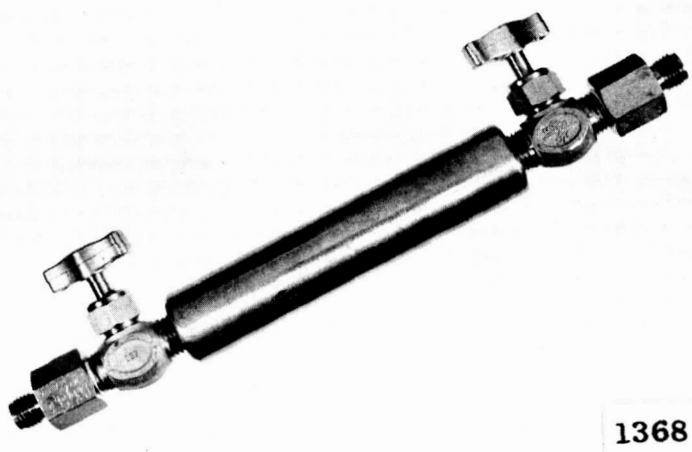

Fig. 5.--Photograph of stainless steel sampling capsule.

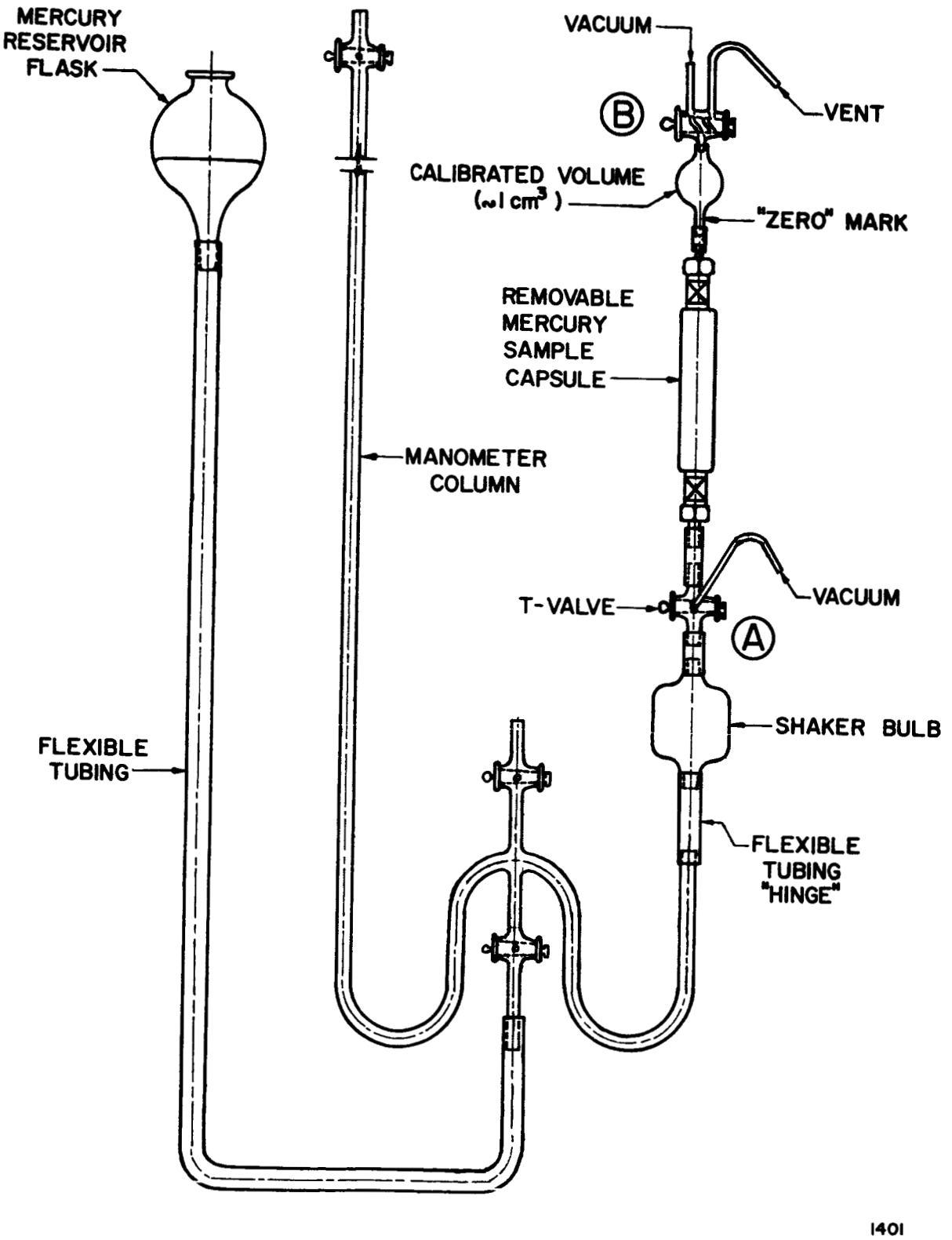

Fig. 6.--Schematic of modified Van Slyke.

from the previously described procedure). Along with a measurement of total sample weight, the volume per cent of gas in the mercury can be computed also from the Van Slyke measurement. The above two independent methods of gas content measurement compared very closely, and the displacement method described first was used for the bulk of the tests, since it was quicker to perform. A combination of the results of both measurements also allowed a computation of mean bubble size.

Several venturis have been fabricated and used over the past few years in this loop for determining the cavitation initiation number with mercury. Figure 7 is a schematic showing the basic geometry of the venturis utilized both in the mercury and water loop (to be described), and Figures 8 through 10 are drawings of the 1/2" plexiglas, 1/8" plexiglas and stainless steel, and 1/2" stainless steel venturis that were used for the cavitation number measurements. This work, consisting of scale effects studies, is currently being carried out as a thesis dissertation in the Nuclear Engineering Department.[6] In addition, several venturis have been fabricated and used in the cavitation damage portion of the investigation. These have been designed with the same basic dimensions as those previously mentioned, Figure 7, although only the 1/2" throat diameter size has been used in this case. It was also desired to observe the effects of specimen orientation in the venturis, as there is some evidence that this substantially affects the cavitation regime.[2] Figure 11 is a drawing of the 1/2" plexiglas venturi as used for the low temperature damage tests in mercury, and Figure 12 is the same for the 1/2" stainless steel venturi. In addition, a forerunner of the

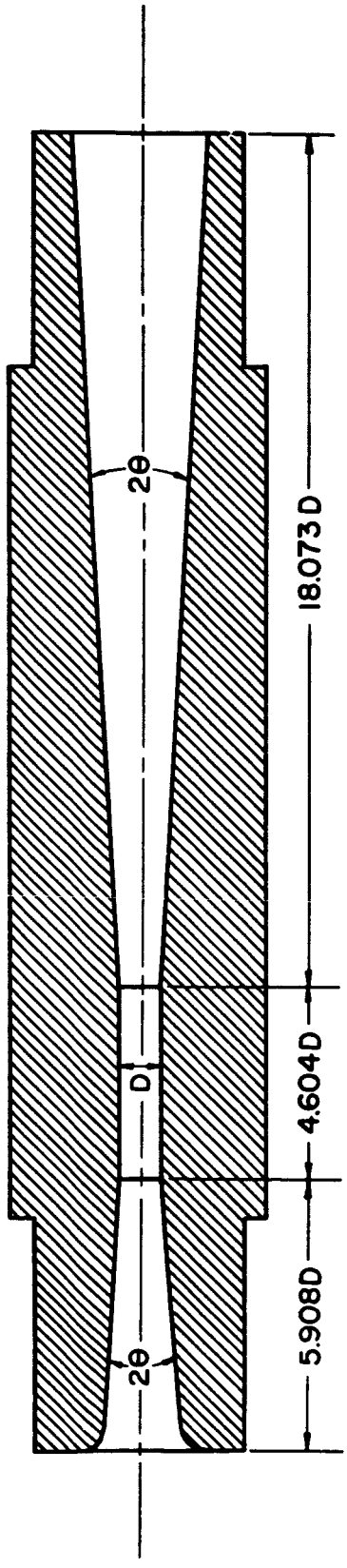

Fig. 7.--Basic venturi flow path dimensions.

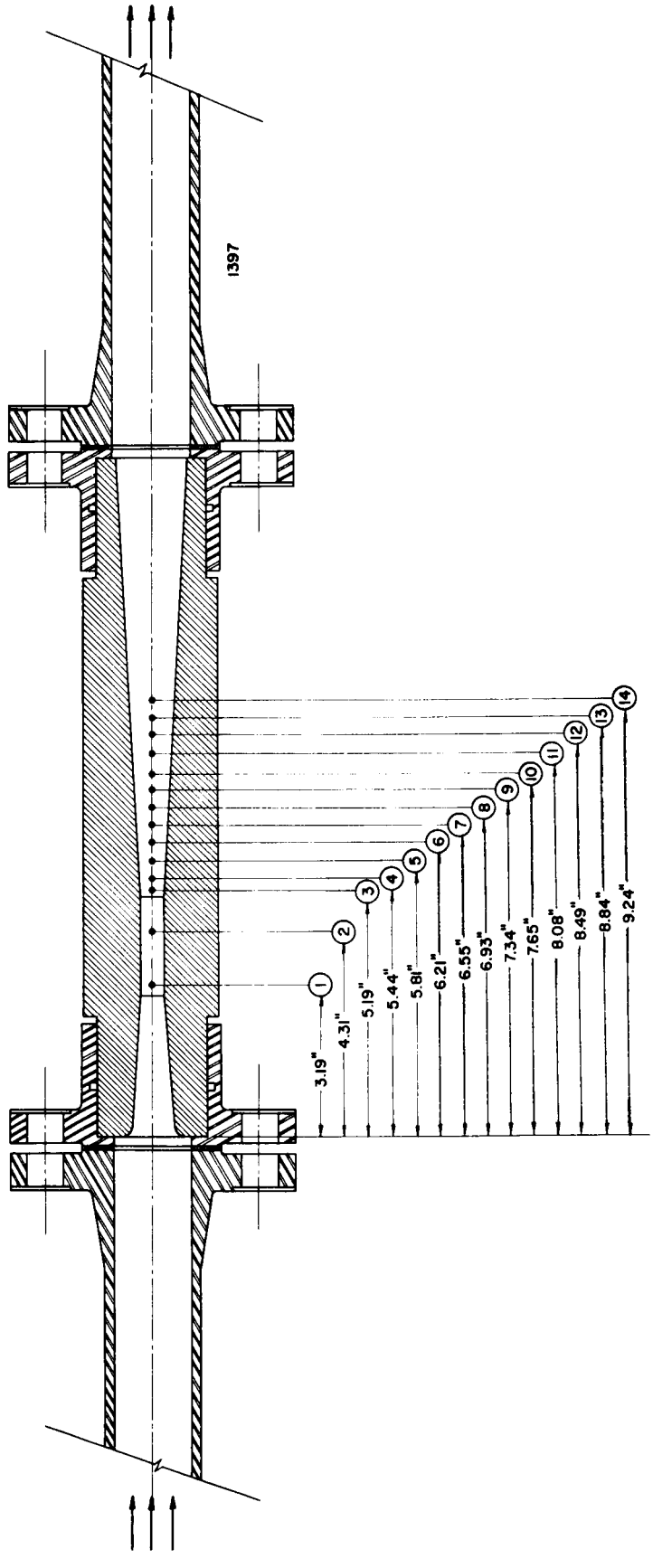

Fig. 8.--Pressure tap locations and mercury loop installation geometry for 1/2" plexiglas venturi.

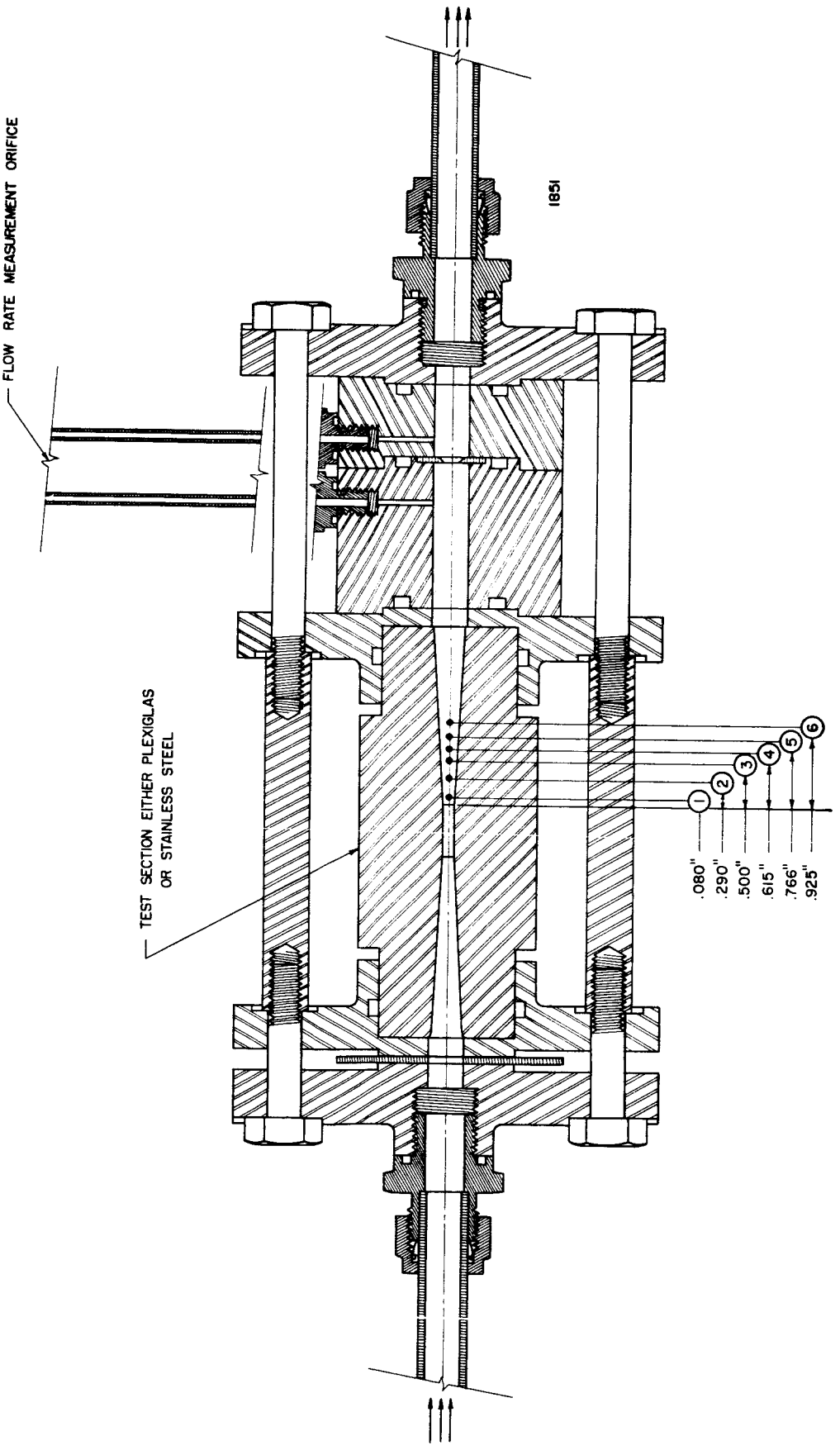

Fig. 9.--Pressure tap locations and mercury loop installation geometry for 1/8" plexiglas and stainless steel venturis.

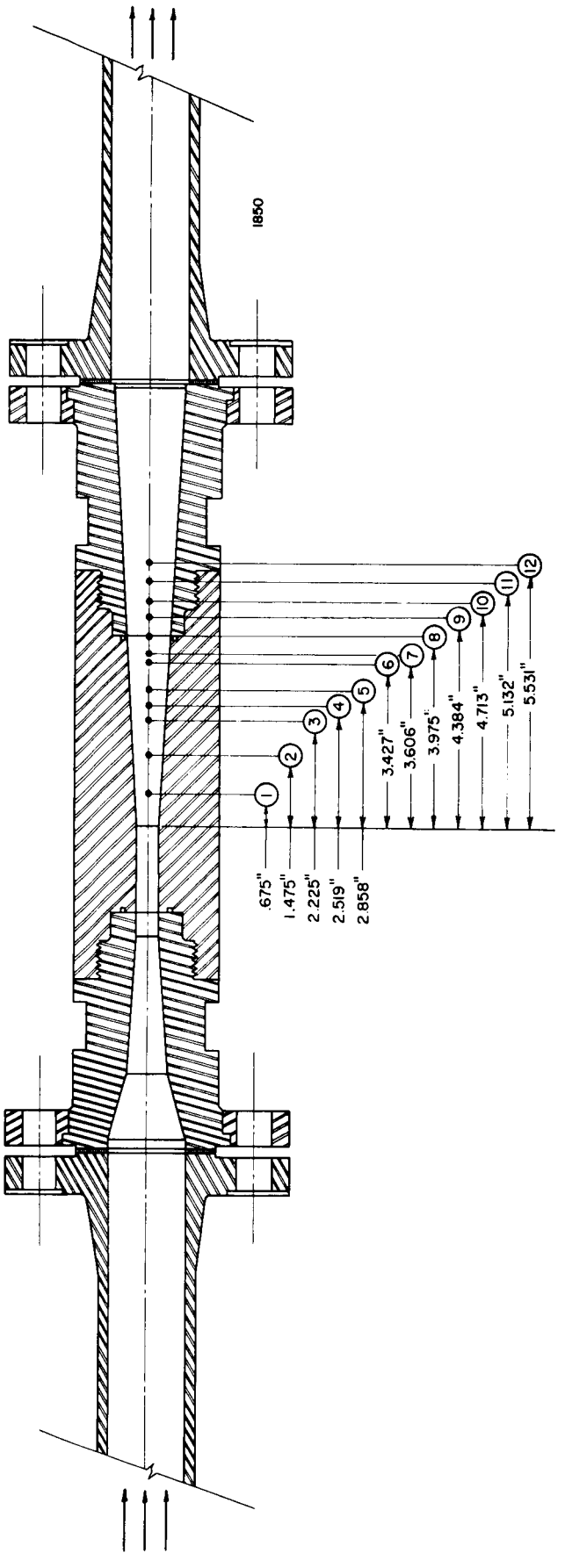

Fig. 10.--Pressure tap locations and mercury loop installation geometry for 1/2" stainless steel venturi.

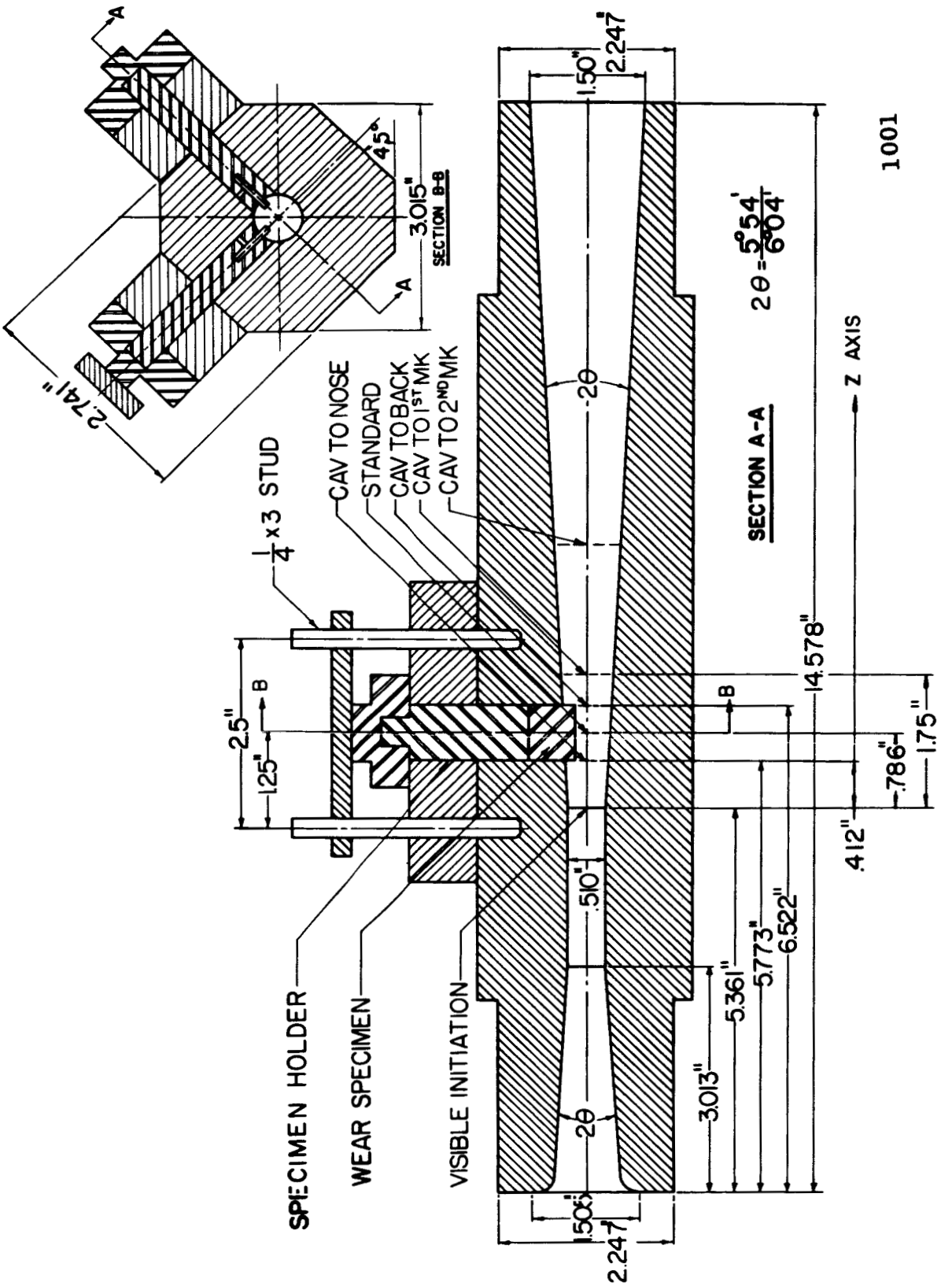

Fig. 11.--1/2" plexiglas damage venturi, 120° 2-specimen orientation, as installed in mercury facility.

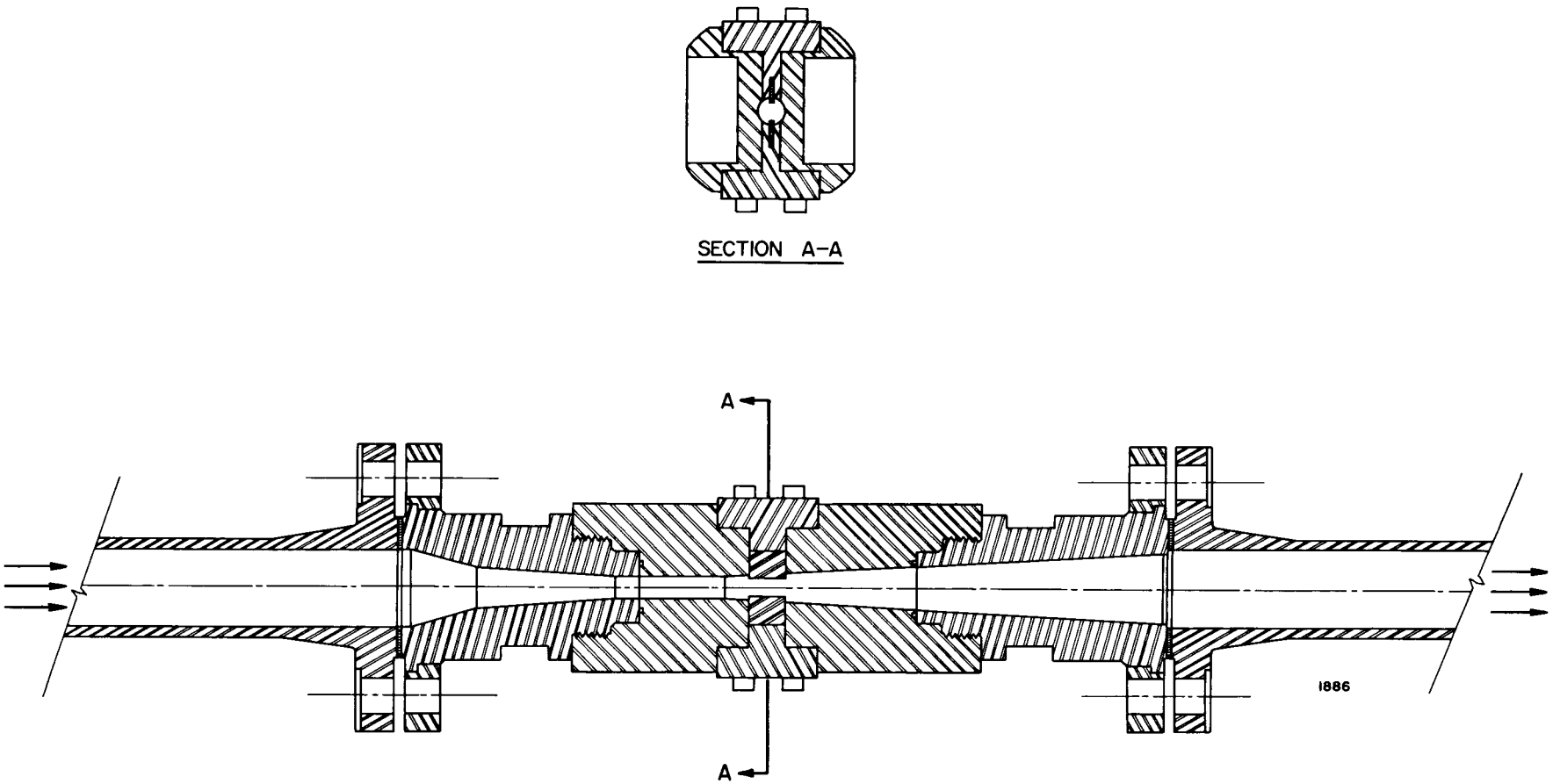

Fig. 12.--1/2" stainless steel damage venturi, 180° 2-specimen orientation, as installed in mercury facility.

stainless steel venturi was constructed of plexiglas with the opposing (180°) orientation of specimen insertion in order that an investigation of prestressed materials (i.e., materials held under an externally imposed stress during the cavitation test) could be made. This venturi is shown in Figure 13.

The apparatus shown in Figure 14 was used for measuring the pressures on the polished surface of the test specimens in conjunction with the overall venturi pressure profile measurements. Also the electrode specimen combination and the specimen-holder combination shown in Figures 15 and 16 were used for measuring the mercury to surface contact time and location, and for the high speed photographic studies, respectively. The sonic probe apparatus, shown schematically in Figure 17, was developed to determine the onset of cavitation in the opaque stainless steel venturis.

B. Water System

The water loop is shown schematically in Figure 18, and Figure 19 is a photograph of this facility. The facility is capable of operating over a temperature range from about 50 to 180°F, the upper limit being dictated by the upper temperature limit of the plexiglas venturis that are used (about 300°F with stainless steel venturis), and a velocity range from about 60 to 200 feet per second, when three loops with 1/2" throat diameter venturis are operated. The system has a bypass filtering and dearation loop by which the water impurity and gas content can be varied. This system is capable of providing water impurity

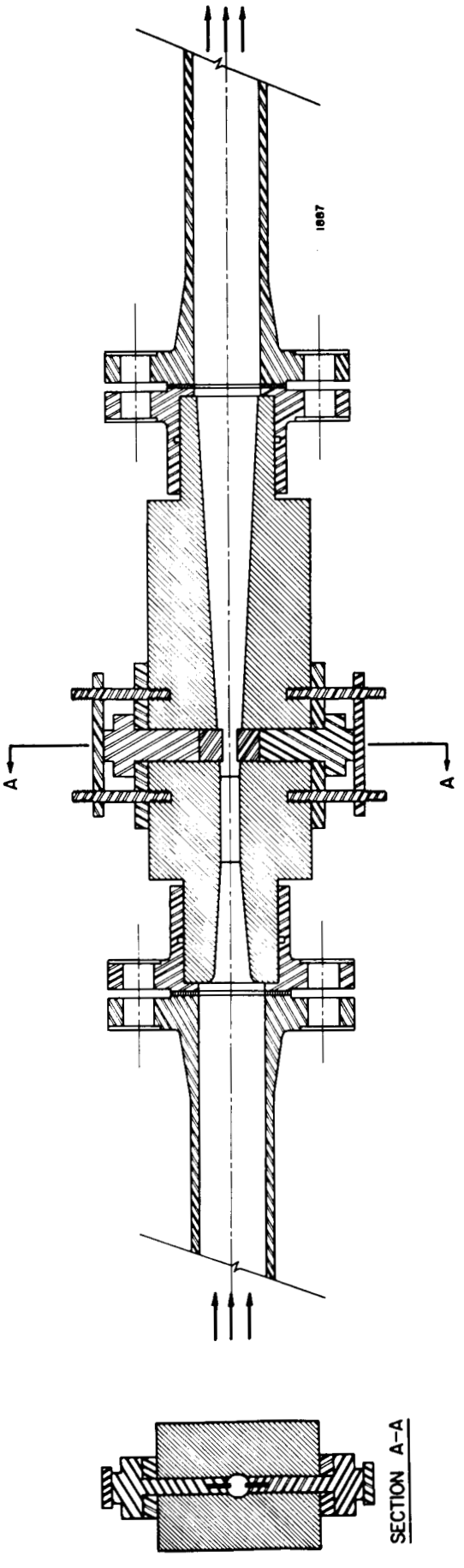

Fig. 13.--1/2" plexiglas damage venturi, 180° 2-specimen orientation, as installed in mercury facility.

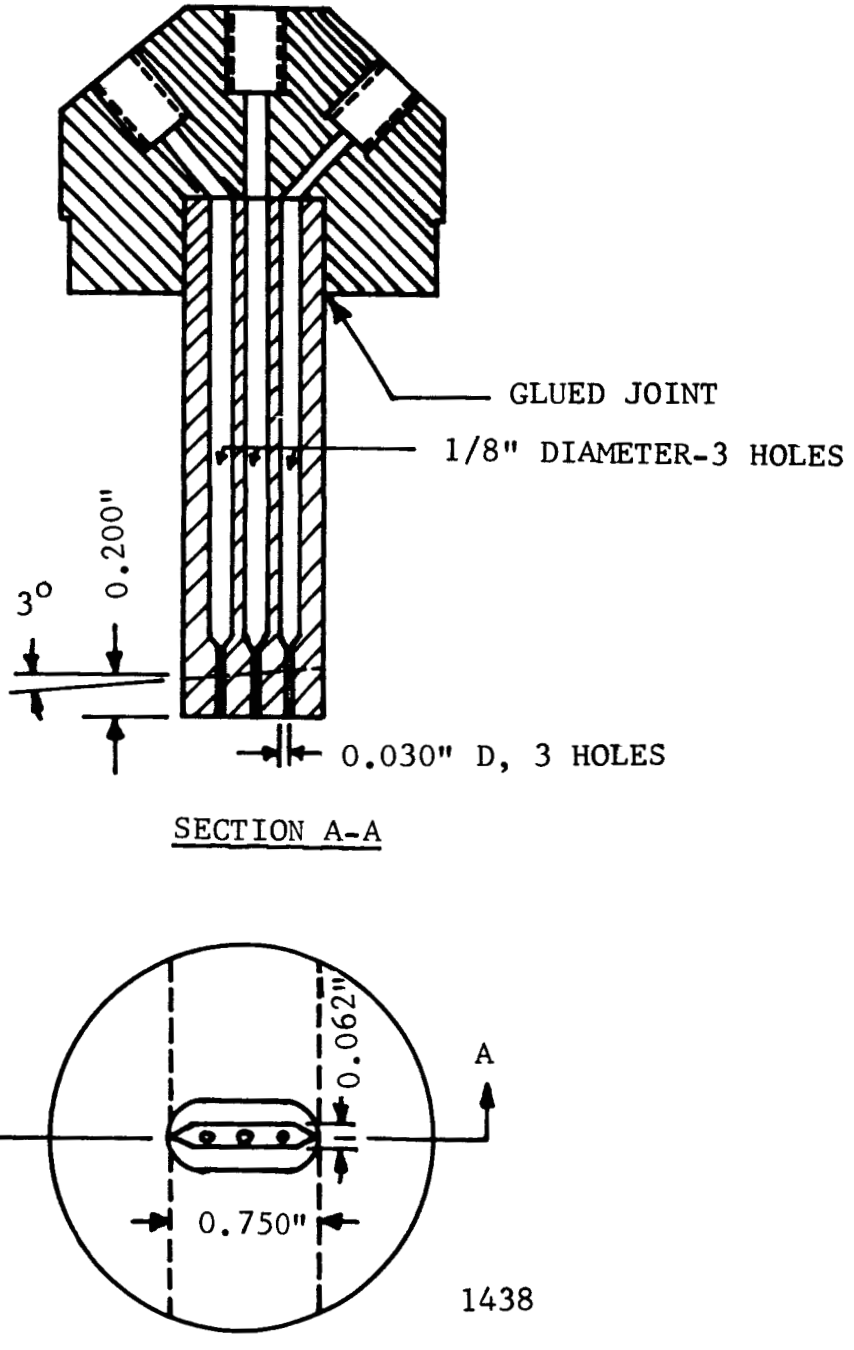

Fig. 14.--Schematic drawing of plexiglas specimen-holder combination for measuring pressures on specimen face.

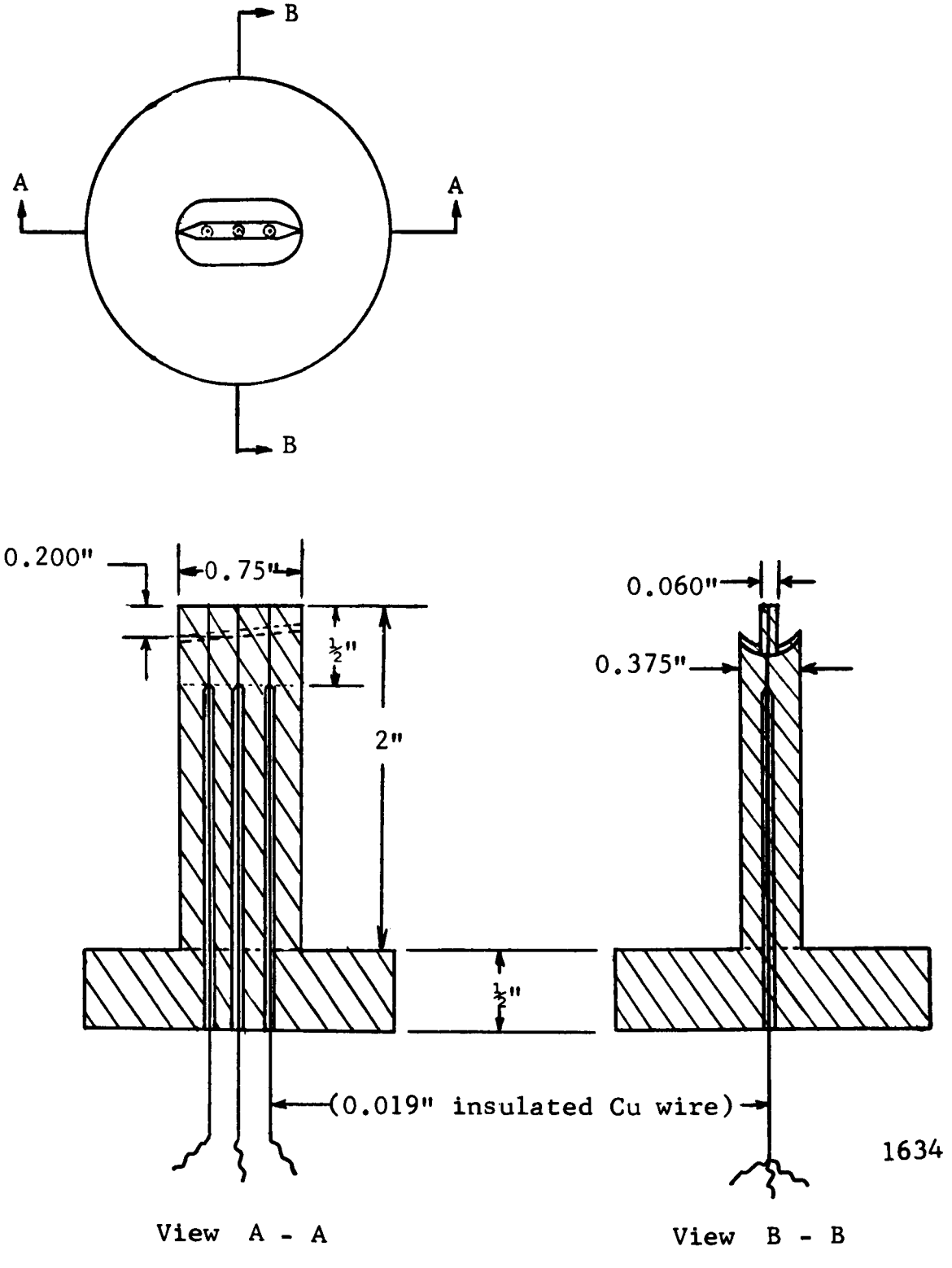

Fig. 15.--Schematic drawing of plexiglas electrode specimen-holder assembly for contact measurements.

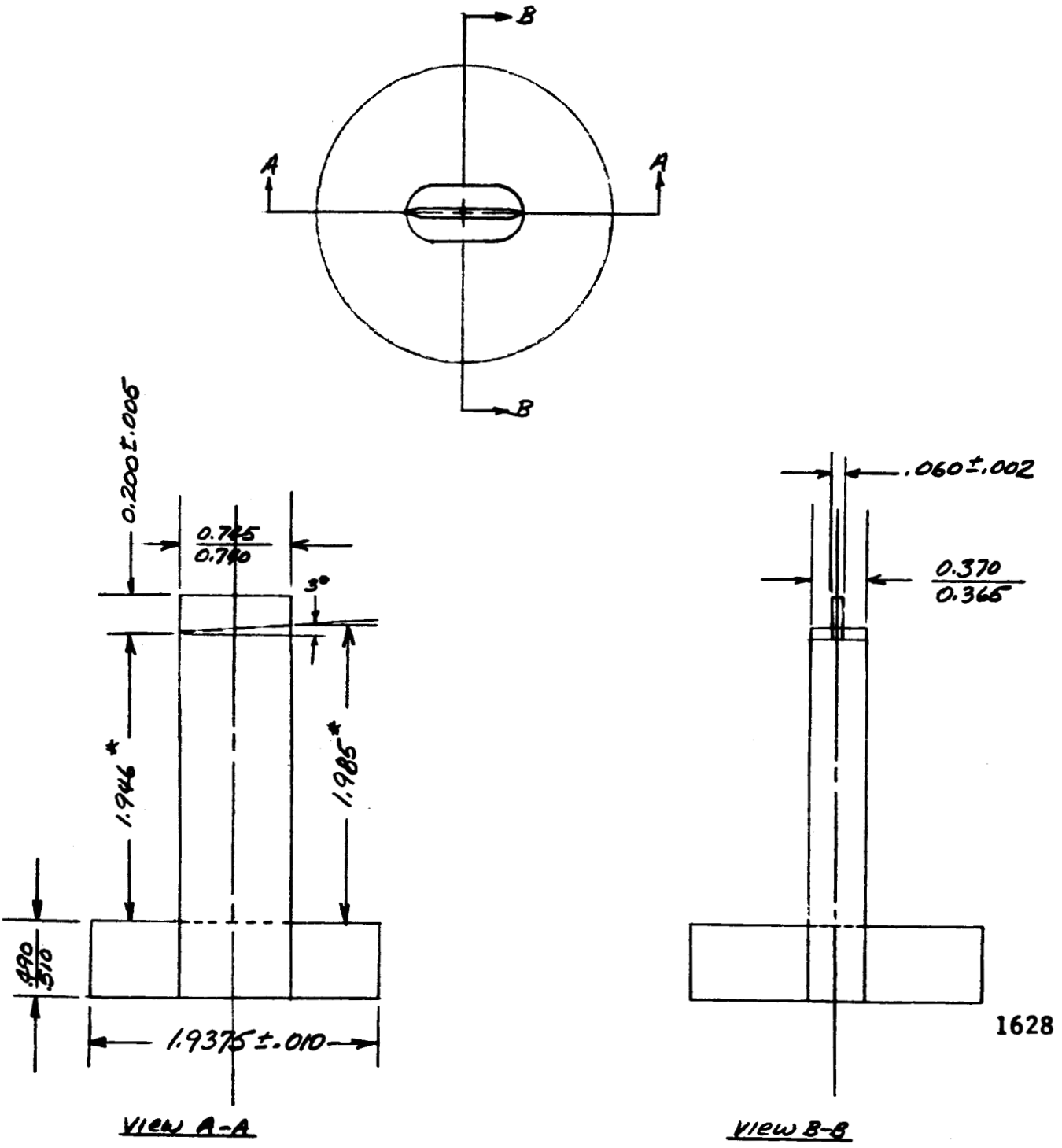

Fig. 16.--Schematic drawing of transparent specimen-holder combination for high-speed photography.

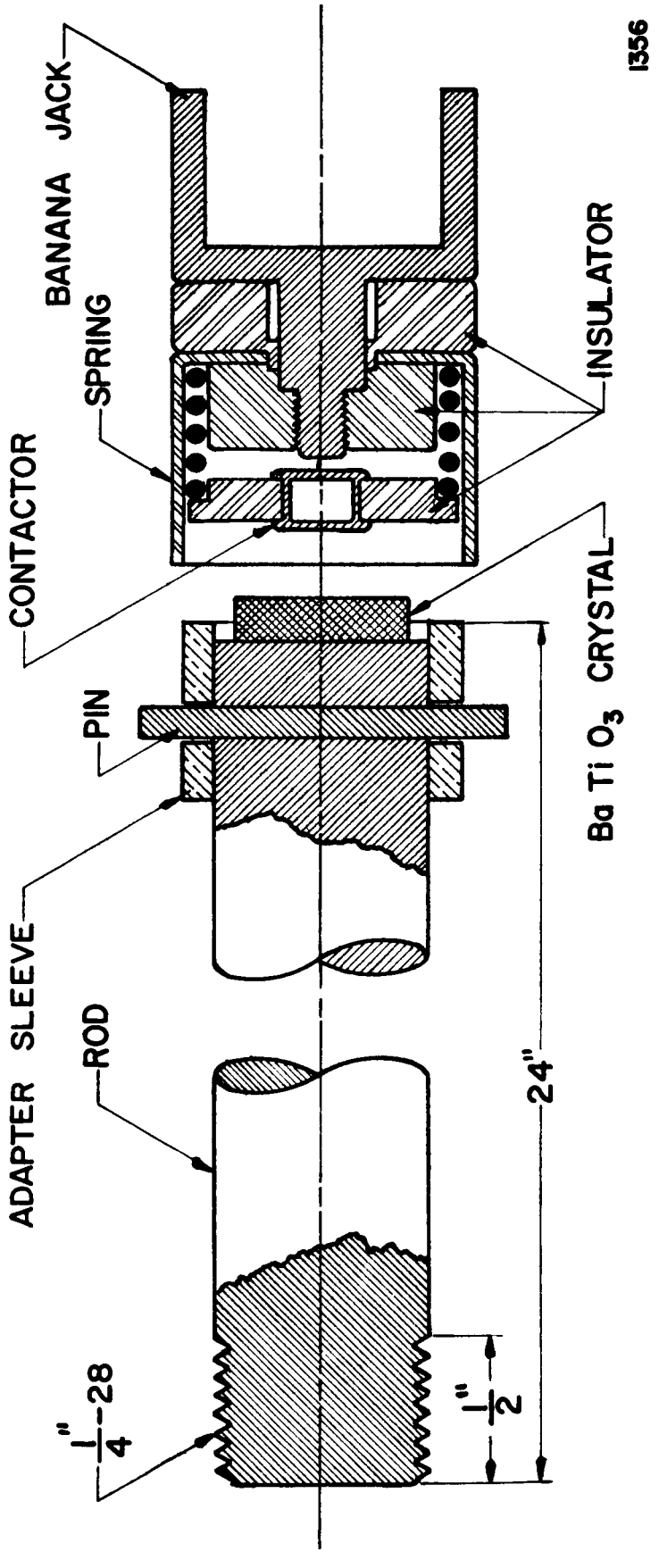

Fig. 17.--Schematic of sonic probe apparatus.

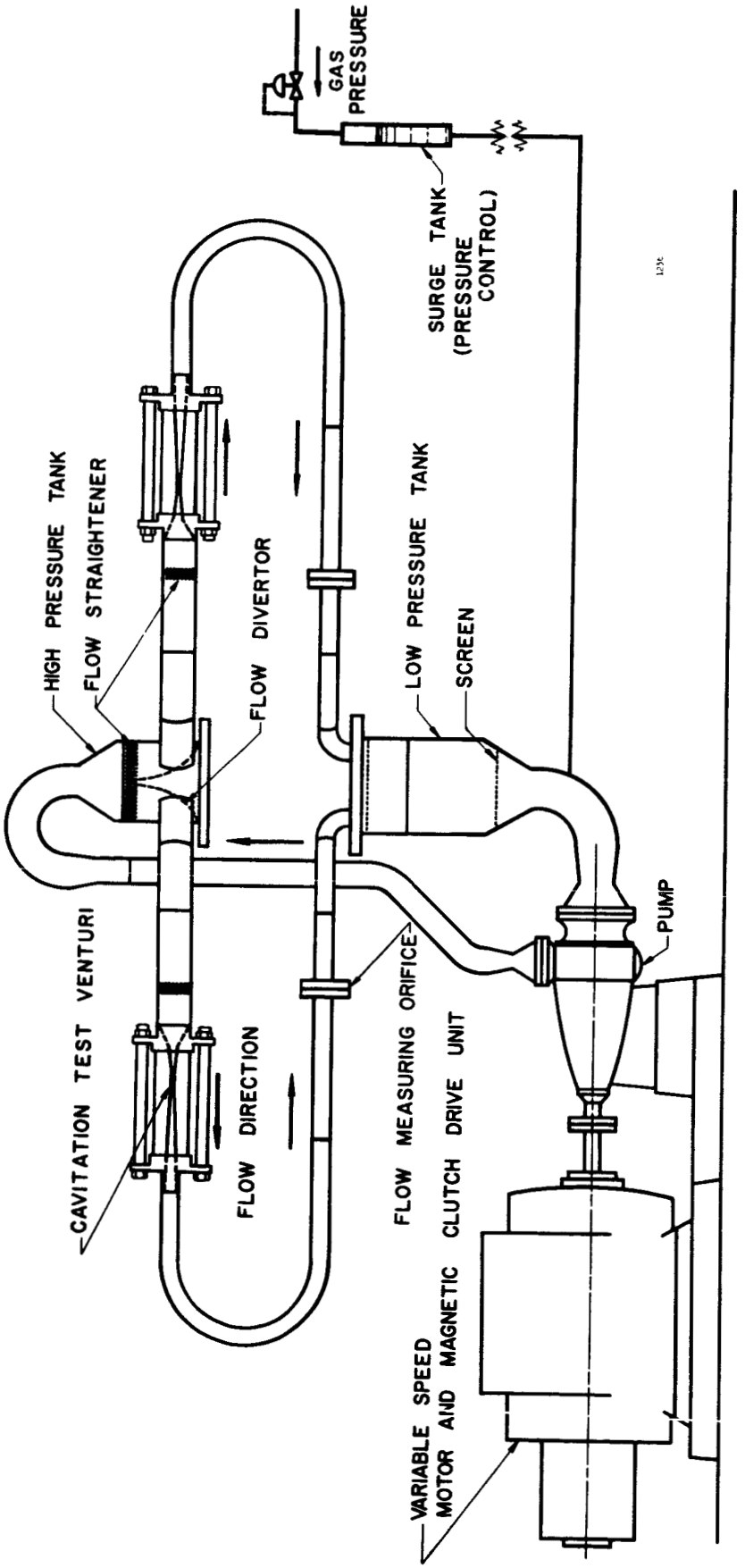

Fig. 18.--Schematic of water cavitation damage facility (only two of the four loops are shown).

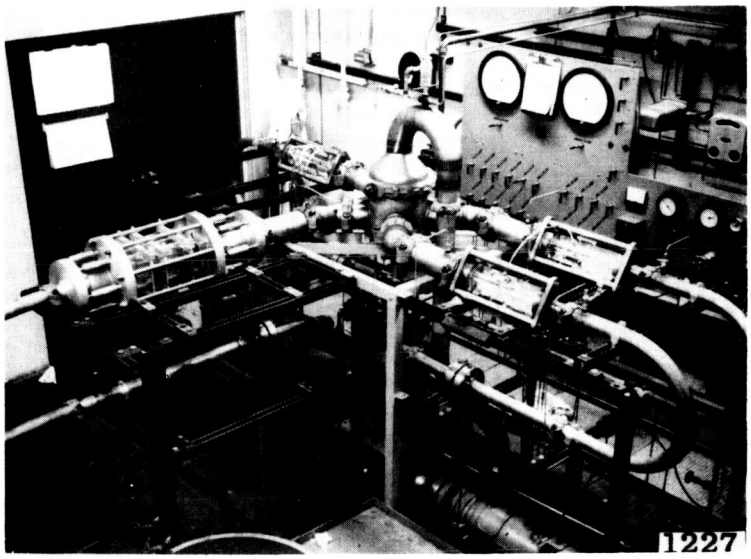

Fig. 19.--Photograph of water cavitation damage, closed loop, venturi facility.

contents from about 10 to 200 ppm solids and dissolved gas contents from about 0.5 to 2.5 per cent by volume. The upper limits here are the values of standard tap water. To the present, the damage studies have used ordinary tap water only, while the scale effects studies[6] have utilized the variable gas content capability.

The gas content of the loop water has been determined by a standard Van Slyke apparatus (Figure 20), and the solids impurity content with a RDE4 Solubridge and a VSO216 Dip Cell.

The venturis utilized in the scale effects studies have all been constructed of plexiglas, with throat diameters of 3/4", 1/2", 1/4" and 1/8". These are shown schematically in Figures 21 through 24. All of the damage tests have been conducted in 1/2" plexiglas venturis as shown in Figure 25. In addition, a two-dimensional venturi was constructed for photographic studies in the water system (Figure 26). The pressure tapped specimen-holder combination and photographic transparent specimen-holder combination shown earlier were also used in the water system.

C. Experimental Procedures

The damage test specimens of all materials (Figure 27) were generally subjected to the following pretest, intermediate, and post-test examinations; weighing, microphotographing of polished surface, pit count of polished surface, and in some cases a post-test examination by proficorder and/or microsection. The samples are stored in a dehumidified storage cabinet between all operations to minimize corrosion and oxidation. The weight loss and pit count data is then analyzed with the aid of a computer program described in Appendix A.

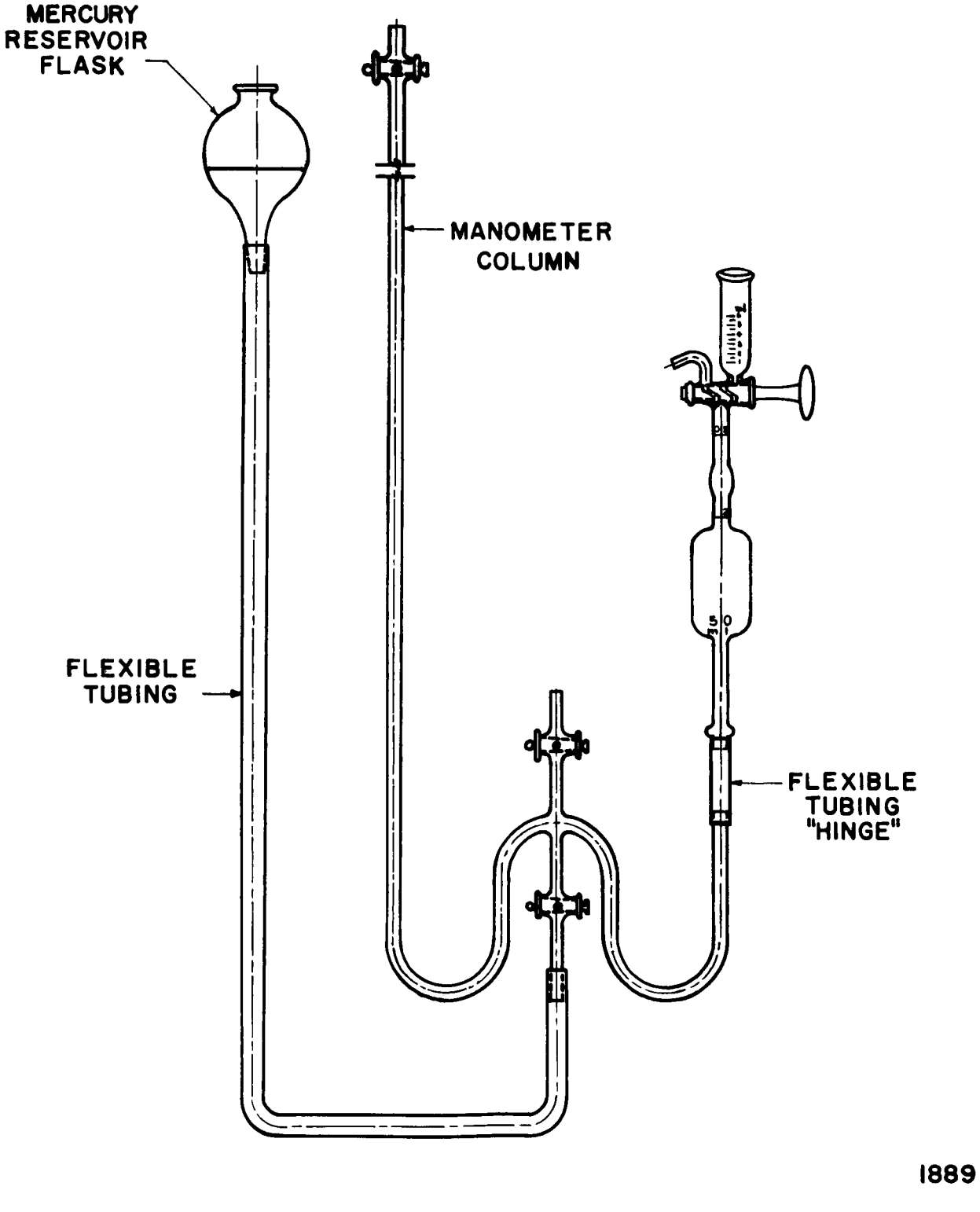

Fig. 20.--Schematic of regular Van Slyke apparatus.

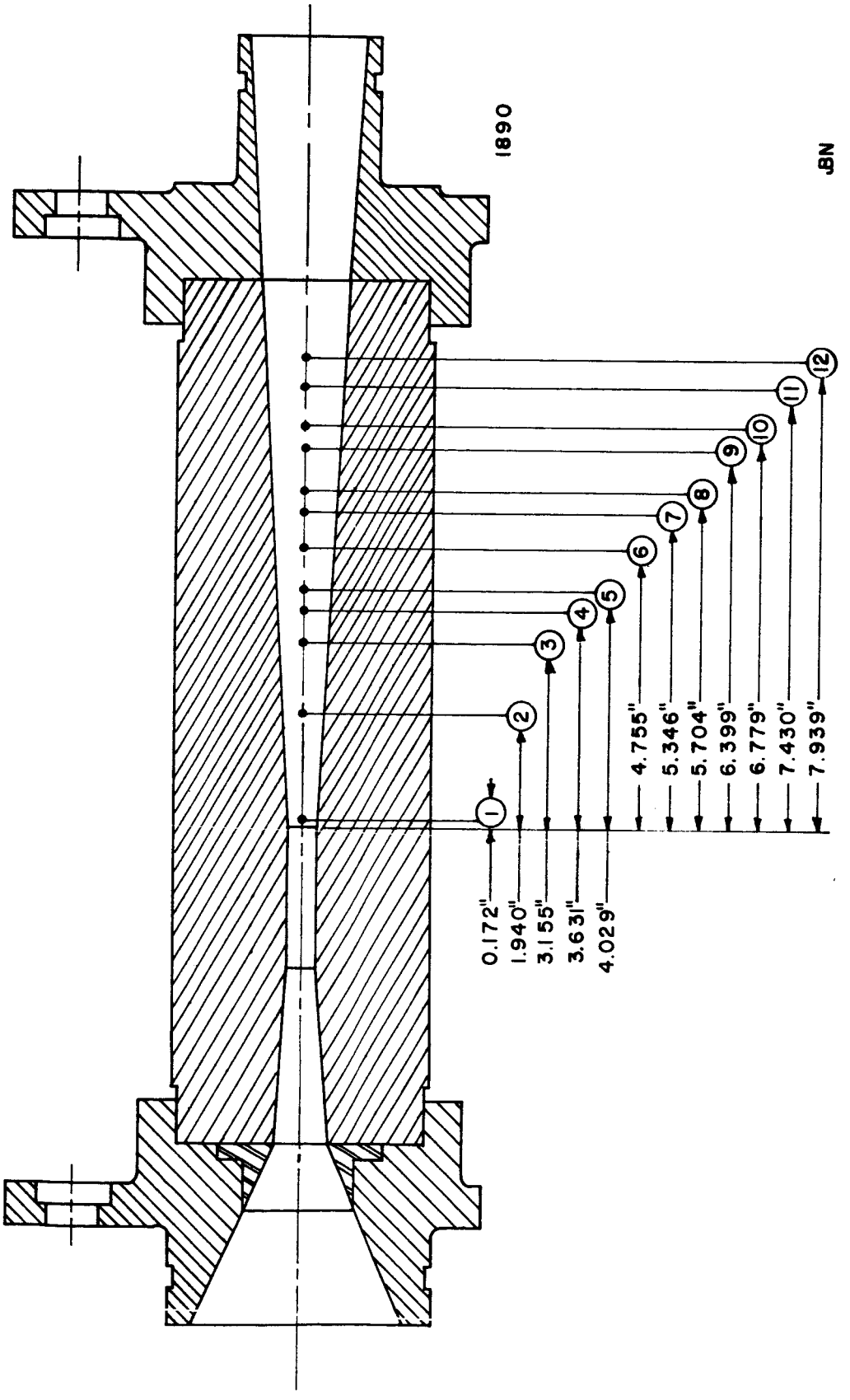

Fig. 21.--Pressure tap locations and water loop installation geometry for 3/4" plexiglas venturi.

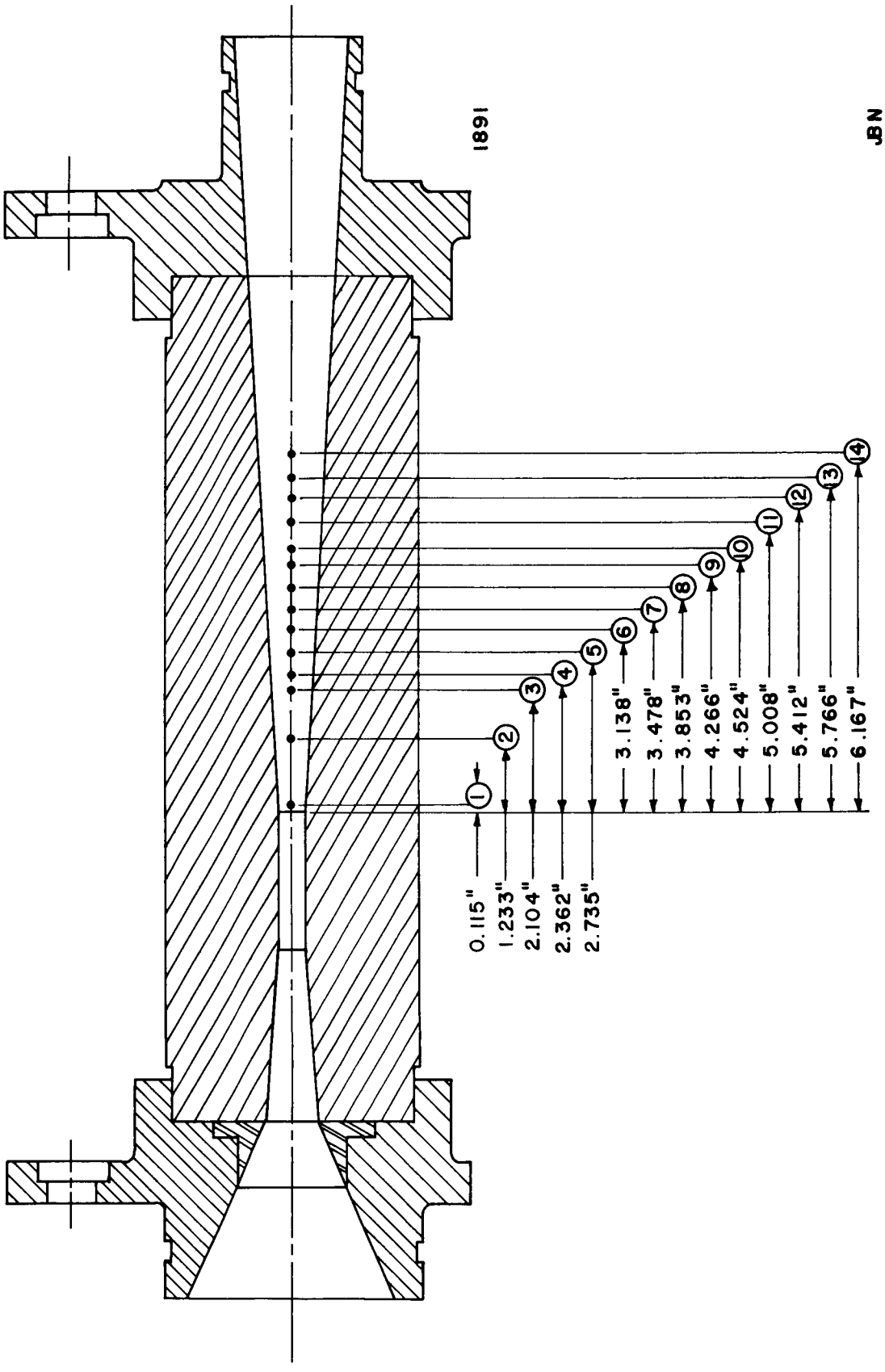

Fig. 22.--Pressure tap locations and water loop installation geometry for 1/2" plexiglas venturi.

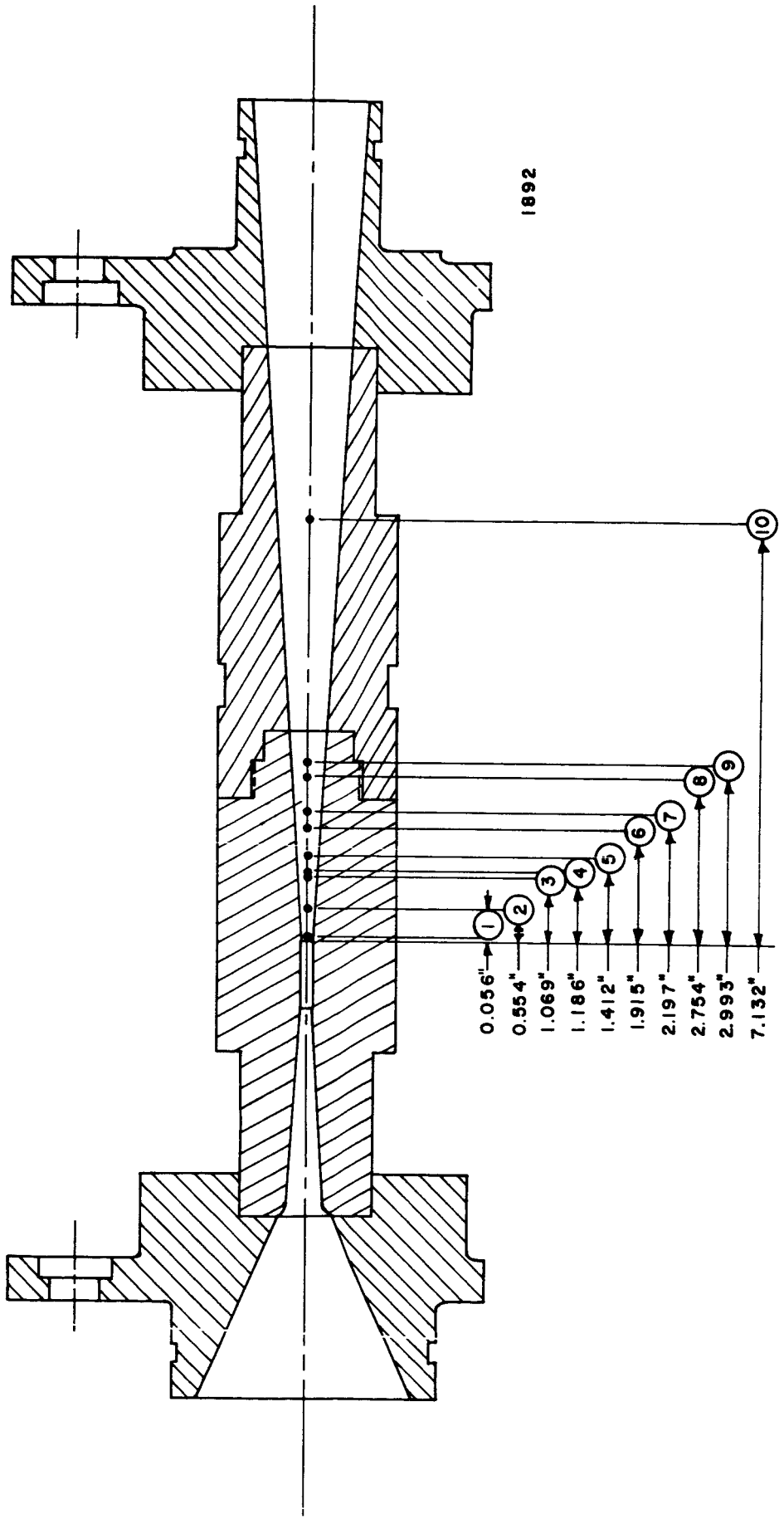

Fig. 23.--Pressure tap locations and water loop installation geometry for 1/4" plexiglas venturi.

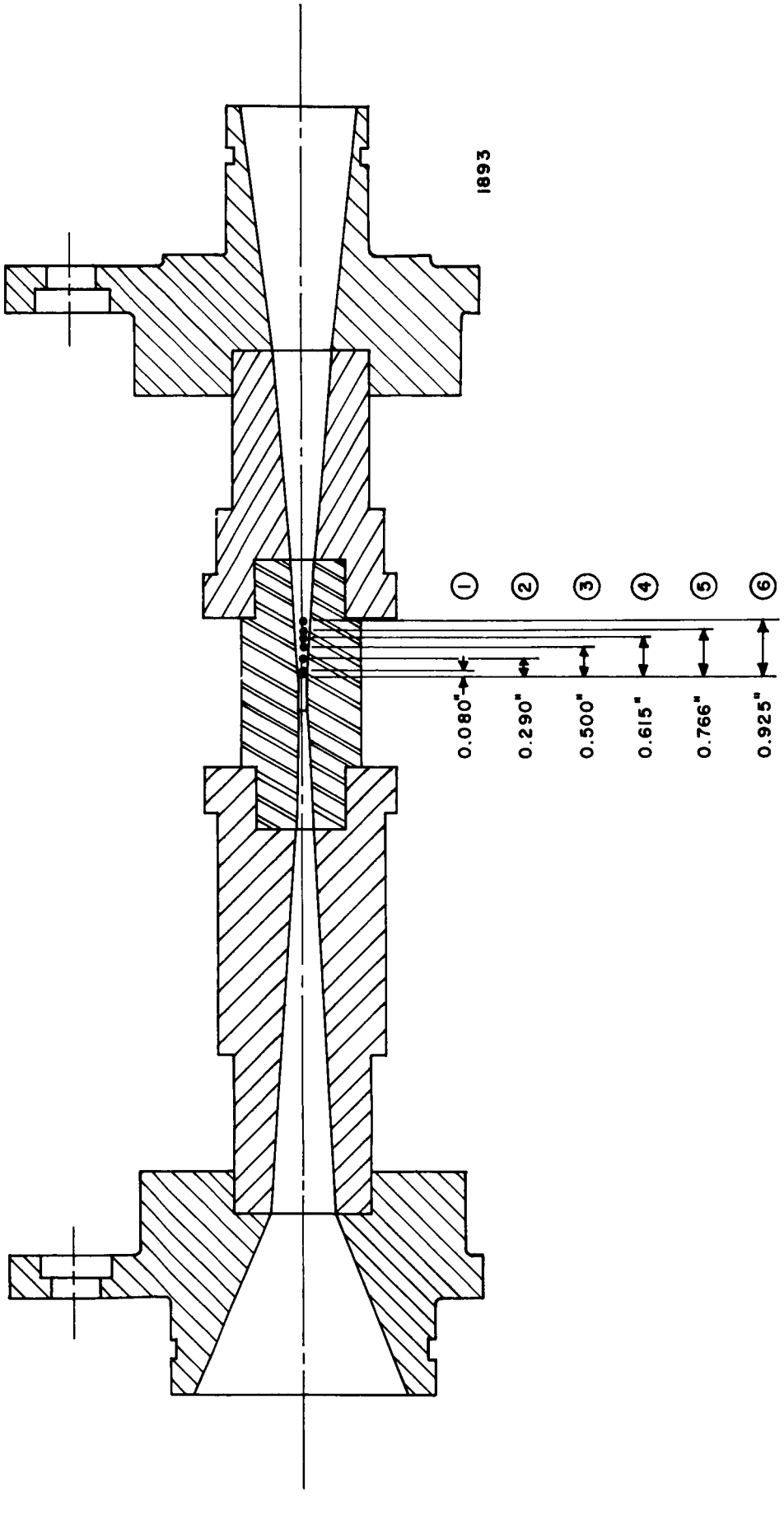

Fig. 24.--Pressure tap locations and water loop installation geometry for 1/8" plexiglas venturi.

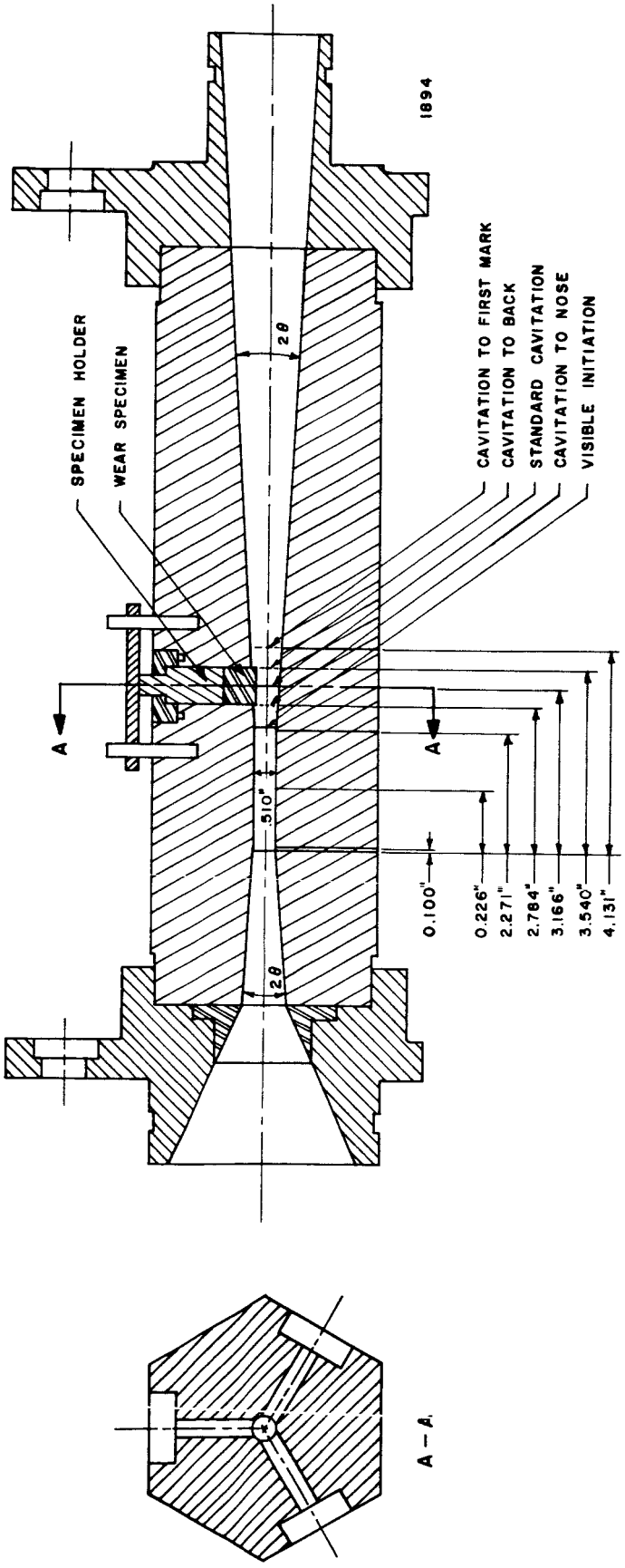

Fig. 25.--1/2" plexiglas damage venturi, 120° 3-specimen orientation, as installed in water facility.

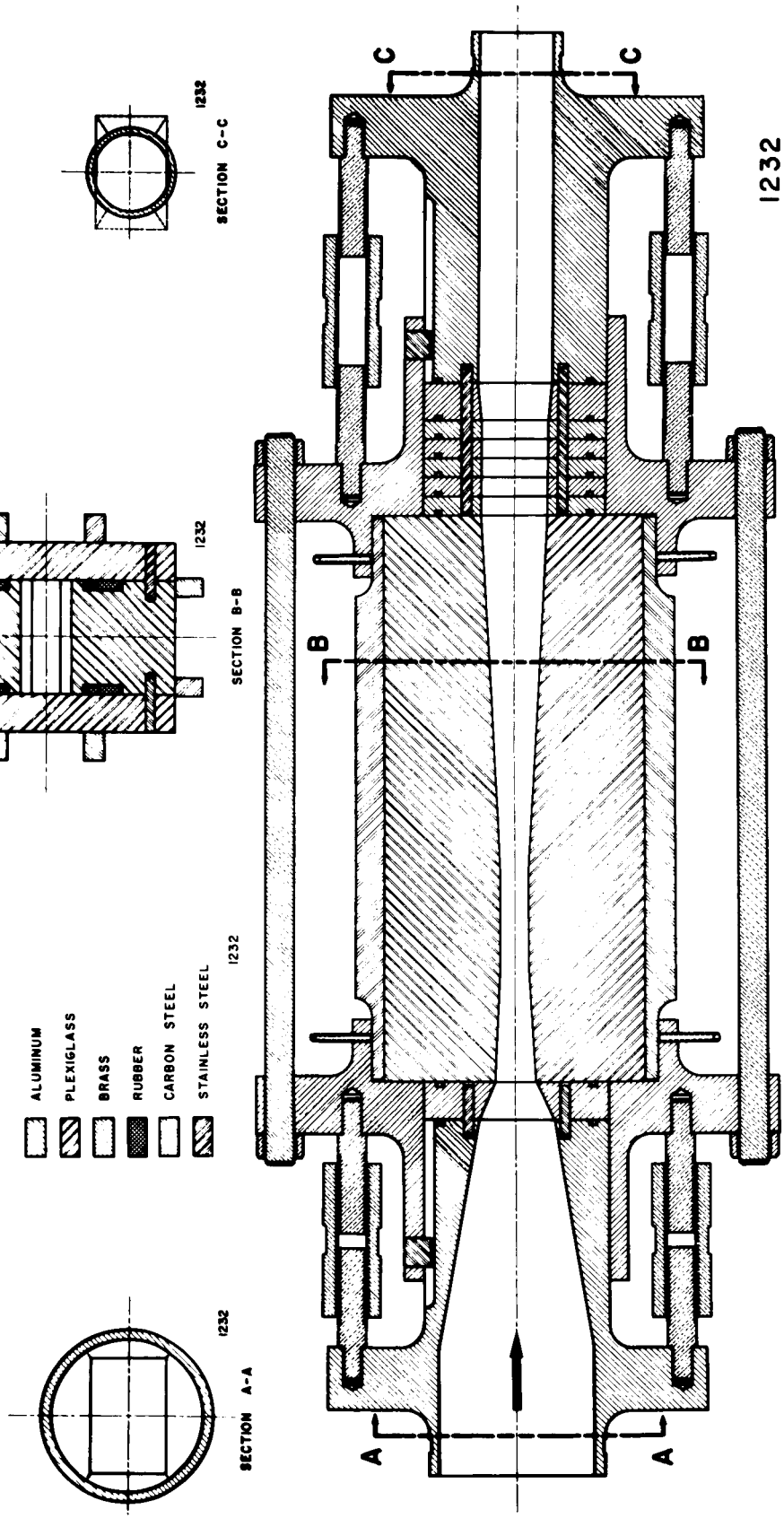

Fig. 26.--Schematic of two-dimensional venturi.

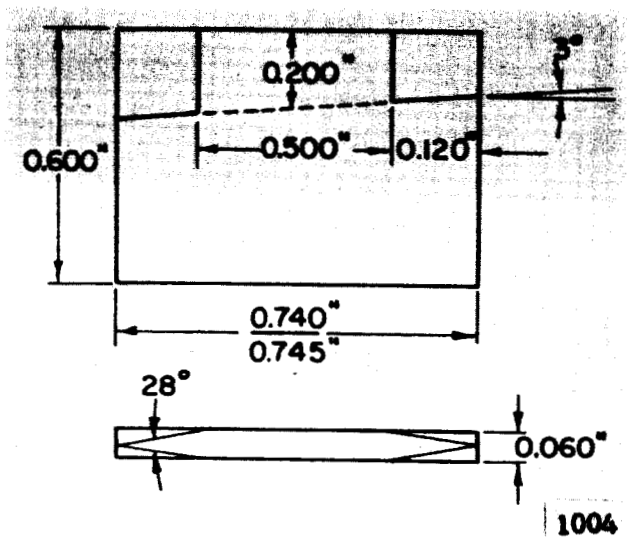

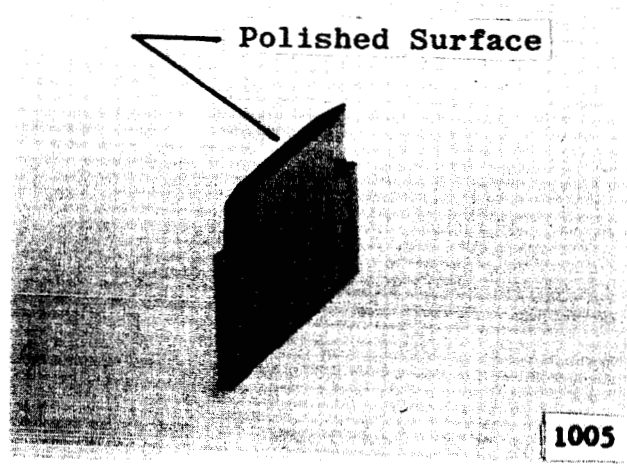

Fig. 27.--Schematic drawing and photograph of damage specimen.

CHAPTER III

MERCURY SYSTEM RESULTS

A. Water Content

In the following discussion of damage results in the mercury system, reference will be made to "wet" and "dry" mercury data. The "wet" mercury damage data was gathered during the period before it was discovered that trace amounts of water were present in the mercury. It was subsequently determined that the amount of water in the mercury for these tests was the order of 500 ppm by weight. However, it was not possible at this time to determine the precise water content for each test. Hence, a preliminary determination of the effect of water content on cavitation damage to stainless steel was made (Figure 28). As shown, a damage maximum occurred for a water content of about 1500 ppm by weight.

The existence of such a maximum seems reasonable if one assumes that the effect of small quantities of entrained water (relatively volatile compared to mercury) is similar either to entrained gas[3] or to an enhanced vapor pressure in the mercury. Its effect is then two-fold;

a) Increased bubble nucleation and growth in a fixed flow regime is afforded,

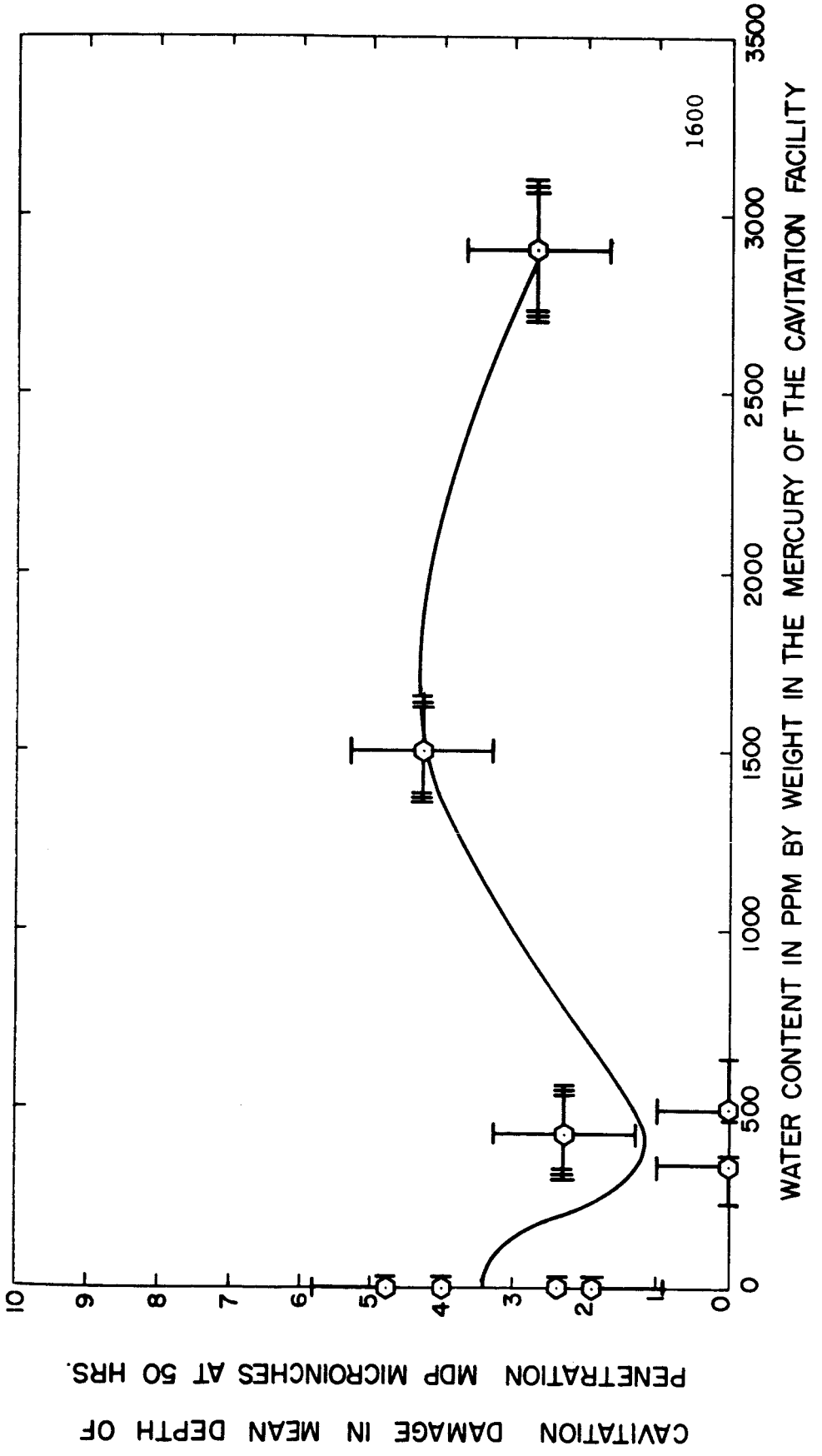

Fig. 28.--Mean Depth of Penetration vs. H_2O content (in ppm) in mercury.

b) A cushioning effect upon bubble collapse is present.

The first mechanism would tend to increase damage while the second would diminish it. However, their relative importance, while unknown at this point, is probably a function of quantity of water. Hence, the existence of a maximum is not surprising. The situation may be analogous to that encountered in vibratory cavitation damage tests in water exposed to atmospheric pressure. Here the damage maximizes when the vapor pressure reaches a value of $\sim 1/15$ of an atmosphere, but diminishes for either higher or lower vapor pressures.

B. Damage Tabulations

All the mercury damage data so far obtained is listed in Table 1 for "wet" mercury, and in Table 2 for "dry" mercury. Specimen material, venturi throat velocity, cavitation condition (extent of cavitation region, see Appendix C), mean depth of penetration (total weight loss times material density divided by surface area exposed to the fluid), observed at selected time intervals, and the number of samples for which the damage data has been averaged are listed. Some of the "wet" data was obtained in a venturi with 120° specimen orientation (Figure 11), while all of the "dry" data is for a venturi with 180° specimen orientation (Figure 12). Hence, these data are not directly comparable.

C. Damage Correlations

As part of the overall effort in understanding and attempting to predict cavitation damage, and of trying to unearth those characteristics of cavitation damage which may be predictable, an attempt has been

TABLE 1

"WET" MERCURY CAVITATION DAMAGE DATA

Material	Velocity (ft/sec)	Cav.Cond.* (Degree)	Mean Depth of Penetration, in. 25 Hrs	50 Hrs	75 Hrs	100 Hrs	No.of Samples
302 SS	24.0	Standard	51.6	58.1	65.5	77.1	2
302 SS	34.0	Zero	--	--	--	--	2
302 SS	34.0	Visible	1.8	1.4	4.2	3.3	4
302 SS	34.0	Nose	3.5	4.5	5.1	5.4	4
1008 CS	34.0	Nose	48.6	94.4	237.6	291.7	2
Cb-1Zr	34.0	Nose	8.7	54.9	--	--	2
302 SS	34.0	Standard	17.1	45.6	86.0	114.8	10
302 SS	34.0	Standard	--	2.0	--	--	14
302 SS	34.0	Standard	--	0.8	--	--	4
1008 CS	34.0	Standard	129.2	107.1	173.8	202.8	4
Cb-1Zr (C-Wkd)	34.0	Standard	90.3	289.6	529.0	637.0	2
Cb-1Zr (Annld)	34.0	Standard	46.7	111.2	219.9	220.7	2
Ta-10W(A)	34.0	Standard	14.2	30.0	41.3	79.6	2
Ta-8W-2Hf(B)	34.0	Standard	13.3	29.0	39.8	66.1	2
Tenelon(F)	34.0	Standard	--	--	--	--	2
Plex(P)	34.0	Standard	2233.5	--	--	--	3
Nickel (As Recd)	34.0	Standard	--	--	--	--	2
302 SS	34.0	Back	7.3	31.0	49.7	94.6	4
302 SS	34.0	1st Mark	--	--	--	--	2
1008 CS	48.0	Nose	290.0	524.7	--	--	1
Cb-1Zr	48.0	Nose	6.3	15.6	17.2	21.0	2
Cb-1Zr	48.0	Standard	31.6	199.3	--	--	2
302 SS	64.0	Zero	--	--	--	--	2
302 SS	64.0	Visible	3.0	3.1	--	--	2
302 SS	64.0	Nose	9.0	15.7	17.2	23.1	2
302 SS	64.0	Standard	2.8	55.0	69.0	84.2	2
302 SS	64.0	Back	5.4	8.1	9.7	9.5	2

*See Appendix C for description of cavitation conditions.

TABLE 2

"DRY" MERCURY CAVITATION DAMAGE DATA

Material	Velocity (ft/sec)	Cav.Cond.* (Degree)	Mean Depth of Penetration-μin. 25 Hrs	50 Hrs	75 Hrs	100 Hrs	No.of Samples
302 SS	34.0	Standard	--	5.7	--	--	8
302 SS	34.0	Standard	--	4.8	--	6.8	4
302 SS	34.0	Standard	--	3.5	--	--	4
1008 CS	34.0	Standard	--	29.4	--	--	4
Ta-10W(A)	34.0	Standard	--	17.1	--	--	2
Ta-8W-2Hf(B)	34.0	Standard	--	8.5	--	--	2
Cb-1Zr (Annld)	34.0	Standard	--	17.9	--	--	2
Tenelon(F)	34.0	Standard	--	3.7	--	--	2
Mo-1/2Ti(E)	34.0	Standard	--	21.0	--	--	2
Nickel (As Recd)	34.0	Standard	--	186.7	--	--	2
Nickel (L.H.Trt.)	34.0	Standard	--	149.2	--	--	2
Nickel (H.H.Trt.)	34.0	Standard	--	65.8	--	--	2
302 SS	48.0	Standard	1.0	--	--	--	2

*Ibid., p. 39.

made to correlate the mechanical properties of the test specimen materials with the observed damage. There are of course many possible interrelated factors that may influence the damaging character of a particular cavitation-material-fluid combination such as: the contribution of pure chemical corrosion and erosion; impurity content of fluid, especially entrained gases; type of fluid; variation of fluid and material properties with temperature; geometry of cavitation flow regime; etc. It has been necessary to eliminate or hold constant as many of these variables as possible, so that the effect of one variable at a time may be investigated. In order to examine only the relationship between mechanical properties and mechanical effects of cavitation damage, materials were selected that had a high resistance to chemical corrosion effects in mercury; and then the test fluid, test velocity, test geometry, test temperature, and cavitation flow regime were held constant. Thus the only variables were the mechanical properties of the different materials being tested. A parallel program for measuring the stress-strain curves and hardness for the same heats of material that were being used for the cavitation damage, and at the test temperatures, was also conducted, since it was found that handbook and vendor catalog values were not sufficiently precise. In addition, other mechanical properties not normally reported in the standard listings, as strain energy to failure, were desired. The resultant mechanical properties data[7] is used herein. The appropriate cavitation damage data that was used for the correlations with mechanical properties are listed in Table 2. This "dry" mercury data is the only full set for mercury where the other parameters have been held constant.

The damage data was subjected to a least mean squares fit regression program (Appendix B) in order that numerous types and combinations of correlating equations could be examined. As an initial step, each property was examined singly to see if a single-property correlation would suffice. These correlations have been reported earlier,[2] and are summarized here in Table 3-a. However, no single property is particularly successful in this regard. This is not surprising since various actual failure mechanisms probably occur, involving strength considerations with regard to resistance to fracture, along with ability to deform away from the very localized bubble-implosion blow without failure. Unfortunately the relation between these characteristics depends on the material. Furthermore, the available mechanical properties are indicative of the materials resistance under semi-static loading conditions, while the actual loading in the cavitation damage case is a very localized pulse of microsecond duration. However, hopefully these semi-static properties may give a rough indication of the type of property which best predicts cavitation failure, i.e., whether a pure strength property as tensile strength, or an energy property as strain energy to failure, or a combination of these types is required for good correlation. Presumably, the type of correlation obtained will influence future work in this area, in the sense of determining whether or not mechanical property data at high rates of loading will be necessary for a good correlation, and which properties of this type should be emphasized. Since single property correlations were not markedly successful, several multiple property correlations[2] were made (Table 3-b). A fairly

TABLE 3-a

TERM BY TERM ANALYSIS OF HG CAVITATION DAMAGE DATA VS. MECHANICAL PROPERTIES

Property	Correlating Equation	F Level	Std. Error	Coef D.
1. True Breaking Stress	$MDP = 0.025 - 0.63 \times 10^{-12}(TBS)^{2}$	12.90	0.008	0.85
2. Engineering Strain Energy	$MDP = 0.028 - 0.54 \times 10^{-6}(ESE)$	10.60	0.009	0.83
3. Percent Elongation	$MDP = 0.029 - 0.24 \times 10^{-1}(\%El.)^{1/2}$	9.20	0.009	0.82
4. True Strain Energy	$MDP = 0.008 + 0.24 \times 10^{12}(TSE)^{-3}$	8.00	0.009	0.80
5. Tensile Strength	$MDP = 0.034 - 0.25 \times 10^{-6}(TS)$	5.80	0.01	0.77
6. Percent Reduction Area	$MDP = 0.022 - 0.11 \times 10^{-6}(\%RA)^{3}$	2.86	0.011	0.70
7. Brinell Hardness	$MDP = 0.007 + 0.10 \times 10^{5}(BHN)^{-3}$	2.60	0.012	0.69
8. Yield Strength	$MDP = 0.009 + 0.17 \times 10^{+3}(YS)^{-1}$	0.415	0.013	0.604
9. Elastic Modulus	$MDP = 0.013 + 0.85 \times 10^{19}(E)^{-3}$	0.11	0.013	0.59
10. Acoustic Impedance	$MDP = 0.024 - 0.64 \times 10^{-2}(AcI)^{1/3}$	0.21	0.013	0.59

TABLE 3-b

BEST CORRELATION WITH ALL TEN PROPERTIES CONSIDERED
(HG CAVITATION DAMAGE VS. MECHANICAL PROPERTIES)

$$MDP = -0.064 + 0.34\times10^{2}(TBS)^{-1/2} - 0.17\times10^{9}(TS)^{-2} + 0.74\times10^{8}(TBS)^{-2}$$

Coefficient of Determination	=	0.994
Standard Error	=	0.00188
Maximum Absolute Deviation	=	0.0034
Maximum Percent Deviation	=	44.56%

good correlation was obtained with a combination of engineering tensile strength (which involves ductility) and true breaking strength.

D. Microexaminations

To explain, control and/or inhibit an event caused by an unknown force regime, such as cavitation, one must first understand the nature of the damaging forces. In the case of cavitation bubble collapse and the resultant damage, there is at present considerable controversy as to the exact nature of the forces and their origin and description. Since these events occur over time intervals on the order of microseconds and the size scale is the order of fractions of a mil, direct observation is difficult. It becomes necessary to examine the "footprints" left by these forces and so attempt to infer the nature of the forces.

The examination of the vertical and horizontal surface displacement with a very sensitive linear tracing device offers a means of enlarging the actual pits so that visual examinations can be accomplished. Such a device was used to examine the detailed profile of many cavitation pits in several materials to obtain a better understanding of the probable mechanisms of damage. A typical trace and corresponding photomicrograph of the surface of a 304 stainless steel specimen is presented in Figure 29. This type of examination is well suited for comparing the cavitation craters with those made by other methods.

An overwhelming preponderence in the mercury damage of circular pits with crater type rims has led to the conclusion that the mechanical forces causing the damage were of a single blow nature. A crater

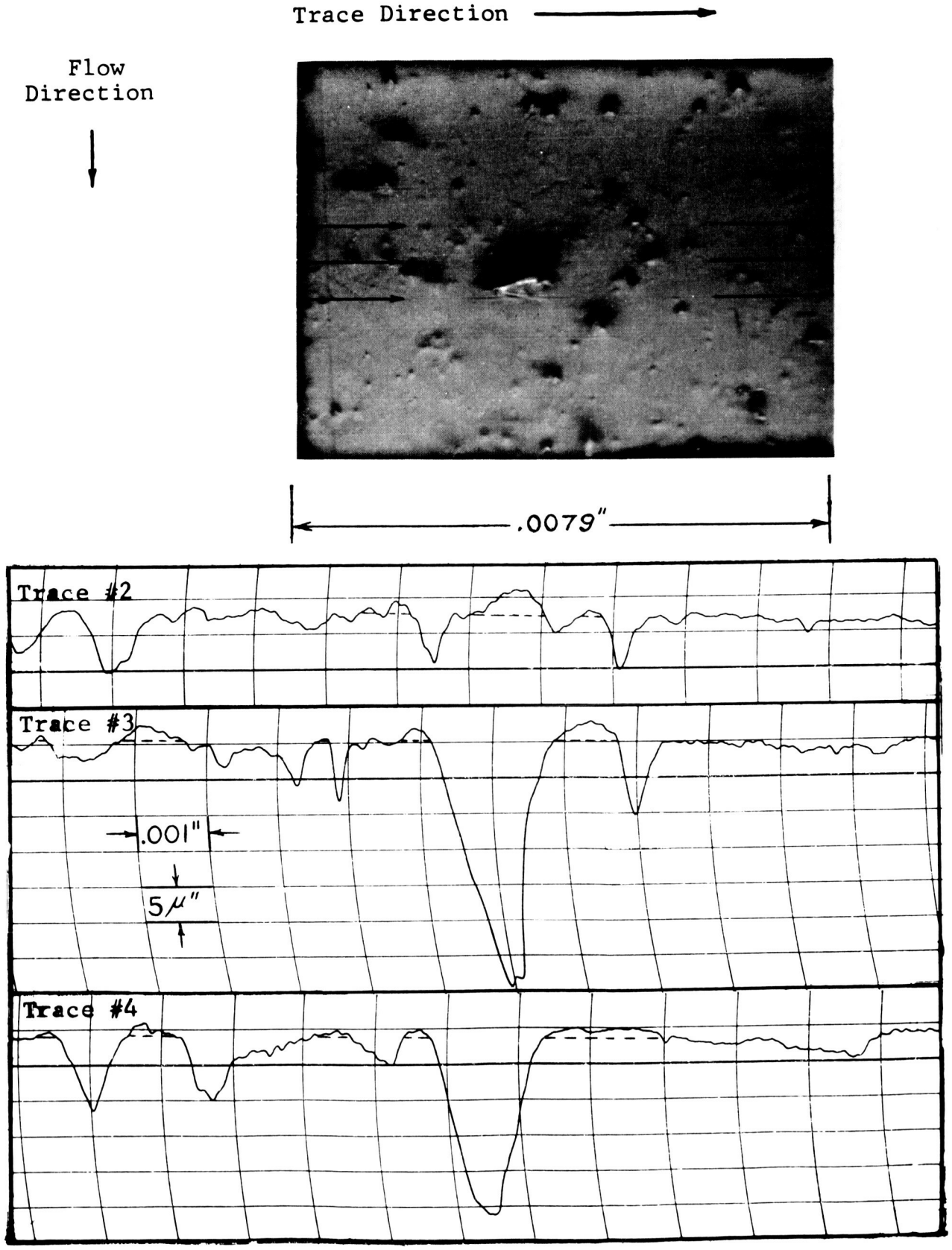

Fig. 29.--Photomicrograph and corresponding proficorder traces of surface of specimen 22-SS (304 stainless steel), after 10 hours exposure to "standard cavitation" in mercury at a throat velocity of 34 feet per second.

produced by simply indenting the surface with a sharp object appears very similar. Such craters were produced for comparison with a hardness indentor. From such a crater it is evident that there will be no material removal, but that the surface will be distorted. A comparison of the crater profiles and the volume displaced above and below the original surface in these two cases,[10] has led to the conclusion that material is indeed removed from the cavitation craters and not removed in the artificial pit case.

It has also been noted that cavitation craters resemble those that are obtained in fluid impact tests. Comparison of typical cavitation crater profiles as obtained here, and those from fluid impact tests[8] (Figure 30) shows that there is an almost exact match, for the particular sets of experimental parameters used. This high degree of similarity lends support to the current theory that the bubble collapses unsymmetrically into a torus shape with a high velocity jet piercing the torus center and impacting the damaged surface. Further evidence, to be presented later, supports this mechanism of collapse.

Detailed proficorder and photographic examinations have also been carried out at several stages during the damage tests, showing that in general craters do not change size or shape with further exposure to the cavitation regime, but that new craters appear next to, and in some cases on, the rims of existing craters.[11] This observation also tends to support the single blow nature of the cavitation forces, at least for the present type of test.

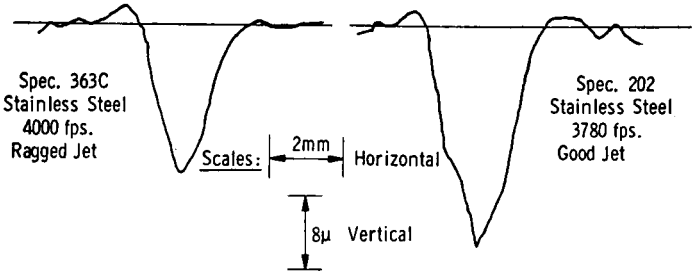

a) Water impact pit profiles from DeCorso[8].

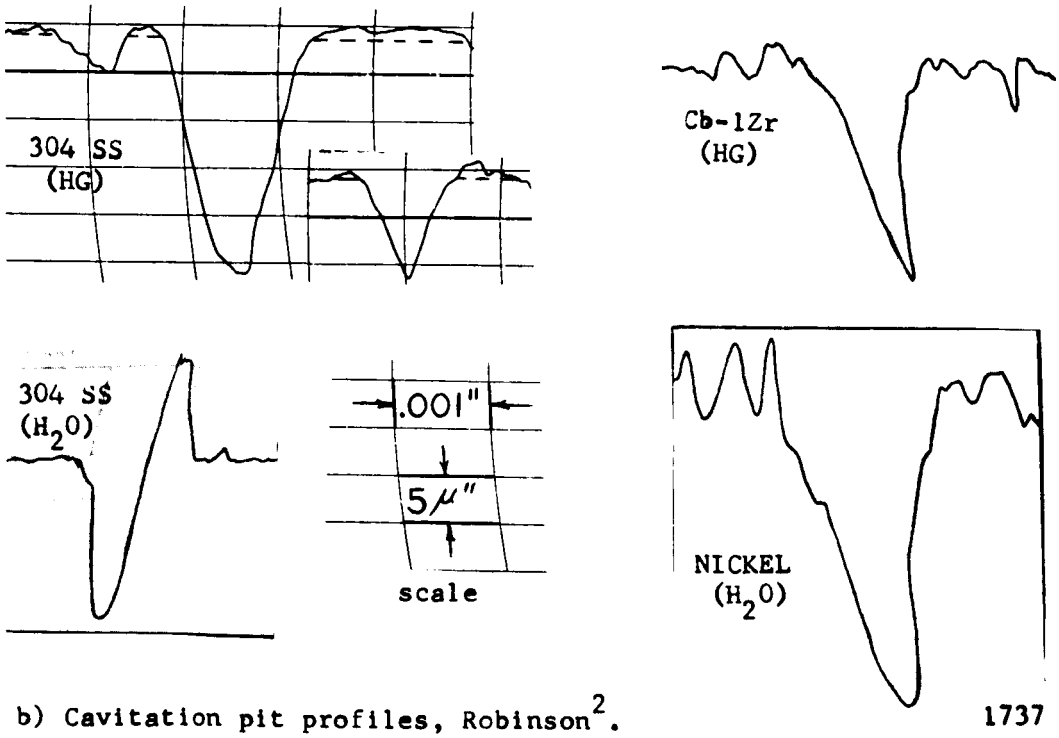

b) Cavitation pit profiles, Robinson[2].

Fig. 30.--Comparison of high velocity water jet impact craters and cavitation damage craters.

It has been noted that the pit depth to diameter ratio for impact tests of mercury on copper for decreasing velocities of impact decreases,[9] and reaches a value that corresponds to that observed in the cavitation pits ($\sim$0.05) at a droplet impact velocity of $\sim$ 600 ft./sec. This value, along with the earlier comparison of size and shape of pits from water impact tests, indicates that a cavitation formed jet, if such exists, would have a velocity of $\sim$ 600 ft./sec. in mercury and $\sim$4000 ft./sec. in water for these particular tests.

E. Pit Correlations

The pressure distribution on the specimen polished surface and the number of bubbles and bubble distribution thereon has been previously reported[2] as a function of cavitation condition, velocity, etc. Hence, detailed pit counts on the polished surface would allow a correlation between flow conditions, number of bubbles, and pits actually formed. Such a count was made at 500X for several axial locations on the specimen surface for two typical materials from the mercury tests. Figure 31 shows the distribution of bubbles* and pits appearing on the polished surface per unit time as well as the pressure above vapor pressure versus distance from the specimen leading edge. The numbers represent total pits of all sizes. Both materials exhibit a pitting rate increasing away from the leading edge, which peaks at about two-thirds the distance towards the downstream end, and then decreases toward the

---

*Bubbles seen in the film by viewing through a transparent specimen[2] must be on the surface because of the opacity of the mercury.

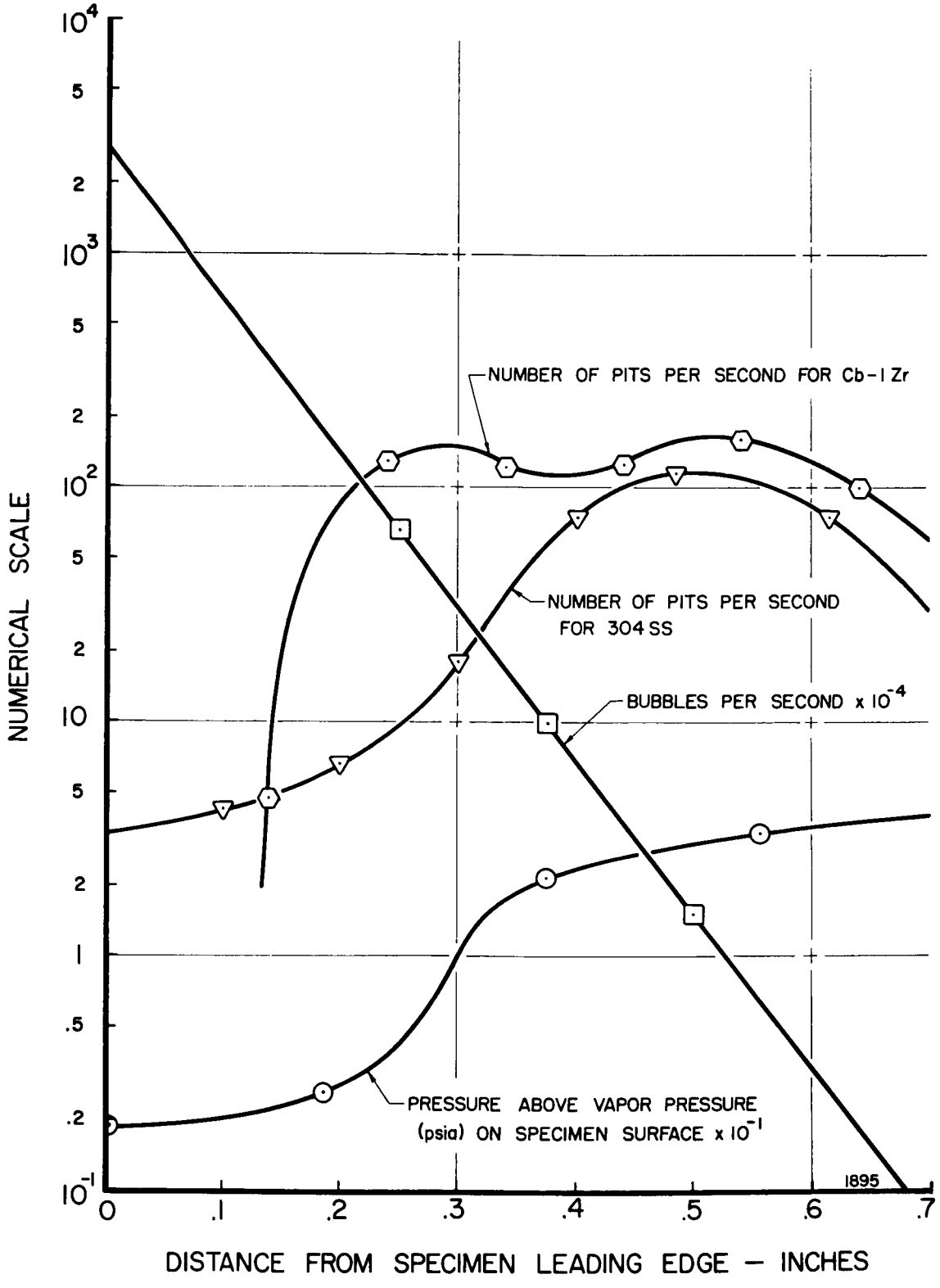

Fig. 31.--Distribution per unit time of pits, bubbles and pressure above vapor pressure on test specimen polished surface vs. distance from specimen leading edge for SS and Cb-1Zr in mercury at 34 ft./sec. and standard cavitation.

downstream end. The bubble population decreases approximately exponentially with distance along the entire length. A strong decreasing trend is expected since the pressure increases strongly above vapor pressure toward the rear of the specimen.

The relation between the bubble population and pressure curves, and the pitting distribution curve shows the expected trend. At the upstream end of the specimen there are many bubbles; however, the pressure on the surface is close to vapor pressure. Thus the bubble driving force for collapse in this region is very small so that few pits are produced. At the downstream end of the specimen, the pressure above vapor pressure is large, but the number of bubbles is small. In the limit of zero bubbles, there would of course be no pits, and the pitting number density does indeed decrease markedly toward this end of the specimen. That a maximum in the pitting rate should occur at some intermediate point where the pressure has risen so that energetic collapses are possible, and yet the number of bubbles is still large, is to be expected. It is also noted that the weaker Cb-1Zr exhibits a sharp increase in pitting rate at a position closer to the upstream end of the specimen and a somewhat higher total pitting rate along the entire specimen (Figure 31) than the stronger stainless steel. The bubble collapse energy threshold for single-event pitting for this material is undoubtedly lower than for the stainless steel and hence many more of these pits are formed in a region of reduced collapse pressure differential.

It may be possible eventually to show that the spectrum of force-time regimes imposed on the surface by bubble collapse in a given cavitating flow system is consistent with the pit size and spatial distribution, and that the different pit spectra for different materials (as Cb-1Zr and stainless steel in the present instance) are both consistent with the same flow regime through the influence of their differing mechanical properties. To accomplish this it would no doubt be necessary to make assumptions on actual mode of bubble collapse, failure mechanism, etc., which are not yet warranted by actual knowledge. However, if such a result could be accomplished, it would be a very long step toward attaining the ability to predict cavitation damage in advance, which is one of the major objectives of investigations in this field.

The size distribution of pits was tabulated for the present tests for three different materials in mercury and one material in water (Figure 32) across a band 0.060 inches wide (the full specimen width) and 0.006 inches long located 0.55 inches downstream from the specimen leading edge. This is in the region of most intense damage. From these curves it is evident that the maximum in the pit size distribution occurs for a diameter of about 0.05 mils for mercury. However, the maximum number of pits for water have a diameter about half that for mercury with the same material, presumably because of the weaker blows with the lower density fluid. For mercury the pits are somewhat smaller for the refractory than for the stronger steels, contrary to expectations.

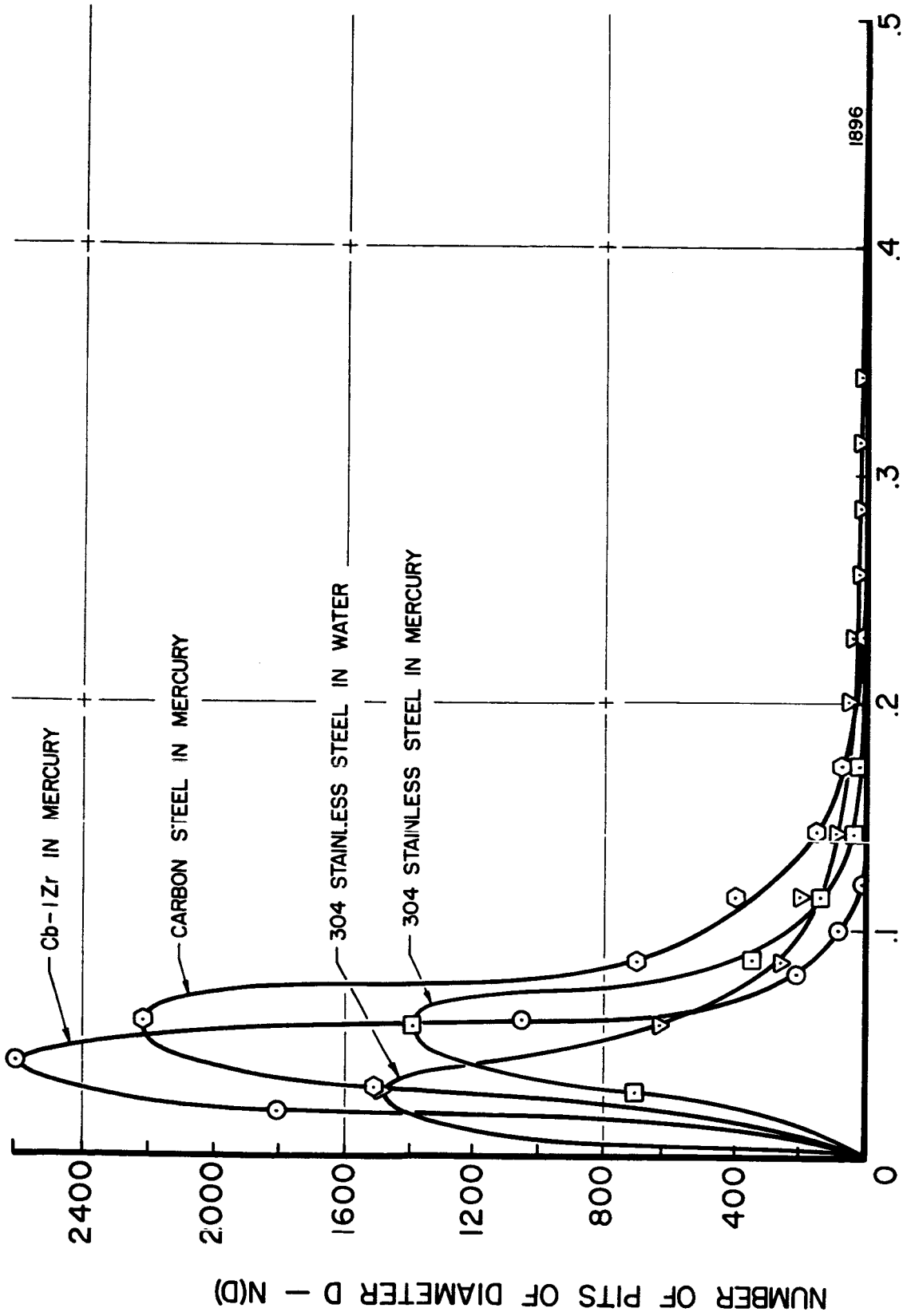

Fig. 32.--Pit size distribution for 1008 carbon steel, 304 stainless steel and Cb-1Zr in mercury at 34 ft./sec. and standard cavitation and 304 stainless steel in water at 200 ft./sec. and standard cavitation.

In the present tests one would expect the pit size to increase with distance along the surface, since only large bubbles could penetrate into the high pressure region at the downstream end of the specimen, and these would see a maximum collapsing pressure differential. To verify this expectation a pit distribution of the type already described was obtained for the Cb-1Zr material at six different axial locations from the leading edge (Figure 33). An examination of the tails of these curves indicates the expected result, i.e., the absolute number of larger pits increases with axial distance from the specimen nose, while the absolute number of all pits decreases.

Another significant observation can be made from Figure 31, which is shown more clearly in Figure 34. The ratio between the number of bubbles on the surface and pits produced is very large. It ranges from 10^9 near the leading edge of the specimen to $\sim 10^4$ to $\sim 10^5$ for that portion of the specimen where the pitting rate is maximum, for both stainless steel and Cb-1Zr (Figure 34). This large decrease in the ratio in the downstream direction is expected since the energy per bubble also increases rapidly in the downstream direction due to the increase in collapsing pressure differential. The effect is greater than it appears from this ratio since the mean pit size is also increasing in this direction.

The existence of a larger ratio of this order has been confirmed both here[13] and elsewhere[14] for a vibratory type of cavitation damage apparatus. Such a large ratio becomes more plausible if one accepts, as is supported by other evidence from these investigations,[2] that the

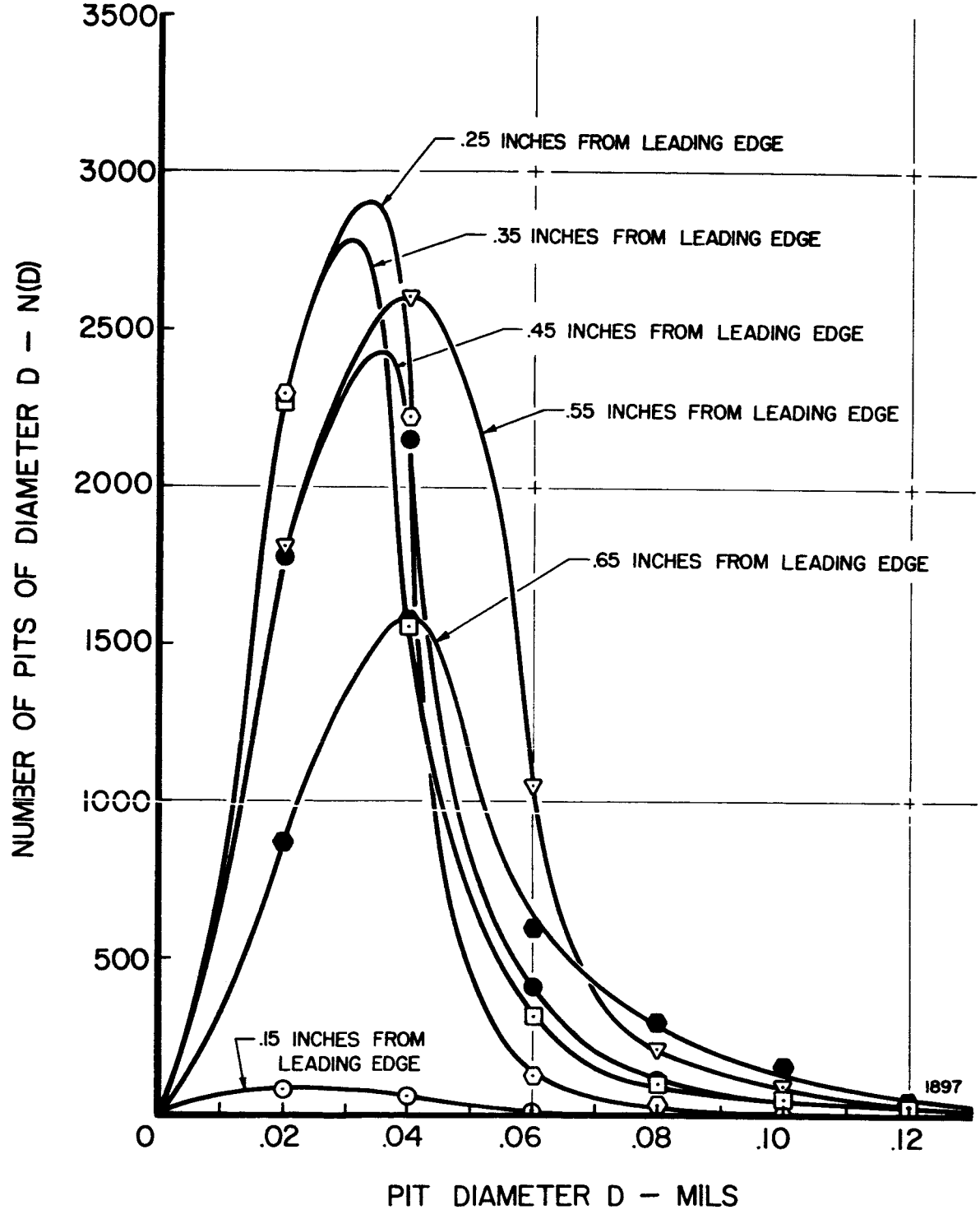

Fig. 33.--Pit size distribution vs. axial distance from specimen leading for Cb-1Zr in mercury at 34 ft./sec. and standard cavitation.

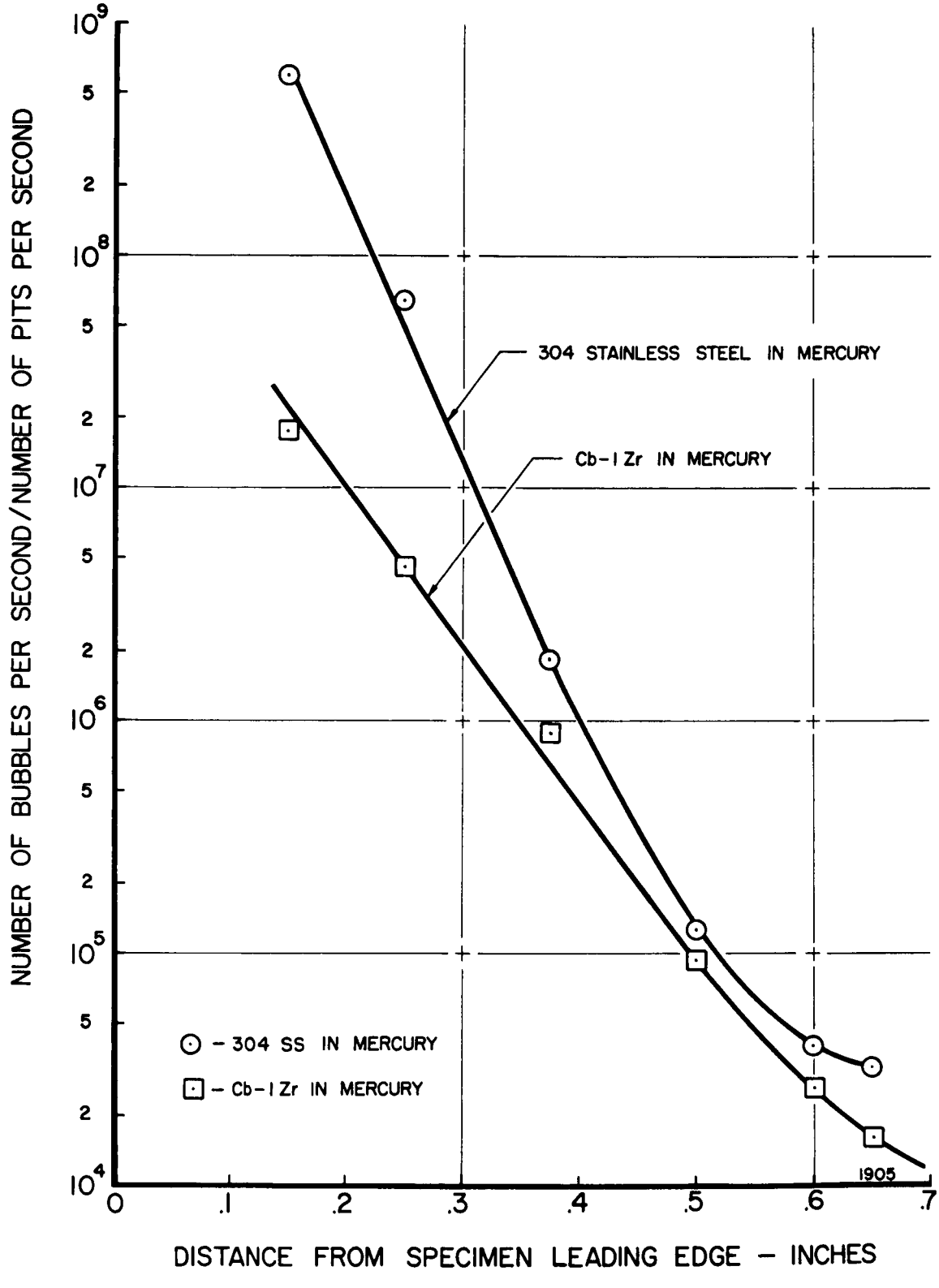

Fig. 34.--Ratio of observed bubbles per pit formed on surface per unit time vs. distance from specimen leading edge for 304 SS and Cb-1Zr in mercury at 34 ft./sec. and standard cavitation.

damage is inflicted by a high velocity fluid jet impinging on the surface and generated from the unsymmetrical collapse of the cavitation bubbles. It has been observed here[15] in a two-dimensional venturi with high speed photographs of the flow, that most bubbles do indeed collapse in this manner, involuting into a torus with axis oriented perpendicular to the pressure gradient, Figure 35, which is nearly parallel to the venturi axis in this case. In order for this type of collapse to cause damage to a surface that is also parallel to the venturi axis, as the present test specimens, the collapse axis must be oriented towards the surface.[2] Earlier photographic studies by Ellis of bubble collapse around a half body[16] show that the bubble collapse front, or flattened side, tends to orient itself normal to the pressure gradients. Very recent pictures also obtained by Ellis[18] of bubbles collapsing in a beaker in the vicinity of a flat plate show the effect of the proximity of such a plate.

Somewhat similar work is now in progress in our venturi.[17] Preliminary results indicate (Figure 36) that the orientation of the torus is indeed affected by the boundary and the pressure gradients. Note also the rebound which occurs in the last picture. Thus as postulated in an earlier report[2] there is indeed a mechanism that may orient the jet towards the surface in such a flowing system, further supporting the unsymmetrical collapse model as a likely damaging mechanism. Further evidence is provided by photomicrographs of cavitation damage in this system[2] on copper-nickel alloy which show a directional variation of the damage pits as the velocity varies. These are reproduced here for

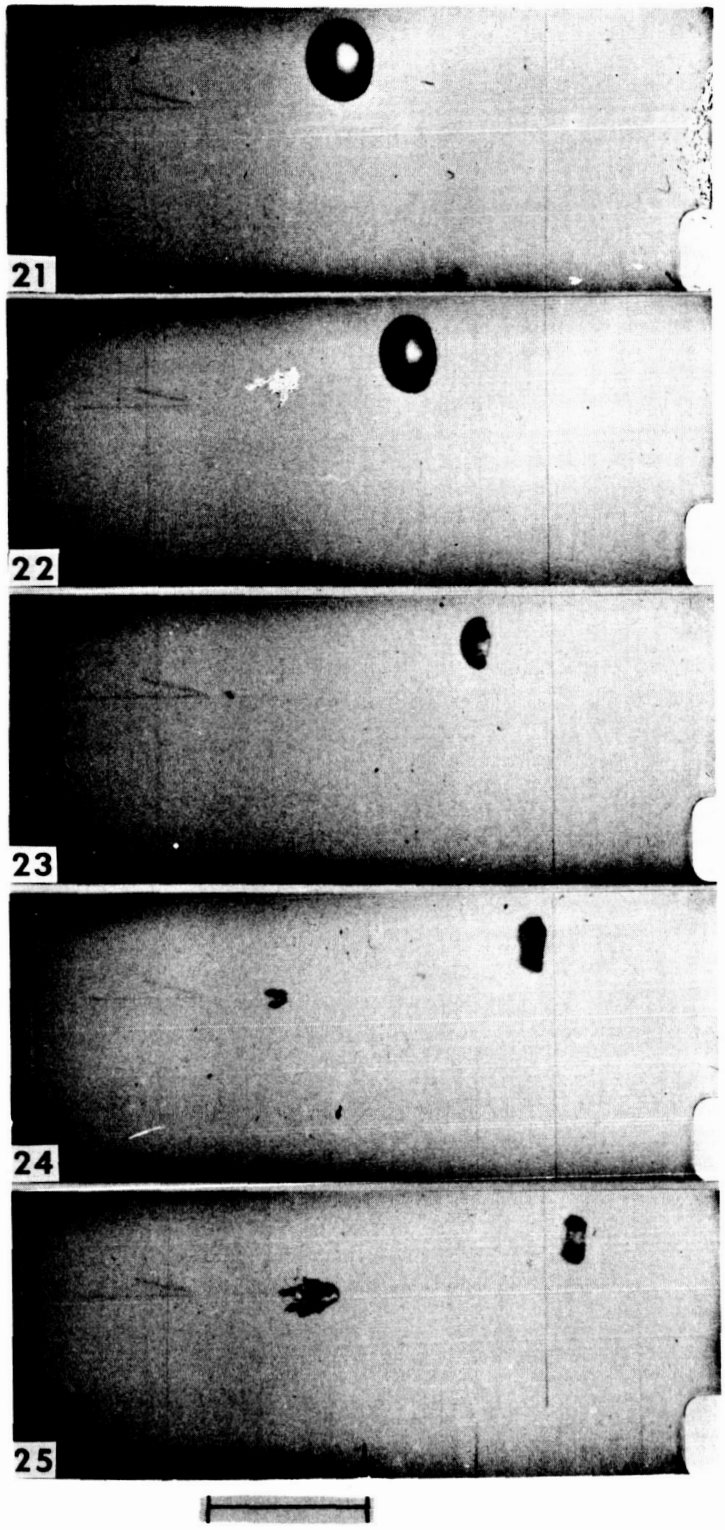

Fig. 35.--High-speed photographs of bubble collapse in two-dimensional venturi with 1/4" throat in water at 74.6 ft./sec. Air content 2.35% by volume, 132 microseconds between frames, 1 microsecond exposure, flow left to right, scale length 0.25 inches.

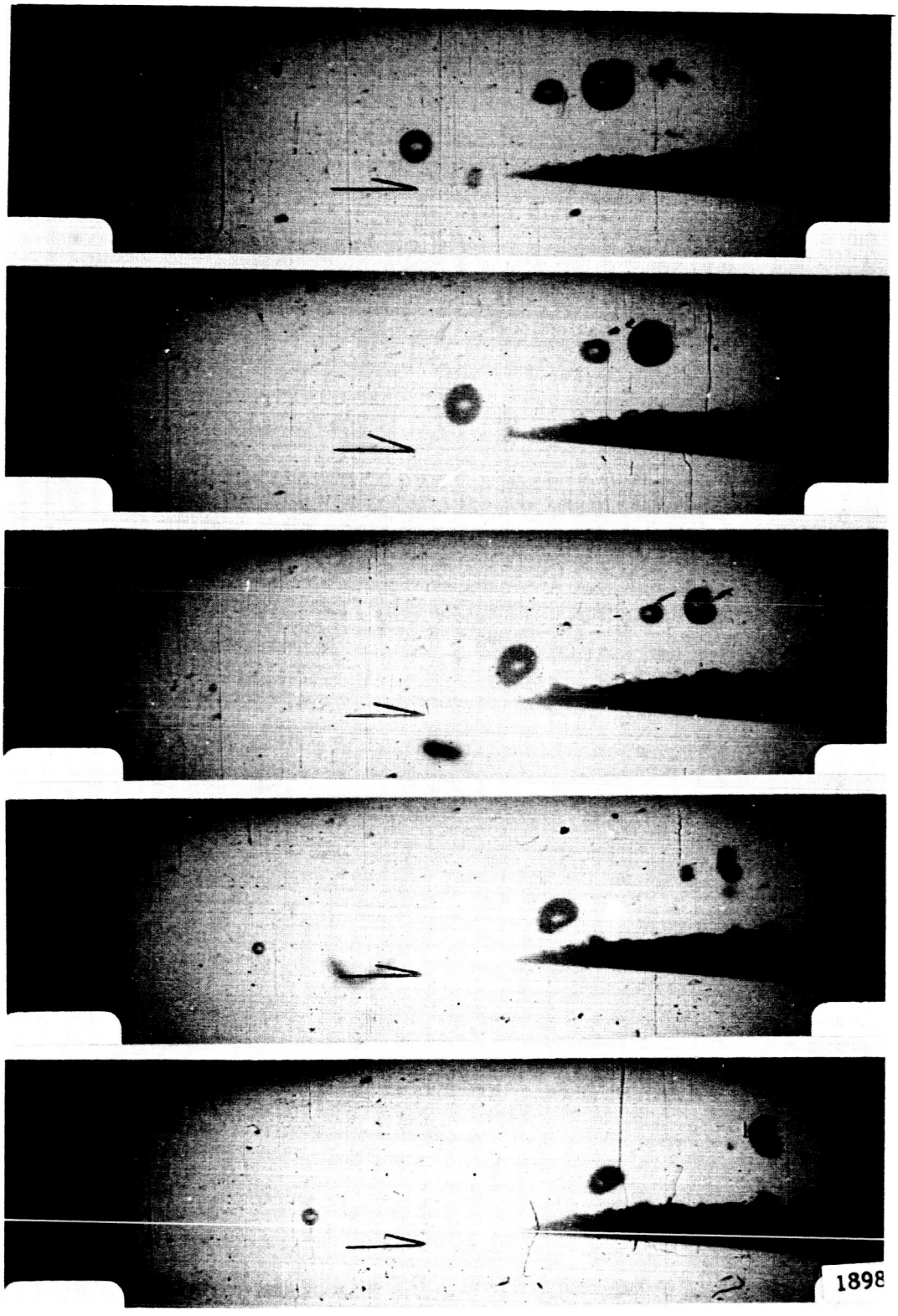

Fig. 36.--High-speed photographs of bubble collapse near a wedge in two-dimensional venturi with 1/4" throat in water at 83.5 ft./sec., air content 1.3% by volume, 126.5 microseconds between frames, 1 microsecond exposure per frame, flow left to right, arrow length is 0.205 inches.

convenience (Figure 37). The pits change from roughly circular craters with raised lip predominantly on the downstream side, to wedges with an apex in the direction of flow, to elongated grooves as the velocity is increased from 65 to 97 and finally to 200 ft./sec. Thus a directional dependence of the damage force capable of being affected either directly or indirectly by the velocity through its effect on boundary layer thickness, velocity and pressure gradients, etc. is indicated. Such a directional dependence of crater shape on flow velocity cannot be explained in terms of the spherical bubble collapse model. The velocity of propagation of the shock wave in the liquid is too much greater than the liquid flow velocity for this velocity to have appreciable effect on the angle of impingement of the shock on the surface.

As also discussed by Ellis,[18] the nonsymmetrical collapse model suggests a much more highly selective process whereby a bubble may cause a pit as compared with the symmetrical model since bubble size, directional orientation and proper distance from the surface are required in the nonsymmetrical model, whereas only size and distance are involved in the symmetrical model. First, the bubble collapse front for a large enough bubble in a large collapsing pressure differential must be oriented towards the surface at the proper time in that portion of its collapse when the jet is being formed. Second, the perpendicularly-oriented jet must be formed at a proper distance from the surface so that the jet energy is not dissipated in the fluid, or so that the jet formation is not inhibited by the nearness of the surface. These stringent criteria make credible the experimentally observed ratio of $\sim 10^4$ observed bubbles on the surface to one observed pit on this surface.

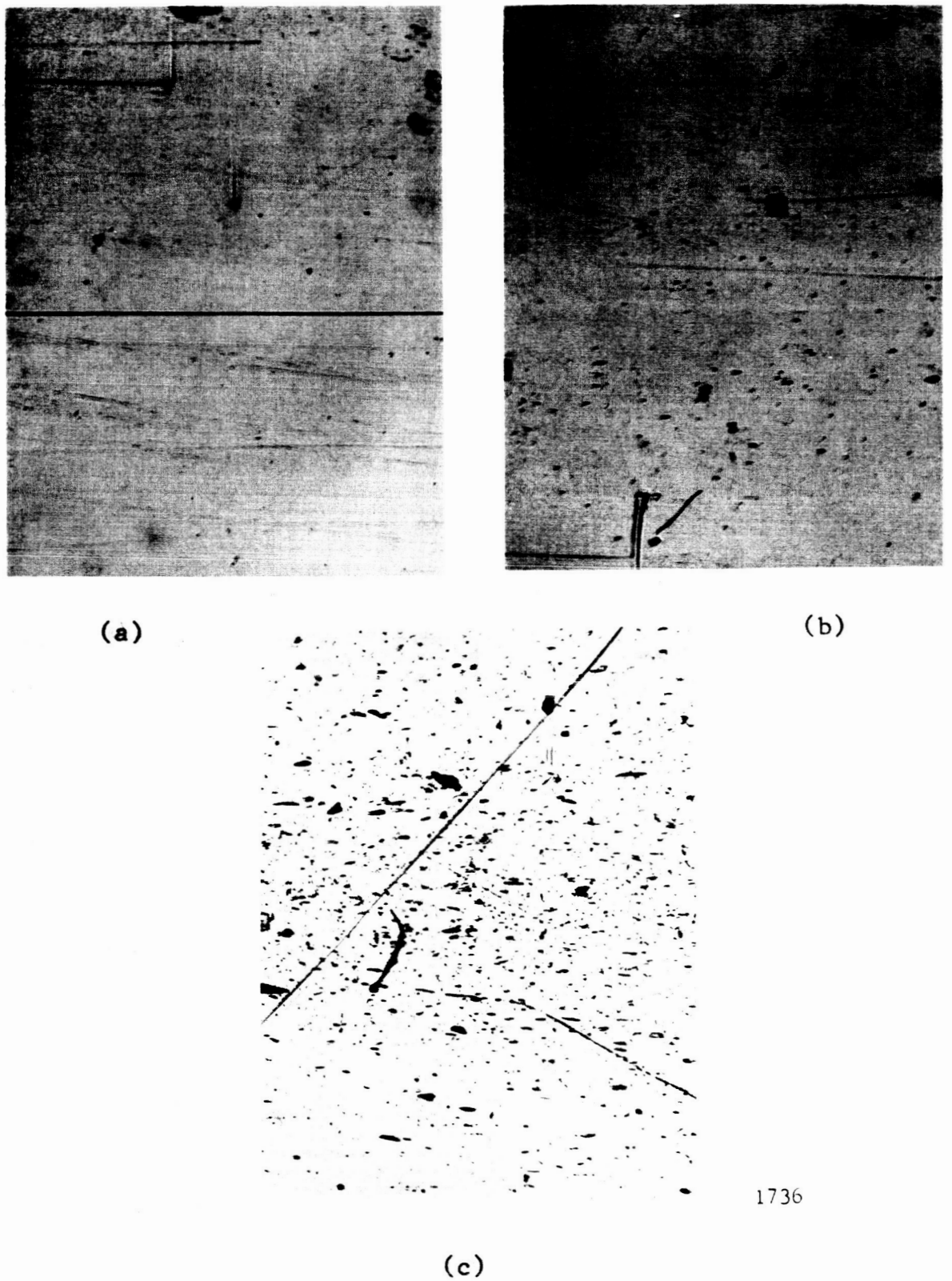

Fig. 37.--Photomicrographs of cavitation damage on copper-nickel alloy (H.H.Trt), for "standard cavitation" in water at one hour duration, (a) 65 ft./sec., (b) 97 ft./sec., (c) 199 ft./sec.

CHAPTER IV

WATER SYSTEM RESULTS

Similar damage tests have been conducted in the water system using identical venturis to those used for the mercury tests. However, two major differences exist. First, three (rather than two) specimens were tested simultaneously so that in each venturi the geometry of specimen insertion differed. (The increased number of test specimen hours required in the water system both because of lower damage rates and a larger number of materials to be tested necessitated the testing of three specimens together.) Secondly, the minimum velocity for the desired cavitation extent was 65 ft./sec. because of loop characteristics (inability to operate with pump suction below atmosphere). Since higher velocities (97 and 200 ft./sec.) were obtainable in the water system, they were utilized to increase damage rates. However, the most commonly used throat velocity in the mercury system was 34 ft./sec. with a maximum of about 55 ft./sec. imposed by equipment limitations.

Another variable not present in the mercury loop is the large solubility range of gases in water ($\sim$2 per cent), whereas for mercury or other liquid metals gas solubility is essentially nil. Finally, many more materials were possible for the water tests since the requirement of chemical compatibility with water is much less restrictive than mercury.

A. Damage Tabulations

The damage data, reduced by the computer program described in Appendix A, is presented in Table 4 for all of the tests performed in the water system to date. Most of the materials have been tested at a "Standard Cavitation" condition for three different velocities. Also, the effect of cavitation condition was examined for almost all materials at the highest velocity, i.e., 200 ft./sec. "Standard Cavitation" and 200 ft./sec. throat velocity were selected for the materials mechanical properties correlations. Therefore, all materials were tested under these conditions. At least three specimens of each material were tested, in most cases for a duration of 100 hours. The definition of the cavitation conditions used in the water system, which differ somewhat from those used in the mercury system, are found in Appendix C. The form of the data presentation in Table 4 is the same as described earlier for mercury (Tables 1 and 2).

B. Damage Correlations

As for mercury, the water data was correlated with the specimen material mechanical properties. The mechanical property data (Table 5) was measured in our own laboratories as reported earlier.[7] Only those materials with good corrosion resistance in water were used in the correlations, i.e., the carbon steel specimens were not included since considerable rust was evident on their surfaces after the tests. Nevertheless, the number of materials used in water is greater than in mercury. Several copper and nickel alloys, tested in three different cold-worked

TABLE 4

WATER CAVITATION DAMAGE DATA

Material	Velocity (ft/sec)	Cav.Cond.* (Degree)	Mean Depth of Penetration-μin. 25 Hrs.	50 Hrs	75 Hrs	100 Hrs	No.of Samples
302 SS	64.7	Standard	1.8	2.6	1.3	1.2	6
1008 CS	64.7	Standard	28.3	28.3	33.4	28.0	3
Brass(cz) (As Recd)	64.7	Standard	7.1	8.8	11.3	15.5	3
Brass(cz) (L.H.Trt.)	64.7	Standard	2.2	5.0	6.0	6.7	3
Brass(cz) (H.H.Trt.)	64.7	Standard	6.6	9.1	10.7	11.3	3
Copper(cu) (As Recd)	64.7	Standard	8.9	11.1	9.6	11.8	3
Copper(cu) (L.H.Trt.)	64.7	Standard	8.9	11.9	12.1	13.4	3
Copper(cu) (H.H.Trt.)	64.7	Standard	10.1	10.3	11.3	14.5	3
Cu-Nickel (As Recd)	64.7	Standard	8.8	10.8	11.0	11.8	3
Cu-Nickel (L.H.Trt.)	64.7	Standard	8.4	10.2	10.7	11.8	3
Cu-Nickel (H.H.Trt.)	64.7	Standard	4.3	5.7	5.8	6.1	3
Nickel(ni) (As Recd)	64.7	Standard	7.0	7.7	7.2	7.8	3
Nickel(ni) (L.H.Trt.)	64.7	Standard	4.2	4.8	4.2	5.3	3
Nickel(ni) (H.H.Trt.)	64.7	Standard	2.7	2.8	3.0	3.5	3
302 SS	97.2	Standard	15.3	12.8	13.8	14.7	3
1008 CS	97.2	Standard	53.1	91.8	106.1	117.0	3
Brass(cz) (As Recd)	97.2	Standard	10.4	13.5	14.6	16.8	3
Brass(cz) (L.H.Trt.)	97.2	Standard	2.9	4.0	6.1	4.9	3
Brass(cz) (H.H.Trt.)	97.2	Standard	5.7	7.1	9.0	7.8	3
Copper(cu) (As Recd)	97.2	Standard	9.4	10.0	9.4	16.8	3
Copper(cu) (L.H.Trt.)	97.2	Standard	9.0	7.4	8.4	10.8	3
Copper(cu) (H.H.Trt.)	97.2	Standard	8.8	8.2	8.1	10.0	3

TABLE 4--Continued

Material	Velocity (ft/sec)	Cav.Cond.* (Degree)	Mean Depth of Penetration-μ in. 25 Hrs	50 Hrs	75 Hrs	100 Hrs	No.of Samples
Cu-Nickel (As Recd)	97.2	Standard	7.6	10.7	10.9	12.3	3
Cu-Nickel (L.H.Trt.)	97.2	Standard	6.2	8.2	9.3	10.0	3
Cu-Nickel (H.H.Trt.)	97.2	Standard	5.3	6.4	7.8	8.1	3
Nickel(ni) (As Recd)	97.2	Standard	12.0	13.0	13.6	14.5	3
Nickel(ni) (L.H.Trt.)	97.2	Standard	5.7	7.3	7.7	8.0	3
Nickel(ni) (H.H.Trt.)	97.2	Standard	2.4	4.8	5.8	7.1	3
1100-0 (2) Aluminum	97.2	Standard	29.0	58.4	63.7	67.4	3
Brass(cz) (As Recd)	200.0	Visible	11.0	15.6	17.7	18.0	3
Brass(cz) (L.H.Trt.)	200.0	Visible	6.1	9.0	11.4	9.5	3
Brass(cz) (H.H.Trt.)	200.0	Visible	8.5	12.3	15.2	14.7	3
Copper(cu) (As Recd)	200.0	Visible	12.4	20.0	31.5	32.6	3
Copper(cu) (L.H.Trt.)	200.0	Visible	8.3	9.6	16.8	20.2	3
Copper(cu) (H.H.Trt.)	200.0	Visible	8.7	12.0	18.0	22.9	3
Cu-Nickel (As Recd)	200.0	Visible	7.5	10.6	11.9	14.4	3
Cu-Nickel (L.H.Trt.)	200.0	Visible	7.3	8.8	9.2	10.6	3
Cu-Nickel (H.H.Trt.)	200.0	Visible	4.5	6.5	7.3	8.3	3
Brass(cz) (As Recd)	200.0	Nose	25.2	25.7	28.7	31.7	3
Brass(cz) (L.H.Trt.)	200.0	Nose	10.7	16.5	17.2	20.6	3
Brass(cz) (H.H.Trt.)	200.0	Nose	12.8	16.5	19.1	21.6	3
Copper(cu) (As Recd)	200.0	Nose	17.9	28.5	32.7	58.3	3
Copper(cu) (L.H.Trt.)	200.0	Nose	17.7	33.1	38.3	42.9	3
Copper(cu) (H.H.Trt.)	200.0	Nose	17.3	28.4	33.9	59.7	3

TABLE 4--Continued

Material	Velocity (ft/sec)	Cav.Cond.* (Degree)	Mean Depth of Penetration-μ in. 25 Hrs	50 Hrs	75 Hrs	100 Hrs	No.of Samples
Cu-Nickel (As Recd)	200.0	Nose	7.6	11.0	9.8	22.6	3
Cu-Nickel (L.H.Trt.)	200.0	Nose	4.3	6.8	6.1	19.1	3
Cu-Nickel	200.0	Nose	6.4	10.8	6.3	13.9	3
302 SS (Ancient)	200.0	Standard	2.0	3.5	3.1	3.0	3
302 SS (Old)	200.0	Standard	3.5	4.1	4.5	5.1	18
302 SS (New)	200.0	Standard	3.8	5.5	6.1	6.5	15
1008 CS	200.0	Standard	19.2	762.3	823.9	848.9	3
Brass(cz) (As Recd)	200.0	Standard	16.5	39.7	41.4	41.1	6
Brass(cz) (L.H.Trt.)	200.0	Standard	18.1	25.7	28.9	28.7	3
Brass(cz) (H.H.Trt.)	200.0	Standard	13.8	25.1	33.8	48.1	6
Copper(cu) (As Recd)	200.0	Standard	16.6	24.0	32.7	46.7	3
Copper(cu) (L.H.Trt.)	200.0	Standard	14.5	23.8	31.6	54.6	3
Copper(cu) (H.H.Trt.)	200.0	Standard	16.9	30.4	35.6	69.1	6
Cu-Nickel (As Recd)	200.0	Standard	15.8	19.2	21.4	23.0	3
Cu-Nickel (L.H.Trt.)	200.0	Standard	10.6	13.3	17.1	19.6	3
Cu-Nickel (H.H.Trt.)	200.0	Standard	4.0	8.6	11.3	13.4	6
Nickel(ni) (As Recd)	200.0	Standard	12.3	15.8	18.2	20.7	3
Nickel(ni) (L.H.Trt.)	200.0	Standard	10.8	15.3	22.6	27.7	3
Nickel(ni) (H.H.Trt.)	200.0	Standard	2.9	5.9	8.2	11.3	3
1100-0 Al	200.0	Standard	926.0	2451.3	3961.0	5489.7	3
2024-Al	200.0	Standard	627.9	1617.0	2705.3	3520.0	3
6061-Al	200.0	Standard	666.7	1976.0	3220.0	4391.7	3
Cb-1Zr (Annld)	200.0	Standard	6.73	20.4	29.63	--	3

TABLE 4--Continued

Material	Velocity (ft/sec)	Cav.Cond.* (Degree)	Mean Depth of Penetration-μin. 25 Hrs	50 Hrs	75 Hrs	100 Hrs	No.of Samples
Cb-1Zr (C-Wkd)	200.0	Standard	1.91	3.49	3.84	5.3	6
Ta-10W(A)	200.0	Standard	9.7	11.1	10.4	--	3
Ta-8W-2Hf(B)	200.0	Standard	4.8	7.6	5.3	--	3
Mo-1/2Ti(E)	200.0	Standard	52.0	99.7	111.3	137.8	6
Tenelon(F)	200.0	Standard	1.8	2.2	2.2	3.1	6
Plex(P)	200.0	Standard	271.9	233.2	84.4	176.3	3

*See Appendix C for definitions of cavitation conditions.

TABLE 5

MECHANICAL PROPERTIES OF TEST SPECIMEN MATERIALS

Material	Tensile Strength	Yield Strength	Engr. Strain Energy	True Strain Energy	True Brkng. Stress	Hard-ness (BHN)	Elastic Modulus	% Elong.	% Red. Area
304 SS	95,200	44,000	44,800	74,500	172,800	133.5	$28x10^6$	54.4	50.9
1008 CS	50,000	30,000	15,500	23,000	55,200	91.5	$28x10^6$	40.0	71.0
Tenelon	131,800	82,000	54,500	94,800	220,900	218.0	$28x10^6$	44.2	46.6
Cb-1Zr Annealed	29,300	14,600	6,000	25,000	30,000	115.0	$12x10^6$	42.5	92.8
Cb-1Zr C-Wrked	56,000	52,500	2,900	10,000	80,000	124.0	$12x10^6$	6.0	84.0
Ta-10W	80,900	72,800	16,800	91,300	117,100	163.0	$29x10^6$	21.0	63.3
Ta-8W-2Hf	89,300	80,400	20,800	96,000	135,600	175.0	$29x10^6$	22.0	59.6
Mo-1/2Ti	94,700	89,600	15,000	83,000	120,000	216.0	$37x10^6$	30.7	54.7
1100-0 Aluminum	14,300	10,500	7,500	52,000	35,600	23.0	$10x10^6$	36.3	89.3
2024-T351 Aluminum	70,300	56,000	14,400	36,000	102,500	120.0	$10x10^6$	21.3	35.1
6061-T651 Aluminum	45,000	41,000	10,300	40,800	86,800	95.0	$10x10^6$	19.0	48.1
Copper-Zinc As Recd.	93,900	82,000	4,700	55,400	137,000	168.0	$16x10^6$	5.3	40.7
Copper-Zinc (L.H.Trt)	47,600	20,000	28,600	57,000	119,500	65.0	$16x10^6$	62.6	60.9
Copper-Zinc (H.H.Trt)	40,400	11,000	15,300	33,000	79,500	29.0	$16x10^6$	58.9	51.7

TABLE 5--Continued

Material	Tensile Strength	Yield Strength	Engr. Strain Energy	True Strain Energy	True Brkng. Stress	Hard-ness (BHN)	Elastic Modulus	% Elong.	% Red. Area
Copper-Nickel (As Recd)	87,300	77,000	6,100	13,200	87,400	162.0	22×10^6	4.5	15.4
Copper-Nickel (L.H.Trt)	57,900	20,000	3,100	36,200	85,900	76.0	22×10^6	34.9	43.5
Copper-Nickel (H.H.Trt)	53,300	18,000	16,300	21,800	70,500	56.0	22×10^6	34.4	34.4
Copper OFHC (As Recd)	53,400	49,500	3,100	11,800	85,600	104.0	17×10^6	6.2	19.8
Copper OFHC (L.H.Trt)	31,500	9,500	13,900	26,900	54,300	66.0	17×10^6	51.3	48.5
Copper OFHC (H.H.Trt)	30,700	5,000	6,100	11,800	43,200	15.0	17×10^6	32.5	33.2
Nickel (As Recd)	93,100	82,000	3,200	8,300	99,100	173.0	30×10^6	3.9	10.2
Nickel (L.H.Trt)	50,500	13,000	18,300	48,300	92,700	55.0	30×10^6	43.8	51.6
Nickel (H.H.Trt)	48,700	7,000	16,100	40,500	79,500	45.0	30×10^6	41.8	49.7

and heat-treated conditions to give varying strength and energy properties for the same physical composition, were included.

A preliminary correlation after 50 hour test duration (same duration used for mercury) showed that either elastic modulus or the acoustic impedance ratio of material to fluid were quite successful as single property correlations, while no reasonable correlations could be obtained with the other eight properties considered in any combination, when the above two properties were not considered (Table 6). Since there is usually more damage in the mercury facility than in the water facility at the same duration, the water tests were continued to 100 hours, and another correlation made. These correlations (Table 7) apply for the three velocities utilized in the water tests and for three cavitation conditions at the highest velocity. The standard cavitation condition at 200 ft./sec., which is the most damaging and the condition that was used for the 50 hour correlations, again shows that the acoustic impedance ratio between material and fluid is a good correlating parameter. A slightly better correlation is obtained when multiple properties are allowed. This improved correlation involves acoustic impedance ratio, tensile strength, and elastic modulus. This also is consistent with the 50 hour results. The other cavitation conditions and velocities (Table 7) were correlatable only as a combination of properties, which did not include the acoustic impedance ratio, but did include engineering strain energy and percent reduction of area in one case, true breaking strength and percent elongation in another case, and engineering strain energy and yield strength in still another. The data

TABLE 6-a

SINGLE VARIABLE CORRELATIONS FOR FULL SET OF WATER DATA EXCEPT CARBON STEEL
(AT 50 HOURS)

Rank	Property	Correlating Equation	Std.Err.	Coef.D.
1	Acoustic Impedance	$MDP = 0.095+4.75(AcI)^{3}-0.239(AcI)^{-1/3}$	0.107	0.970
2	Elastic Modulus	$MDP = -31.23+0.639\times10^{22}(E)^{-3}-0.134\times10^{17}(E)^{-2}$	0.117	0.966
3	Percent Elongation	$MDP = 0.010 + 0.173\times10^{-1}(\%El)^{-2}$	0.411	0.542
4	Tensile Strength	$MDP = 0.070 + 0.673\times10^{13}(TS)^{-3}$	0.428	0.503
5	True Breaking Stress		0.551	0.179
6	Percent Reduction Area	(No more correlating equations listed	0.562	0.145
7	Engineering Strain Energy	since the data does not show	0.564	0.138
8	Brinell Hardness	sufficient correlation.)	0.565	0.135
9	True Strain Energy		0.569	0.123
10	Yield Strength		0.573	0.110

TABLE 6-b

SINGLE VARIABLE CORRELATIONS FOR WATER DATA SUBSET OF MATERIALS
AS USED IN MERCURY
(AT 50 HOURS)

Rank	Property	Correlating Equation	Std.Err.	Coef.D.
1	Elastic Modulus	$MDP = 0.0536+0.105\times10^{-22}(E)^3-0.357\times10^{-15}(E)^2$	0.0016	0.998
2	Percent Reduction Area	$MDP = -1.72-0.109\times10^{4}(\%RA)^{-2}+0.864\times10^{2}(\%RA)^{-1}+0.172\times10^{-3}(\%RA)^2$	0.010	0.946
3	Yield Strength	$MDP = 0.054-0.616\times10^{-10}(YS)^2+0.714\times10^{-15}(YS)^3$	0.020	0.765
4	Engineering Stress Energy	$MDP = -0.146-0.275\times10^{11}(ESE)^{-3}+0.249\times10^{4/3}(ESE)^{-1/3}$	0.023	0.692
5	Brinell Hardness		0.028	0.497
6	True Breaking Stress	(No more correlating equations listed	0.030	0.438
7	Percent Elongation	since the data does not show	0.033	0.321
8	Acoustic Impedance		0.033	0.300
9	Tensile Strength	sufficient correlation.)	0.034	0.275
10	True Strain Energy		0.034	0.255

TABLE 6-c

SINGLE VARIABLE CORRELATIONS FOR WATER DATA SUBSET OF MATERIALS
AS TESTED IN WATER ONLY
(AT 50 HOURS)

Rank	Property	Correlating Equation	Std.Err.	Coef.D.
1	Elastic Modulus	$MDP = 56.63+0.476\times10^{23}(E)^{-3}-0.690\times10^{16}(E)^{-2}$ $-0.106\times10^{-1}(E)^{1/2}+0.273\times10^{-21}(E)^{3}$	0.156	0.971
2	Acoustic Impedance	$MDP = -0.119+0.248\times10^{1}(AcI)^{3}$	0.149	0.970
3	Percent Elongation	$MDP = 0.0105 + 0.167\times10^{-2}(\%E1)^{-3}$	0.562	0.547
4	Tensile Strength	$MDP = 0.131 + 0.656\times10^{13}(TS)^{-3}$	0.577	0.521
5	True Breaking Stress	(No more correlation equations listed since the data does not show sufficient correlation.)	0.683	0.330
6	True Strain Energy		0.719	0.258
7	Engineering Strain Energy		0.743	0.208
8	Percent Reduction Area		0.747	0.200
9	Yield Strength		0.761	0.169
10	Brinell Hardness		0.763	0.165

TABLE 7

BEST MULTIPLE PROPERTY CORRELATIONS OF FULL SET OF WATER DATA
EXCEPT CARBON STEEL AT 100 HOURS

Velocity (ft/sec)	Cav. Cond.		Correlation	Std.Err.	Coef.D.
64.7	Standard		$MDP = K_1 - K_2(\%RA)^{1/3} - K_3(ESE)^{1/2} + K_4(\%RA)^3$	0.0041	0.924
97.2	Standard		$MDP = K_1(TBS)^{-2}$	0.0277	0.497
200.0	Visible		$MDP = K_1 - K_2(TBS)^{1/2} + K_3(\%E1)^{-1/2}$	0.0037	0.978
200.0	Nose		$MDP = K_1(ESE)^{-1} + K_2(YS)^{-1}$	0.0085	0.963
200.0	Standard	1)	$MDP = -K_1 + K_2(AcI)^2 - K_3(E)^2 + K_4(YS)^{-1} + K_5(TS)^{-1/2} - K_6(YS)^{-1/2} + K_7(E)$	0.141	0.989
		2)	$MDP = -K_1 + K_2(AcI)^2 + K_3(TS)^{-2} + K_4(E)^{1/3}$	0.198	0.976
		3)	$MDP = -K_1 + K_2(AcI)^2 + K_3(TS)^{-2} + K_4(E)^2$	0.235	0.967
		4)	$MDP = K_1 - K_2(AcI)^2 + K_3(AcI)^3$	0.269	0.956

at 97.2 ft./sec. did not show a good correlation with any combination of properties. The best correlation for this data was with true breaking strength alone. However, the coefficient of determination is very low. The lack of good correlations for the lower velocity and "non-standard" cavitation conditions may be because fewer materials and samples of each material were used, and the total damage was less severe so that the precision of the weight loss measurements is reduced.

C. Microexaminations

The damage test specimens from the water system were subjected to the same types of analyses as the mercury specimens, in an attempt to examine the "tracks" left by the damaging bubble collapses and thus infer the damage mechanisms. The following subtopics show the results of these investigations.

1. Proficorder Techniques

The damage inflicted on the materials in the water cavitation facility, with conditions of standard cavitation and throat velocity of 200 ft./sec., appeared typically as shown in Figures 38, 39 and 40. Figure 38 shows damage on stainless steel. The pits consist of elongated grooves in the direction of flow, with a typical length to width ratio of about four. As indicated on the accompanying traces of the surface, there is a predominant ridge on the downstream end of the groove, indicating that the damaging force was directed partially in the downstream direction, i.e., the pit is slightly "tipped." The same type of general damage and damage orientation was observed on all materials

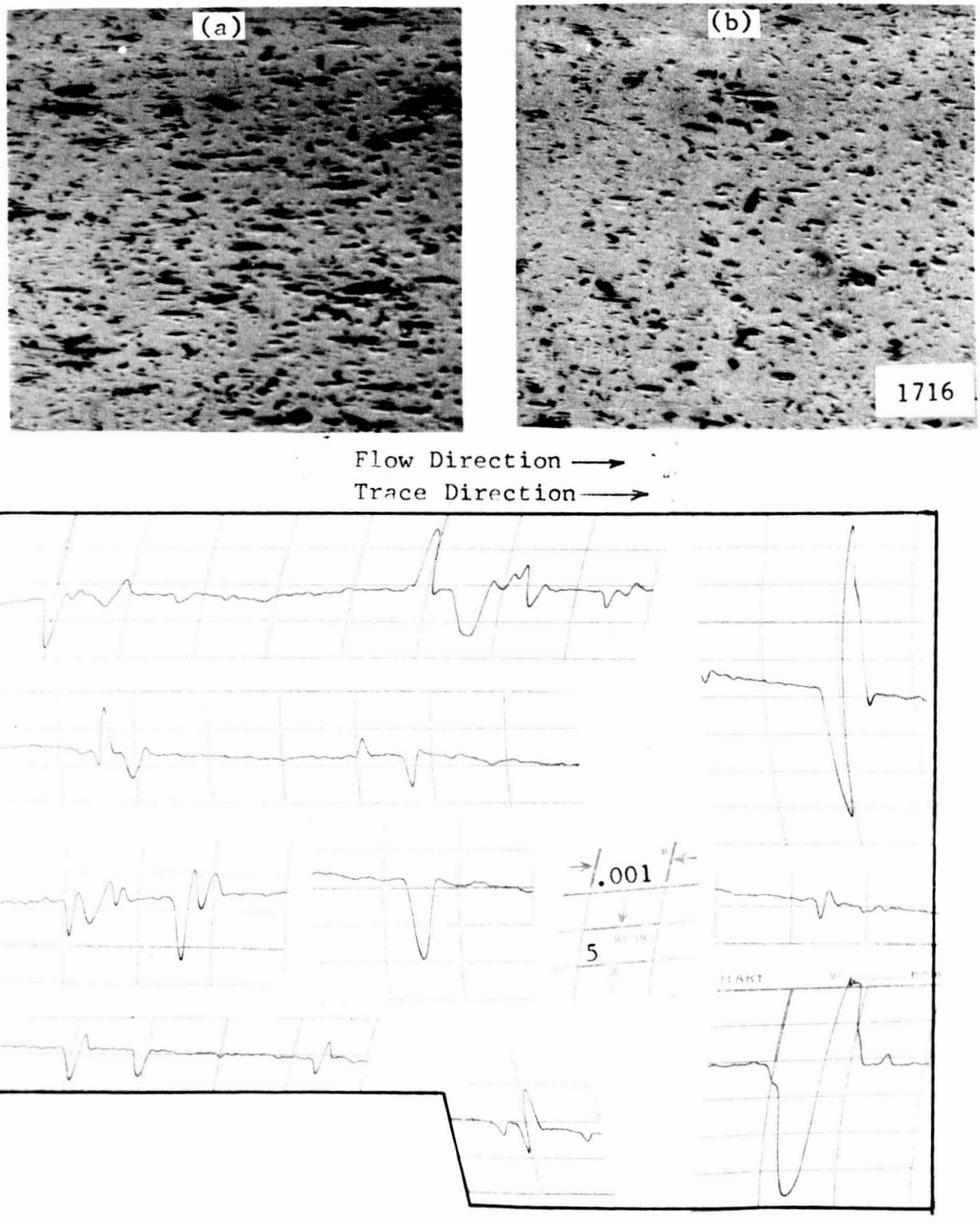

Fig. 38.--Typical photomicrographs and typical axial proficorder traces of cavitated surface of specimen No. 139-3 (304 SS) after 100 hours in water at a throat velocity of 200 ft./sec. for "standard cavitation" (a) nose area, (b) tail area.

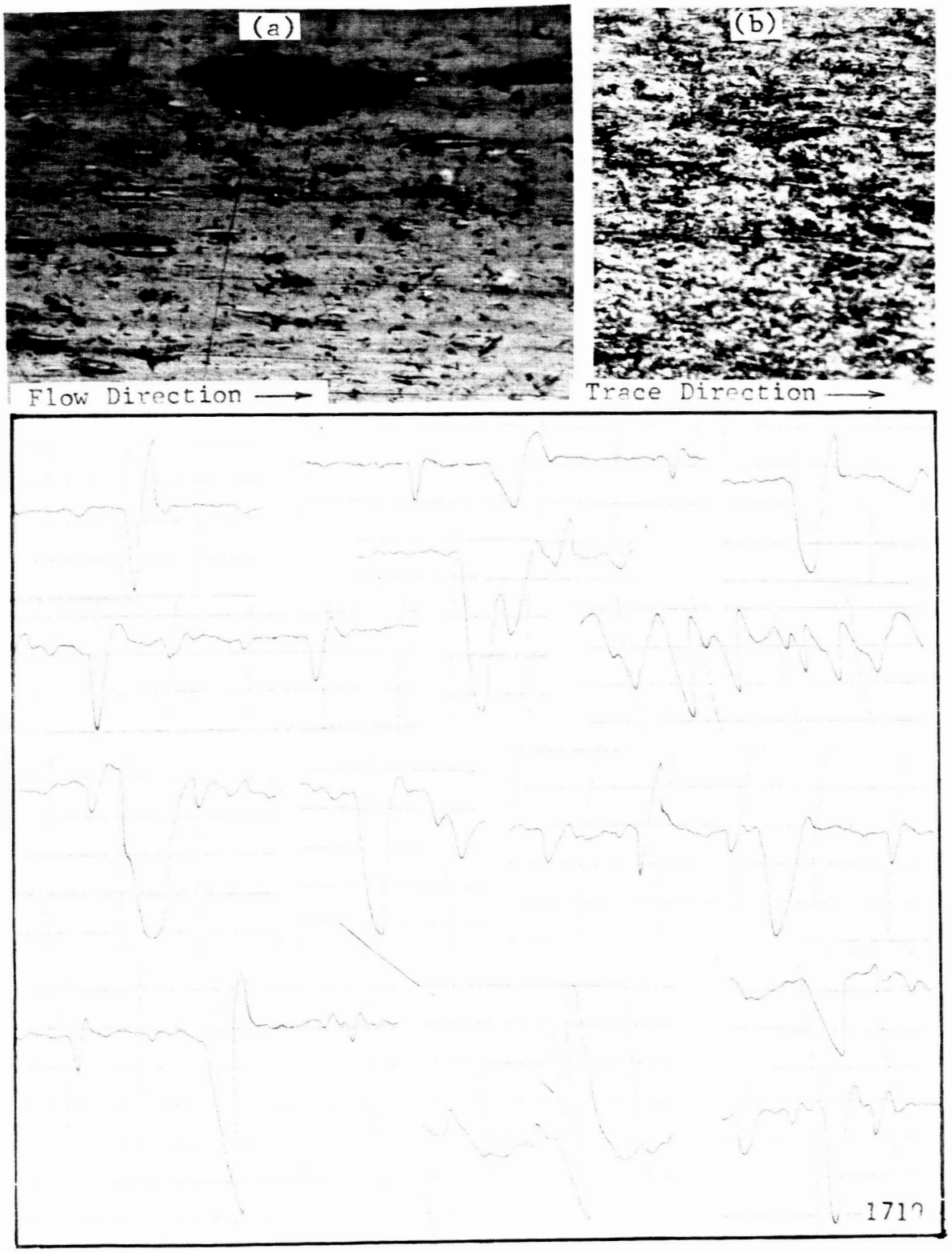

Fig. 39.--Typical photomicrographs and typical axial proficorder traces of cavitated surface of specimen No. 8-cn (as rec'd copper-nickel) after 100 hours in water at a throat velocity of 200 ft./sec. for "standard cavitation" (a) nose area, (b) tail area.

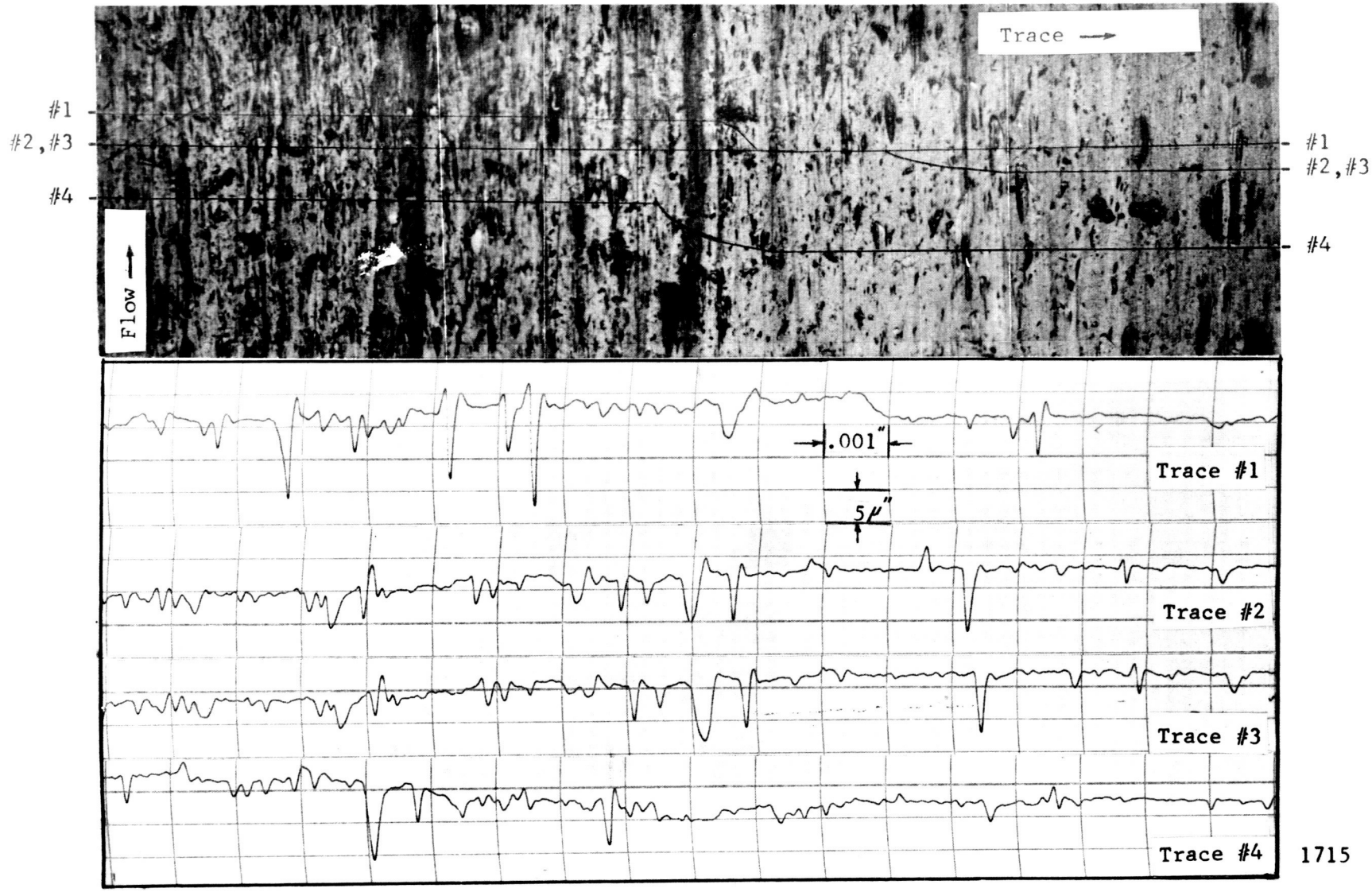

Fig. 40.--Typical photomicrographs and corresponding transverse proficorder traces of cavitated surface of specimen No. 8-cn (as rec'd copper-nickel) after 100 hours in water at a throat velocity of 200 ft./sec. for "standard cavitation."

at this velocity. Figures 39 and 40 show this effect for copper-nickel alloy. By tracing the surface in a direction perpendicular to the flow (Figure 40) it was found that there are raised rims on either or both sides of the grooves, indicating that the raised rim is not a characteristic bump of the tracing tip as it passes through a pit. If this were the case, no rim would appear on the side from which the tracer is approaching. A tabulation of many pits from all materials tested in the water facility gives an average depth to diameter ratio of ~ 0.03 as compared with ~ 0.05 from the mercury tests, and ~ 0.06 from the water jet impact tests,[8] compared earlier in Figure 30. A discussion of the relation of the impact tests to the cavitation case is included later.

Comparing the mean depth of penetration data at 50 hours duration for water (Table 3) to that found for "dry" mercury (Table 2), it is noted that for stainless steel the values are about equal. However, the mercury data was taken at a velocity of 34 ft./sec. and the water data at 200 ft./sec., and also the geometry of specimen insertion was different. Unfortunately no data for the two fluids for precisely the same geometry and velocity is available since the capabilities of the two flow facilities do not allow this overlap.

2. Microhardness Examinations

It is evident from the pitting size distributions that there are force-time regimes of varying magnitude applied to the surface, so that the surface is probably exposed to many blows below the damaging threshold during a sustained cavitation test. To evaluate the extent of cold-working of the surface, microhardness axial profiles were

measured along the centerline of the polished surface on the fully annealed pure copper, copper-zinc, and copper-nickel alloys at selected time intervals during a 100 hour cavitation test (Figures 41, 42, and 43). On the pure copper specimens (Figure 41) there was the greatest increase in surface hardness as the tests progressed. The increase was largest near the upstream end, but still existed at the downstream end. That the hardness increase should be greatest at the upstream (low pressure) end and for the softest material indicates that the implosions in this region are relatively very numerous and weak, having an effect in many cases only on the weakest material. Thus in the softest material the blows effective in producing cold-work cover most of the surface and cause a substantial increase in hardness. At the high pressure end there are many fewer bubbles and hence only a small portion of the surface is covered so that cold-working is much more local (even though the individual blows are relatively stronger) and does not affect the hardness readings as significantly.

For the other two alloys, which were considerably harder initially, some increase in hardness was noted in the upstream areas, while a small decrease in hardness occurred in the downstream areas (Figures 42 and 43). It is felt that the decrease is probably merely experimental scatter. The fact that the increase for these harder materials is less than that for the soft copper is reasonable in that a smaller portion of the surface would be exposed to blows intense enough to cause significant cold-work for these stronger materials, i.e., the effect is quite localized. Figure 44 is a full surface magnified view of one of these

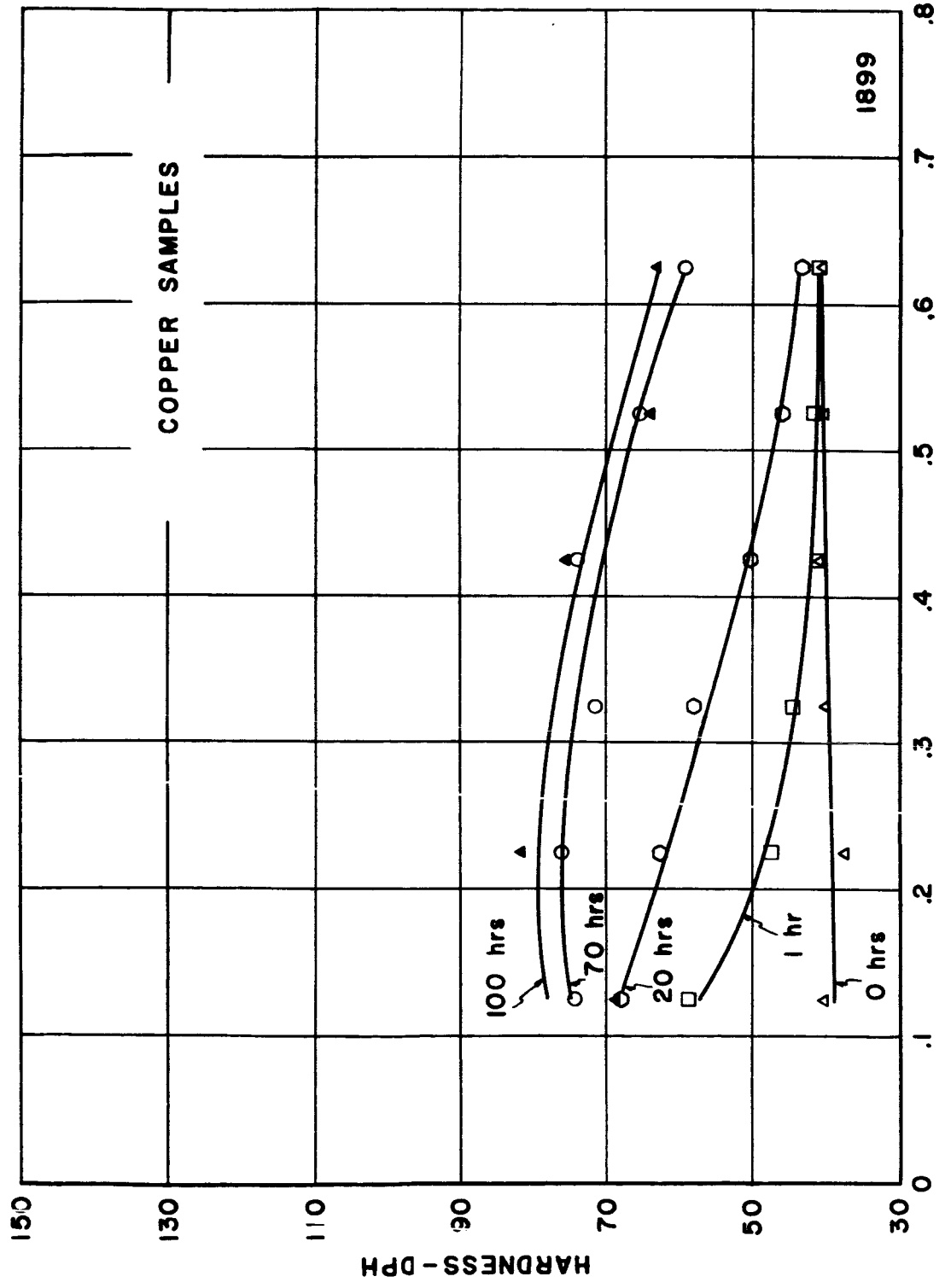

Fig. 41.--Hardness on surface vs. exposure time and distance from specimen leading edge for copper (H.H.Trt) in water at 200 ft./sec. and standard cavitation.

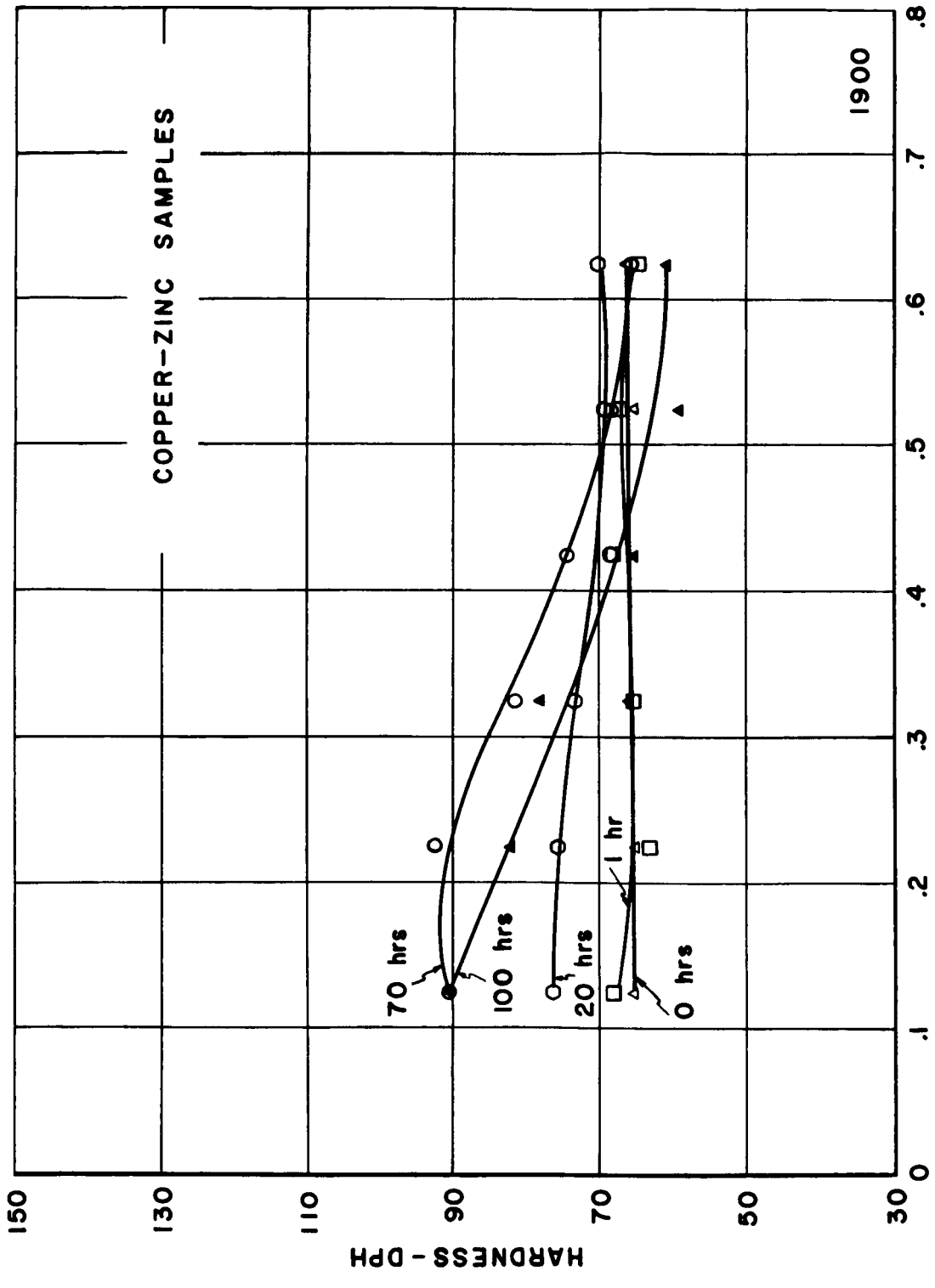

Fig. 42.--Hardness on surface vs. exposure time and distance from specimen leading edge for copper-zinc (H.H.Trt) in water at 200 ft./sec. and standard cavitation.

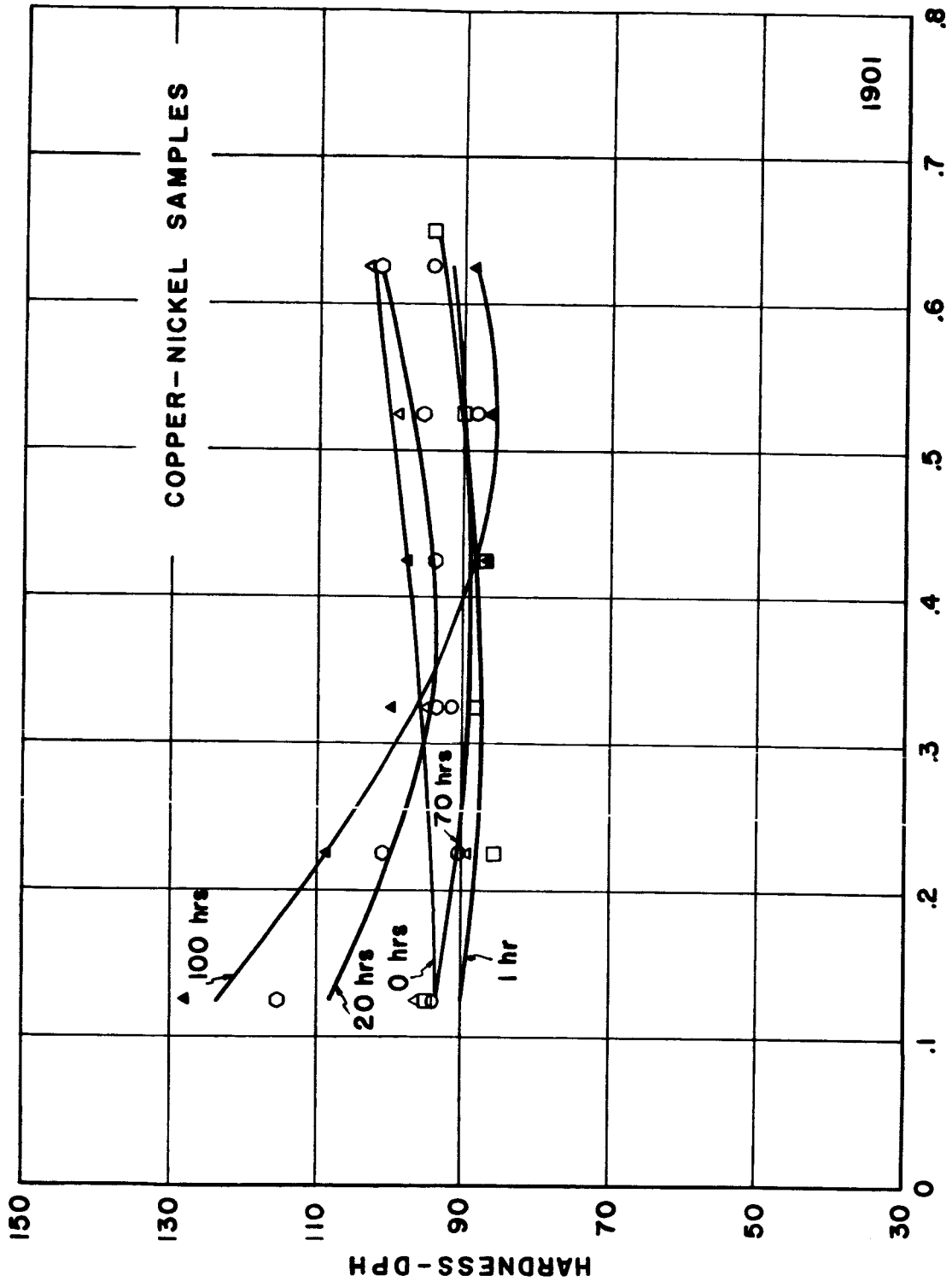

Fig. 43.--Hardness on surface vs. exposure time and distance from specimen leading edge for copper-nickel (H.H.Trt) in water at 200 ft./sec. and standard cavitation.

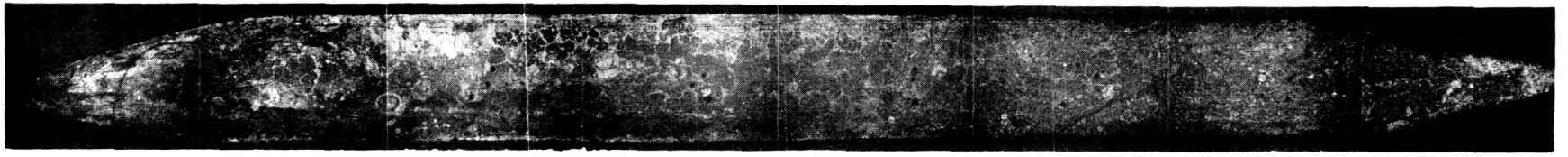

Fig. 44.--Full surface photograph of copper specimen from hardness test series showing damage distribution and location of DPH hardness marks for standard cavitation in water at 200 ft./sec. Exposure time hours.

samples showing the surface pitting distribution and the general location of the microhardness readings.

3. Grain Size Effects

Examination of surfaces that had been etched and photographed before and after exposure to cavitation in the mercury facility shows that the location of pits seems completely random with respect to grain boundaries.[12] Previous investigations[19,20,21] have been made of the effect of grain size on cavitation damage. Generally, it is difficult to isolate this variable, since the material properties such as tensile strength, yield strength, etc., are obviously affected by the heat treatment necessary to effect a change in grain size. In the present tests four similar alloys of copper, zinc and nickel, were available. Hence, an attempt has been made to correlate grain size with damage on this set of four materials, each in three different heat treat conditions. It was possible, by dividing the mechanical properties into suitable ranges, to obtain a plot of grain size versus damage for these materials. This curve (Figure 45) shows a decrease in damage with decreasing grain size to a point and then an increase starting with a grain size of 7. The data for the grain sizes of 7 and smaller are not really comparable with that for the larger sizes, since the material was in a 60% cold-worked condition and the grains were clearly very elongated and difficult to measure. Thus, for the more accurate portion of the curve (grain size of 1 to 6), damage decreases for smaller grain size. The decrease is by a factor of about 3 over this range of variation if grain dimension (factor of $\sim (6)^{1/2}$). This trend is consistent

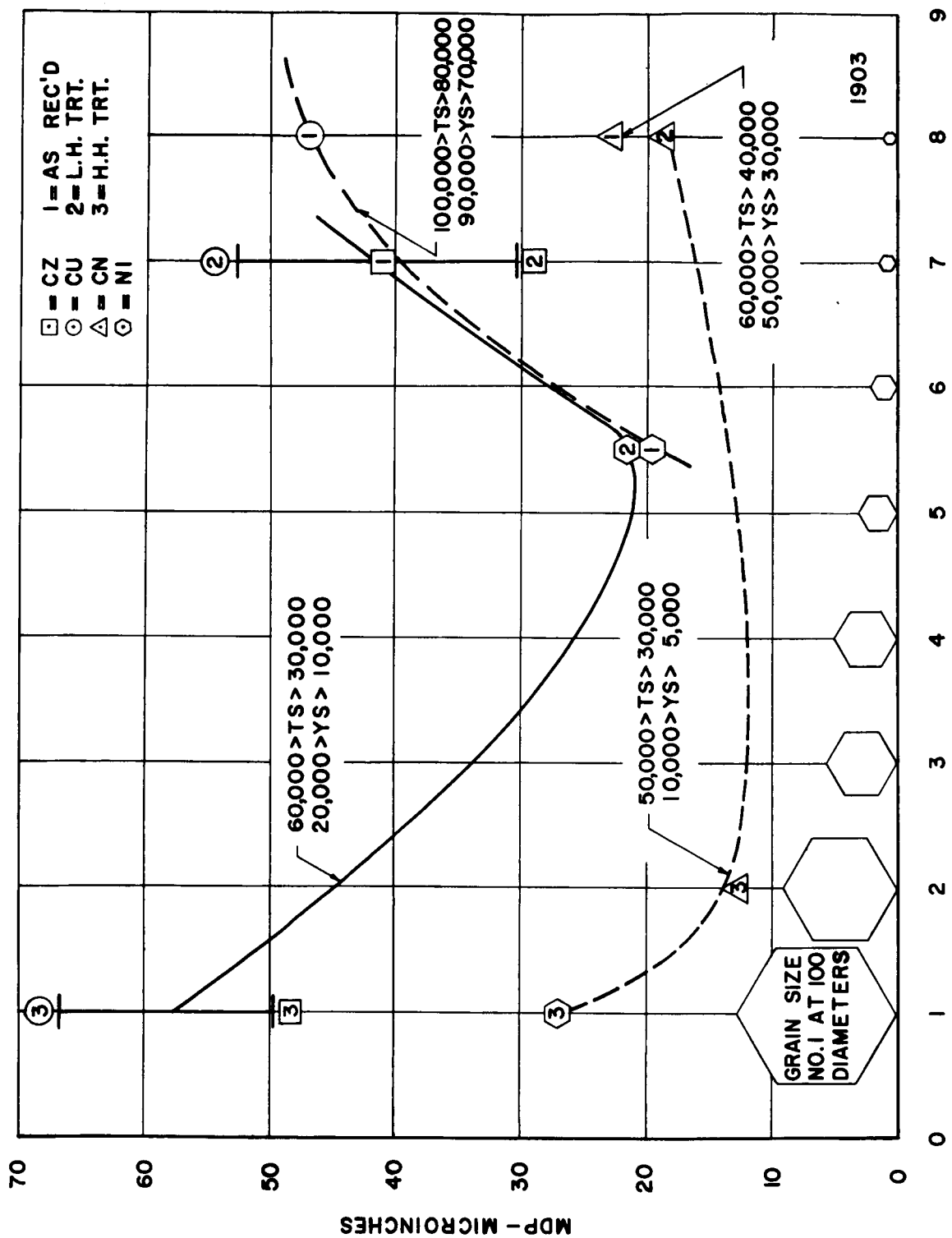

Fig. 45.--Cavitation damage at 100 hours vs. grain size for copper-zinc-nickel alloys for water at 200 ft./sec. and standard cavitation.

with earlier observations by Mousson[19] and Boetcher.[21]

These tests appear to indicate that since grain size affects cavitation damage significantly even though other mechanical properties are constant, a correlation of damage with mechanical properties alone is not possible.

CHAPTER V

CONCLUSIONS

Several general conclusions can be drawn on the basis of this investigation.

A. Damage Correlations

In general, there has been little success in obtaining a correlation of the cavitation damage data in the mercury system with a single mechanical property of the specimen materials. In the water system both elastic modulus and the ratio of the material and fluid acoustic impedance seem to correlate well with the damage. In both fluids a good correlation has been obtained with a group of several mechanical properties, involving a combination of strength and energy properties. This included tensile strength and true breaking strength in mercury, and acoustic impedance ratio, tensile strength, yield strength, and elastic modulus in water. No general correlation to apply for both fluids has been found. It is suspected that such general correlations based on the conventional semi-static material mechanical properties do not in fact exist.

B. Microexaminations

1. Proficorder Techniques

Examinations with a very sensitive linear tracing technique show that:

a) the size and shape of cavitation produced pits indicates a single-blow nature of the event producing the damage, during the early phases of damage. Later, the surface becomes largely covered by such single-event craters so that their interaction begins to cause fatigue failures, which are also enhanced by weaker blows unable to leave a permanent distortion. This early phase of damage when single-event craters predominate may be the "incubation period" often noted in the literature. However, from our data, there is weight loss during this period although perhaps less than sometimes detected.

b) There is an almost one to one comparison in the size, shape and depth to diameter ratio between impact pits from liquid impact tests and cavitation pits, where the corresponding velocities of impact are 4000 ft./sec. for water, and about 600 ft./sec. for mercury.

c) There is a directional variation in the assumed angle of incidence of the damaging blow for the water tests with varying test fluid velocity.

2. Microhardness Examinations

There is a significant increase in surface hardness on the copper, zinc, and nickel alloy specimens tested, with increased duration of exposure up to one hundred hours. This indicates that the surface is undergoing cold-work due to the repeated application of blows from

collapsing bubbles, some of which do not leave visible craters. The effect is greatest for the softest materials in the region where the largest number of bubbles exists (even though in a small collapsing pressure differential).

3. Grain Size Effects

There is a general decrease in damage in the water tests on the copper, zinc, and nickel alloys with decreasing grain size for comparable strength ranges of the materials. If a significant damage effect exists with grain size, even though other mechanical properties are constant, it is clear that a correlation in terms of mechanical properties alone cannot be completely successful.

C. Pit Correlations

Pitting rate and size distribution data, along with pressure and bubble distribution on the specimen polished surface, shows that:

a) In general, there is at least a 10^4:1 ratio between the number of bubbles observed on the specimen surface and the resulting number of pits observed there per unit time. The ratio becomes much greater in regions of low collapsing pressure differential;

b) The pit size number distribution has a maximum at about 0.05 mils diameter for most of the materials in both fluids;

c) The pitting rate varies with axial position and exhibits a maximum at an intermediate axial location due to the interaction of a decreasing number of bubbles and an increasing collapse pressure in the direction of downstream motion;

d) The pit size number distribution shifts in the direction of a relatively larger number of larger pits as the observer moves downstream since the pressure increases in this direction and the number of bubbles decreases.

APPENDIX A

COMPUTER ANALYSIS OF CAVITATION DAMAGE DATA

The computer program used to compute the mean depth of penetration, both from the pit count data and the weight loss measurements, is listed on the following pages. Included also is a page of typical output showing the numbers calculated, etc.

```
$COMPILE MAD,EXECUTE,DUMP,PUNCH OBJECT
R                              PROGRAM A
R                  REVISED AS OF FEB 23, 1965.
R
 Z=Z
 READ DATA FLUID
 PRINT FORMAT TABLE
 PRINT FORMAT TITLE, FLUID
 J=0
 K=1
START  READ FORMAT RFMT,MATL,NO,VEL,CAV
 MDPR = 0
 AMDPR = 0
 MDP2 = 0
 AMDP2 = 0
 H2 = 0
 I=0
AGAIN  READ DATA HRS,N1,N2,N3,N4,AWL
 WHENEVER Z.E.3
 PRINT COMMENT $0                                                NEXT SAMP
1LE DATA WERE OBTAINED IN THE OLD WATER LOOP$
 J = J + 1
 Z = 1
 OR WHENEVER Z.E.4
 PRINT COMMENT $0                                                NEXT SAMP
1LE DATA WERE OBTAINED IN DRY MERCURY $
 J = J + 1
 Z = 2
 END OF CONDITIONAL
 WHENEVER J.E.25
 K = K + 1
 PRINT FORMAT PAGE, K
 PRINT FORMAT TITLE, FLUID
 J = 0
 END OF CONDITIONAL
 WHENEVER HRS.L.0, TRANSFER TO START
 WHENEVER I.E.0
 FLAG = HRS
 N10=N1
 N20=N2
 N30=N3
 N40=N4
 I=1
 END OF CONDITIONAL
 WHENEVER Z.E.2
 N1 = 0
 N2 = 0
 N3 = 0
 N4 = 0
 OTHERWISE
 N1=N1-N10
 N2=N2-N20
 N3=N3-N30
 N4=N4-N40
 END OF CONDITIONAL
 WHENEVER MATL.E.$SS$.OR.MATL.E.$CS$
 RO = 7.85
```

```
OR WHENEVER MATL.E.$FLEX$
RO = 1.23
OR WHENEVER MATL.E.$CBZR$
RO = 8.72
OR WHENEVER MATL.E.$AL$
RO = 2.77
OR WHENEVER MATL .E.$CZ$
RO = 8.616
OR WHENEVER MATL.E.$A$.OR.MATL.E.$B$
RO = 17.655
OR WHENEVER MATL.E.$CU$
RO = 9.0248
OR WHENEVER MATL.E.$CN$
RO = 9.040
OR WHENEVER MATL.E.$NI$
RO = 8.973
OR WHENEVER  MATL .E.$SS1$
RO = 7.994
OR WHENEVER MATL.E.$F$
RO = 7.810
OR WHENEVER MATL.E.$D$
RO = 9.832
OR WHENEVER MATL.E.$G$
RO = 4.52
OR WHENEVER MATL.E.$E$
RO = 10.215
END OF CONDITIONAL
AUX1  =            .5216*N1+6.0363*N2+71.1547*N3+334.4513*N4
KO = 7.346E-3
KP = 1.172
KS = 3.601
WLPS = 1.642E-8*RO*KO*KP.P.3*AUX1
WL = KS * WLPS
APS = 3.72E4
AT = 3.362E5
MDPPS = KO * KP.P.3 * AUX1 /APS
MDP = KO * KP.P.3 * KS *AUX1/AT
AUX2 =     .6480*N1 + 3.1525*N2 + 16.4799*N3 + 46.6233 * N4
PDAPS = 25.*3.14159 * KP.P.2 *AUX2/APS
PDA = 25.*3.14159*KP.P.2 *KS *AUX2/AT
AMDP = AWL/(AT * 1.642E-8 * RO)
WHENEVER  WL.E.0
APDA = 0
OTHERWISE
APDA = PDA * AWL / WL
END OF CONDITIONAL
WHENEVER HRS.E.0
MDPR = 0
AMDPR = 0
MDP2 = 0
AMDP2 = 0
H2 = 0
OTHERWISE
H1 = H2
MDP1 = MDP2
AMDP1 = AMDP2
H2 = HRS
MDP2 = MDP
AMDP2 = AMDP
```

```
 MDPR = (MDP2 - MDP1)/(H2-H1)
 AMDPR = (AMDP2 -AMDP1)/(H2-H1)
 END OF CONDITIONAL
 WHENEVER HRS.G.FLAG
 WHENEVER Z.E.1
 PRINT FORMAT PFMT1,HRS,N1,N2,N3,N4,MDP,PDA,MDPR,AMDP,APDA,
1 AMDPR,AWL
 OR WHENEVER Z.E.0
 PRINT FORMAT PFMT1,HRS,N1,N2,N3,N4,MDP,PDA,MDPR
 OR WHENEVER Z.E.2
 PRINT FORMAT PFMT2,HRS,AMDP,      AMDPR,AWL
 END OF CONDITIONAL
 OTHERWISE
 PRINT FORMAT PFMT,MATL,NO,VEL,CAV,HRS,N1,N2,N3,N4,MDP,PDA,
1 MDPR,AMDP,APDA,AMDPR,AWL
 END OF CONDITIONAL
 J=J+1
 WHENEVER J.E.25
 K=K+1
 PRINT FORMAT PAGE,K
 PRINT FORMAT TITLE, FLUID
 J=0
 END OF CONDITIONAL
 TRANSFER TO AGAIN
 FORMAT VARIABLE Z
 INTEGER MATL,NO,N1,N2,N3,N4,J,K,I,Z,FLUID, CAV
R
R               FORMAT VALUES
R
 VECTOR VALUES TABLE=$1H1,S63,8HTABLE   *$
 VECTOR VALUES TITLE=$1H0,S50,30HCAVITATION  DAMAGE  DATA  IN
1 ,C6//S10,103H         WL = WEIGHT LOSS,  MDP = MEAN DEPTH OF
2PENETRATION,  PDA = PERCENT DAMAGED AREA,  R = RATE     ///S9
3,119HTHROAT  CAV. HOURS  PIT COUNT DATA     ---- CALCULATED
4VALUES ----          ----- ACTUAL (OR MEASURED) VALUES -----
5  /129HMATL NO. VEL-FPS COND  RUN    N1  N2  N3 N4    MDP-MIL
6S   PDA-PERCENT MDPR-MILS/HR MDP-MILS   PDA-PERCENT MDPR-MILS
7/HR   WL-GRAMS *$
 VECTOR VALUES PAGE=$1H1,S63,5HPAGE ,I2*$
 VECTOR VALUES RFMT=$C4,S6,I3,S7,F5.1,S5,C4*$
 VECTOR VALUES PFMT=$1H0,C4,   I3,S2,F5.1,S2,C4,S1,F5.1,S1,I4,
1S1,I3,S2,I2,S1,I2,S3,1PE10.3,S2,1PE10.3,S2,1PE10.3,S2,1PE10.3
2,S2,1PE10.3,S2,1PE10.3,S2,1PE10.3*$
 VECTOR VALUES PFMT1=$1H0,S21,                          F5.1,S1,I4,
1S1,I3,S2,I2,S1,I2,S3,1PE10.3,S2,1PE10.3,S2,1PE10.3,S2,1PE10.3
2,S2,1PE10.3,S2,1PE10.3,S2,1PE10.3*$
 VECTOR VALUES PFMT2 = $1H0,S21,F5.1,55H         ---- PIT COUNT
1ING WAS NOT POSSIBLE ----         ,1PE10.3,S14,          1PE10
2.3,S2,1PE10.3*$
 END OF PROGRAM
```

CAVITATION DAMAGE DATA IN WATER

WL = WEIGHT LOSS, MDP = MEAN DEPTH OF PENETRATION, PDA = PERCENT DAMAGED AREA, R = RATE

MAIL	NO.	THROAT VEL-FPS	CAV. COND	HOURS RUN	PIT COUNT DATA N1	N2	N3	N4	---- CALCULATED VALUES ---- MDP-MILS	PDA-PERCENT	MDPR-MILS/HR	----- ACTUAL (OR MEASURED) VALUES ----- MDP-MILS	PDA-PERCENT	MDPR-MILS/HR	WL-GRAMS
CW	84	200.0	STND	.0	0	0	0	0	.000E 00	.000E 00	.000E 00	.000E 00	.000E 00	.000E 00	.000E 00
				1.0	51	8	0	0	9.486E-06	6.733E-02	9.486E-06	3.212E-03	2.279E 01	3.212E-03	1.600E-04
				4.0	53	36	1	3	1.671E-04	3.515E-01	5.255E-05	5.219E-03	1.098E 01	6.691E-04	2.600E-04
				10.0	120	54	2	6	3.214E-04	6.479E-01	2.572E-05	9.635E-03	1.942E 01	7.360E-04	4.800E-04
				20.0	161	50	3	3	2.030E-04	5.214E-01	-1.184E-05	1.285E-02	3.300E 01	3.212E-04	6.400E-04
				30.0	293	64	7	4	3.008E-04	8.013E-01	9.784E-06	1.806E-02	4.812E 01	5.219E-04	9.000E-00
				40.0	643	124	11	9	6.177E-04	1.627E 00	3.169E-05	2.328E-02	6.135E 01	5.219E-04	1.160E-03
				50.0			---- PIT COUNTING WAS NOT POSSIBLE ----					2.509E-02		1.806E-04	1.250E-03
				75.0			---- PIT COUNTING WAS NOT POSSIBLE ----					3.352E-02		3.372E-04	1.670E-03
				100.0			---- PIT COUNTING WAS NOT POSSIBLE ----					5.600E-02		8.992E-04	2.790E-03
CW	157	200.0	STND	.0	0	0	0	0	.000E 00	.000E 00	.000E 00	.000E 00	.000E 00	.000E 00	.000E 00
				1.0	44	6	2	1	6.788E-05	1.468E-01	6.788E-05	3.412E-03	7.377E 00	3.412E-03	1.700E-04
				4.0	107	30	4	2	1.508E-04	3.733E-01	2.763E-05	6.423E-03	1.590E 01	1.004E-03	3.200E-04
				10.0	193	59	11	7	4.535E-04	9.460E-01	5.046E-05	1.285E-02	2.679E 01	1.071E-03	6.400E-00
				20.0	242	56	11	6	4.121E-04	9.179E-01	-4.142E-06	1.465E-02	3.263E 01	1.806E-04	7.300E-04
				30.0	381	67	12	7	4.811E-04	1.135E 00	6.897E-06	1.827E-02	4.309E 01	3.613E-04	9.100E-04
				40.0	1521	160	14	13	8.997E-04	2.689E 00	4.186E-05	2.108E-02	6.298E 01	2.810E-00	1.050E-03
				50.0			---- PIT COUNTING WAS NOT POSSIBLE ----					2.148E-02		4.014E-05	1.070E-03
				75.0			---- PIT COUNTING WAS NOT POSSIBLE ----					3.593E-02		5.781E-04	1.790E-03
				100.0			---- PIT COUNTING WAS NOT POSSIBLE ----					7.025E-02		1.373E-03	3.500E-03
CW	158	200.0	STND	.0	0	0	0	0	.000E 00	.000E 00	.000E 00	.000E 00	.000E 00	.000E 00	.000E 00
				1.0	0	0	1	1	5.138E-05	7.292E-02	5.138E-05	3.212E-03	4.558E 00	3.212E-03	1.600E-04
				4.0	0	1	5	4	2.153E-04	3.143E-01	5.464E-05	5.419E-03	7.913E 00	7.360E-00	2.700E-04
				10.0	139	27	5	6	3.291E-04	6.209E-01	1.897E-05	9.835E-03	1.856E 01	7.360E-04	4.900E-04
				20.0	179	31	5	4	2.500E-04	5.577E-01	-7.903E-06	5.821E-03	1.298E 01	-4.014E-04	2.900E-04

APPENDIX B

COMPUTER REGRESSION ANALYSIS OF DAMAGE DATA VERSUS MECHANICAL PROPERTIES

Due to the length and complexity of the regression program it is not reproduced in detail here as it appears in the original reference.[22] However, it is desirable to describe in general the characteristics and unique operational features of the program in order to better understand the predictions resulting from the use of it with respect to the damage data.

The program is in essence a least mean square fit regression analysis. It is capable of handling 59 independent variables, one dependent variable, 36 terms per variable, i.e., 36 powers per independent variable, and third order interactions of terms, i.e., a term of this latter type would be $X(1)^{a}X(2)^{b}X(3)^{c}$. Due to the tremendous number of possible terms available if the program is utilized to full capacity, it has incorporated into it a process of learning. The program selects a subset of up to 59 terms for a single pass out of the possible large number of terms generated for the entire number of variables considered to their different powers and interaction orders, e.g., for 8 variables, 10 terms per variable, there are 80 possible terms to analyze. However, if second order interactions are permitted, the total number of possible terms becomes 2880. Thus, it is soon obvious that it would take a long

time to examine all possible terms in this manner. The simple learning technique incorporated in this program consists of a weighting of the terms in the matrix, such that the probability of selecting terms of the type that have been selected in a previous pass as good fits are increased, and vice versa, for the terms of a type that have not been shown to have a good fit in a previous pass. Thus, the program is able to converge more rapidly on a statistically good fit of the observed data points with a function of the independent variables that were presented to it. The regression analysis is terminated when either of three criterion are satisfied: (1) The probability of inserting another term or removing a term from the current predicting equation is such that the chance of getting a bad term in or of taking a good term out is greater than the control value specified, (2) the total number of possible terms is exhausted and there are none left to insert, (3) the total number of trial passes specified is exceeded.

The sequence of analysis events occurs as follows:

The program reads in the specified control information and data sets, sets up a labeling system for the total possible number of terms, and then randomly picks out a subset of up to 59 of these for the first pass. It then computes individual correlation coefficients for each term with respect to the observed data values listed. The term with the highest correlation coefficient is selected to be entered into the equation and the least mean squares analysis is used to generate the coefficients for an equation of the following form:

$$Y = a_o + a_1 X_1$$

and the statistical information regarding the fit of this equation to the data is computed. The program then computes an importance factor for the test of the terms not in the equation with regard to how each will best account for the deviations between the actual data and the predicted values. The best term in this respect is entered into the equation if the test for the probability of insertion and deletion error is passed. If not, the regression is terminated. This process is continued until the best fit predicting equation possible with the first subset of terms is achieved. This completes a standard trial. Then, still working with the same subset of terms, a random trial is performed. The above process is repeated through the entering of the first term. The second term in this case is chosen randomly from the remaining terms of the subset with respect to the importance factors. This process is continued as for the standard trial until the regression is terminated for one of the three reasons mentioned previously. Several random trials are possible per pass, and in some cases result in a better predicting equation than the standard trial due to the combination of several terms that did not have as high of importance factors being better than another single term with the highest importance factor as selected in the standard trial.

At this point, the learning technique is employed by increasing the probability of picking terms of the type that got into the equation in the last pass and decreasing the probability of picking those types of terms that did not get in. The terms that are in the equation from the last pass are entered in the subset for the next pass and a random

process of selection, with respect to the changed probabilities of term selection, is employed to select enough other terms from the total possible to fill out the subset to its normal value. Another pass as described above is then initiated and carried out. At the end of the prescribed number of passes, the best trial of the best pass is indicated and the statistics of degree of fit to the data are generated and printed out along with the predicted equation. A typical pass would use the following data and control parameters.

Control parameters used for typical pass:

Prescribed Coefficient of Determination	=	0.97
Prescribed Standard Error of Y	=	0.00
Probability of insertion error	=	0.01
Probability of deletion error	=	0.01
Number of independent variables	=	10
Number of terms per variable	=	10
Interaction order	=	1
Number of terms per pass	=	40

Thus the total possible terms is 100.

In the program used, the mechanical properties were read in as follows, i.e., as dependent variables:

X(1) = Tensile Strength

X(2) = Yield Strength

X(3) = Engineering Strain Energy

X(4) = Elastic Modulus

X(5) = Brinell Hardness

X(6) = Acoustic Impedance = $\frac{(\rho (E/\rho)^{1/2})_{\text{fluid}}}{(\rho (E/\rho)^{1/2})_{\text{material}}}$ =

$$\frac{(\text{Density x Sonic Velocity})_{\text{fluid}}}{(\text{Density x Sonic Velocity})_{\text{material}}}$$

X(7) = True Breaking Stress

X(8) = True Strain Energy

X(9) = % Elongation

X(10) = % Reduction of Area

X(11) = MDP (Independent Variable)

APPENDIX C

DEFINITION OF CAVITATION CONDITIONS

The degree of cavitation as defined in the overall damage investigations in this laboratory and in this particular investigation differ between mercury and water. In the mercury venturi, where only two specimens are used, cavitation initiates at the throat outlet for all velocities used thus far, and the degree of cavitation applied to the mercury tests describes the extent of the cavitation cloud starting at the throat outlet and extending downstream to the point indicated, i.e., "cavitation to nose" is self explanatory. However, in the case of water, where three specimens are used, thus presenting more blockage to the venturi, the cavitation cloud initiates on the nose of the specimens and extends downstream to some point arbitrarily labeled by the degree of cavitation terminology. The first visible manifestation of cavitation occurs on the nose of the test specimen, and thus the term "visible initiation" was applied in this case. Then, succeeding degrees of more fully developed cavitation followed the old progression, regardless of the termination point on the specimen. The following are the definitions of the degrees of cavitation as used in this investigation:

Mercury

Visible Initiation - continuous ring of cavitation at the throat outlet, about 1/8" long.

Cavitation to Nose - cavitation cloud extends from throat outlet to termination at the nose of the specimen.

Standard Cavitation - cavitation cloud extends from throat outlet to termination at the middle of the specimen.

Cavitation to Back - cavitation cloud extends from throat outlet to termination at the rear of the specimen.

Water

Visible Initiation - cavitation cloud extends from nose of specimen to a point downstream on specimen about 1/8" long.

Cavitation to Nose - cavitation cloud extends from nose of specimen to termination at the middle of the specimen.

Standard Cavitation - cavitation cloud extends from nose of specimen to termination at the rear of the specimen.

From the pressure profile data in this report, the correspondence between water and mercury from a standpoint of degree of cavitation is as follows:

Mercury Condition	corresponds to	Water Condition
Cavitation to Nose	--	Visible Initiation
Standard Cavitation	--	Cavitation to Nose
Cavitation to Back	--	Standard Cavitation

This would result in the pressure gradients on the surfaces and the termination points on the surfaces being approximately the same for corresponding conditions from water to mercury.

BIBLIOGRAPHY

1. Hammitt, F. G., "Cavitation Damage and Performance Research Facilities," ASME Fluids Engr. Conf., Philadelphia, Pa., May, 1964, Symposium on Cavitation Research Facilities and Techniques, 175-184.

2. Robinson, M. J., "On the Detailed Flow Structure and the Corresponding Damage to Test Specimens in a Cavitating Venturi," Ph.D. Thesis, Nuclear Engineering Department, The University of Michigan, Ann Arbor, August, 1965. Also ORA Technical Report No. 03424016-T, Laboratory for Fluid Flow and Heat Transport Phenomena, Nuclear Engineering Department, The University of Michigan, August, 1965.

3. Rasmussen, R. E. H., "Some Experiments on Cavitation Erosion in Water Mixed with Air," Symposium on Cavitation in Hydrodynamics, National Physical Laboratory, Teddington, England, Sept. 14-17, 1955, 20 p.1 to 20 p.25.

4. Hammitt, F. G., Ericson, D., Ivany, R., Garcia, R., and Robinson, M. J., "Feasibility Investigations of Cavitation Number Measurements in Mercury and Water with Gas Injection," ORA Technical Report No. 06110-2-T, Laboratory for Fluid Flow and Heat Transport Phenomena, Nuclear Engineering Department, The University of Michigan, July, 1964.

5. Hammitt, F. G., Robinson, M. J., Ericson, D. M., Robinson, R. A., Koopman, R. P., Ahmed, O. S. M., "An Investigation of Entrained Gas Effect on Cavitation Number in Mercury in a Venturi," ORA Technical Report No. 06110-3-T, Laboratory for Fluid Flow and Heat Transport Phenomena, Nuclear Engineering Department, The University of Michigan, February, 1966.

6. Ericson, USAF Capt. D. M., Jr., Ph.D. Thesis in progress, Nuclear Engineering Department, The University of Michigan.

7. Harrison, C. A., Robinson, M. J., Siebert, C. A. Hammitt, F. G., and Lawrence, J., "Complete Mechanical Properties Specifications for Materials as Used in Venturi Cavitation Damage Tests," ORA Internal Report No. 03424-29-I, Department of Nuclear Engineering, Laboratory for Fluid Flow and Heat Transport Phenomena, The University of Michigan, August, 1965.

8. DeCorso, S. M., "Erosion Tests of Steam Turbine Blade Materials," ASTM Proceedings, Am. Soc. Testing Mats., Vol. 64, pp. 782-796.

9. Engel, O. G., "Pits in Metals Caused by Collision with Liquid Drops and Soft Metal Spheres," J. of Res. of Nat. Bur. Stds., Vol. 62, No. 6, Research Paper No. 2958, June, 1959, pp. 229-246.

10. Cramer, V. F., and Hammitt, F. G., "Cavitation Pit Diameter-Depth Observations for Stainless Steel in Water," ORA Report No. 03424-9-I, Department of Nuclear Engineering, Laboratory for Fluid Flow and Heat Transport Phenomena, The University of Michigan, Aug., 1961.

11. Hammitt, F. G., "Observations of Damage in a Flowing System," Trans. ASME, J. Basic Engr., Vol. 85, Sept., 1963, pp. 347-359.

12. Hammitt, F. G., et. al., "Cavitation Damage in Mercury and Water in a Cavitating Venturi and Other Components," ORA Technical Report No. 03424-9-T, Laboratory for Fluid Flow and Heat Transport Phenomena, The University of Michigan, Department of Nuclear Engineering, Sept., 1963.

13. Olson, H. G., unpublished thesis data, Ph.D. thesis, Nuclear Engineering Department, The University of Michigan, thesis in progress.

14. Plesset, M. S., "Pulsing Techniques for Studying Cavitation Erosion of Metals," Corrosion, May, 1962, pp. 181-188.

15. Ivany, R. D., Hammitt, F. G., and Mitchell, T. M., "Cavitation Bubble Collapse Observations in a Venturi," ASME Paper No. 65-WA/FE-20, to be published Trans. ASME, J. Basic Engr., abstracted Mechanical Engineering, Feb., 1966, p. 80.

16. Ellis, A. T., "Observations on Cavitation Bubble Collapse," Ph.D. thesis, Hydrodynamics Laboratory, California Institute of Technology, December, 1952.

17. Mitchell, T., unpublished thesis data, Ph.D. thesis, Nuclear Engineering Department, The University of Michigan, thesis in progress.

18. Ellis, A. T., "Parameters Affecting Cavitation and Some New Methods for Their Study," Report No. E-115.1, Hydrodynamics Laboratory, C.I.T., October, 1965.

19. Mousson, J. M., "Pitting Resistance of Metals Under Cavitation Conditions," ASME Trans., Hydraulic Division, June, 1937, pp. 399-408.

20. Wood, G. M., Knudsen, L. K., and Hammitt, F. G., "Cavitation Damage Studies with Rotating Disk in Water," ASME Paper No. 66-FE-11, to be published ASME Trans., J. Basic Engr.

21. Boetcher, H. N., "Failure of Metals Due to Cavitation Under Experimental Conditions," HYE-58-1, Trans. ASME, Vol. 58, 1936, pp. 355-360.

22. Westervelt, F. H., "Automatic System Simulation Programming," Ph.D. Thesis, The University of Michigan, November, 1960.